UNIVERSITY OF CALIFORNIA, SAN DIEGO

New roles for *Id3* in B and T cell development

A dissertation submitted in partial satisfaction of the requirements for
the degree Doctor of Philosophy

in

Biology

by

Shuwen Chen

Committee in Charge:

Professor Cornelis Murre, Chair
Professor Catriona Jamieson
Professor Li-Fan Lu
Professor David Nemazee
Professor David Traver
Professor Elina Zuniga

2016

The Dissertation of Shuwen Chen is approved, and it is acceptable in quality and form for publication on microfilm and electronically:

_____

_____

_____

_____

_____

_____
Chair

University of California, San Diego

2016

TABLE OF CONTENTS

LIST OF FIGURES

Chapter II

Chapter III

Chapter IV

ACKNOWLEDGMENTS

First, I would like to thank my advisor, Cornelis Murre, for all the help and the guidance he offered me throughout my PhD study. His insights and support allowed me to move forward my project while remaining optimistic about my future.

Current and former members of the Murre lab have always been a source of courage and help for me. I am so lucky to receive so many sharp-minded scientific insights, career suggestions, and other various advices. Working at Murre lab is an incredibly enjoyable experience.

I would like to thank my family for always believing in me more than I do. In particular my younger cousin, Beibei, for reminding me that every day could be a happy day as long as you keep smiling and laughing. Because of you, life outside lab also becomes so rewarding and refreshing.

People from the Biological Sciences department have always done their best to help students achieve as much as they can from the program. During my PhD study, I've witnessed the constant improvement of the program. I really appreciated and felt honored that I was admitted into such an excellent program. It paved the way for me to start my exploration in the scientific field for my future career success.

Lastly, I would like to thank my friends who have always stood behind me to give me courage and confidence. In particular, I would like to thank Masaki Miyazaki, for teaching me all those experimental procedures, and more importantly, for sharing his experience and advices for a PhD career with me.

Chapter II, in full, is a reprint of the material as it appears in Miyazaki M, Miyazaki K, Chen S, Itoi M, Miller M, Lu LF, Varki N, Chang AN, Broide DH, Murre C. (2014). *Id2 and Id3 maintain the regulatory T cell pool to suppress inflammatory disease*. Nature Immunology. The dissertation author was a co-first author on this publication.

Chapter III, in full, is a reprint of the material as it appears in Miyazaki M, Miyazaki K, Chen S, Chandra V, Wagatsuma K, Agata Y, Rodewald HR, Saito R, Chang AN, Varki N, Kawamoto H, Murre C. (2015). *The E-Id protein axis modulates the activities of the PI3K-AKT-mTORC1-Hif1a and c-myc/p19Arf pathways to suppress innate variant TFH cell development, thymocyte expansion, and lymphomagenesis.* Genes Development. The dissertation author was a co-author on this publication.

Chapter IV, in part, is based on the material as it appears in Chen S, Miyazaki M, Fisch K, Chang AN, Murre C. *The antagonist HLH protein Id3 acts to enforce the germinal center checkpoint in B-lineage cells.* (In preparation, 2016). The dissertation author was the primary author of this draft in preparation.

VITA

2010 Bachelor of Science, Fudan University, Shanghai, China

2016 Doctor of Philosophy, University of California, San Diego

PUBLICATIONS

Miyazaki M, Miyazaki K, **Chen S**, Itoi M, Miller M, Lu LF, Varki N, Chang AN, Broide DH, Murre C. *Id2 and Id3 maintain the regulatory T cell pool to suppress inflammatory disease.* (Nature Immunology, 2014)

Miyazaki M, Miyazaki K, **Chen S**, Chandra V, Wagatsuma K, Agata Y, Rodewald HR, Saito R, Chang AN, Varki N, Kawamoto H, Murre C. *The E-Id protein axis modulates the activities of the PI3K-AKT-mTORC1-Hif1a and c-myc/p19Arf pathways to suppress innate variant TFH cell development, thymocyte expansion, and lymphomagenesis.* (Genes & Development, 2015)

Yang G, Chen S, Zhu X, Liang S, Liu L, Ren D. *A synthetic multi-epitope antigen enhances hepatitis C virus-specific B- and T-cell responses.* (Viral Immunology, 2011)

ABSTRACT OF THE DISSERTATION

New roles for *Id3* in B and T cell development

by

Shuwen Chen

Doctor of Philosophy in Biology

University of California, San Diego, 2016

Professor Cornelis Murre, Chair

E proteins have been shown to play an important role during various stages of B and T cell development. E proteins execute this regulatory function mainly via binding to the E-box sequence around the target genes. However, the activity of E proteins can be inhibited by Id proteins, such as Id2 and Id3 in the immune system.

Previous studies have suggested crucial roles played by Id2 and Id3 in the differentiation process of certain T cell lineages. Id2 was required for CD8 T cell differentiation and activation, while Id3 was required to inhibit E2A activity upon pre-TCR and TCR signaling. During my PhD study, I performed a wide array of experiments to probe into the functions of Id2 and Id3 during the development of

regulatory T cells (Treg) and innate-like follicular helper T (Tfh) cells. My work helped unveil that Id2 and Id3 expression was required for Treg cells to suppress the onset of fatal Th2-mediated inflammation. Meanwhile, I also discovered that thymic Id2 and Id3 expression was indispensable for inhibiting the expansion of innate-like Tfh cells and the pathogenesis of αβ T cell lymphoma.

Besides T cells, B cells are also a target population to be regulated by Id proteins like Id3. Ablating *Id3* expression specifically in the B cells, I found that these *Id3*-deficient B cells were clearly impaired in their ability to differentiate into germinal centers upon antigen stimulation. In addition, without *Id3* expression, these B cells can no longer elicit any IgG1 response during the memory phase upon encountering a secondary challenge.

To summarize, my PhD study helped to reveal the important functions played by *Id2* and *Id3* during the differentiation and activation of different lymphocytes.

Chapter I:

General introduction to early B cell development, B cell terminal differentiation, and T cell development and differentiation in periphery

Early Hematopoiesis

Hematopoiesis is initiated by a small population of cells called hematopoietic stem cells (HSCs). They are localized in the yolk sac, fetal liver, and bone marrow. HSCs are characterized by their ability of self-renewal and multi-potency over the lifetime of an organism [1]. The establishment of HSCs takes place in a sequential manner: During embryogenesis, mesodermal precursor cells migrate to the yolk sac for commitment to red blood cells. Later during embryogenesis other HSCs colonize the developing fetal liver for expansion and differentiation until the stage of fetal life, when bone marrow hematopoiesis is initiated [2]. Progenitors from both fetal liver and bone marrow can give rise to the lymphoid compartment. Populations derived from HSCs gradually lose their multi-potency as they differentiate into various cell types of the lymphoid, myeloid, and other cell lineages. The ability of HSCs to self-renew fades with senescence and the choice of lymphoid versus myeloid lineage become skewed with age.

HSCs lack expression of genes specific to the committed lineages, such as B220 and CD19 for B cells or CD4 and CD8 for T cells (Lin-), but express other surface markers such as Sca-1, c-kit, and CD150 [3,4]. HSCs have been further divided into 2 subpopulations named long-term HSCs and short-term HSCs [5]. Within the bone marrow, a fraction of long-term HSCs transit into short-term HSCs, which can only self-renew for a limited period of time [6,7]. The HSCs then give rise to multi-potent progenitors (MPPs), which lose self-renewal ability while maintain the potential of differentiation into all lineages [8]. MPPs then advance to the common lymphoid

progenitors (CLPs) or the common myeloid progenitors (CMPs). These oligo-potent progenitors can then differentiate into all lineage-committed cell populations of the hematopoietic system [9]. CLPs give rise to various lymphoid lineage populations including T cells, B cells, and natural killer (NK) cells. The choice of next developmental fate within the CLP compartment is reflected by Ly6D expression. Ly6D+ CLPs, termed B cell biased lymphoid progenitors (BLPs), commit their lineage to B cells, while Ly6D- CLPs, termed all-lymphoid progenitors (ALPs), usually move along the differentiation track to become NK cells, T cells, or B cells [10-12].

T-Lineage Development

Mammalian T cells are commonly derived from pluripotent precursors in the bone marrow or fetal liver, which localize to the thymus for initiation and maintenance of T cell differentiation. After extensive proliferation, these progenitors undergo gene rearrangements that are associated with the T cell receptor (TCR) loci [13]. After T cell lineage commitment, the αβ and γδ lineages segregate. αβ T cells development is initiated upon interaction of the alpha-beta TCR with MHC. CD4 and CD8, the two co-receptors, can be used as cell surface markers along with other molecules to distinguish between the αβ T-lineage cells. The earliest thymic precursors express neither CD4 nor CD8 and are named double-negative (DN) cells. The DN population contains multiple subsets that are associated with differential expression of two additional surface markers, CD25 and CD44. The DN1 (CD44+CD25-) compartment contains cells of other lineages such as dendritic cells and B cells. During the DN2 (CD44+CD25+) and the DN3 (CD44-CD25+) stage, the process of T cell lineage commitment is completed. During DN3 stage, the rearrangement of the variable segments occurs until an in-frame and proper TCR is generated, verified by the β-selection checkpoint. The rearranged TCR β-chain then associates with pre-Tα, resulting in the expression of a pre-TCR complex to promote proliferation and expression of CD4 and CD8 to progress into the double-positive (DP: CD4+CD8+) stage, during which α-rearrangement is carried out. The interaction between TCRαβ with self peptide-MHC complexes (pMHC) then gives rise to either CD4 single-positive (CD4SP) or CD8 single-positive (CD8SP) thymocytes [14,15].

T Cell Differentiation in Periphery

Previous studies indicated that CD4+ T cells are required for GC formation and the generation of Ag-specific responses. Further studies revealed that T follicular helper (Tfh) cells are the key player during this process. Characterized by high expression levels of surface molecules (CXCR5, ICOS, and PD-1) and transcription factors (Bcl-6), Tfh cells display unique patterns of localization and function [16]. Loss of T cell area-homing chemokine receptor CCR7, along with high CXCR5 expression, redirect Tfh cells from the T cell zone to the B cell follicles, where Tfh cells provide supportive signaling for B cell proliferation and differentiation [17].

Regulatory T (Treg) cells are a distinct T cell subpopulation as they play a vital role in maintaining self-tolerance and immune homeostasis, characterized by the transcription factor Foxp3, which is essential for Treg cell development and function. Mice carrying mutations of *Foxp3* display Treg deficiency and develop fatal autoimmunity [18]. Treg development involves affinity-based TCR-pMHC interaction. High strength TCR signaling within the thymus initiates negative selection in most CD4SP thymocytes. However, some CD4SP thymocytes only receive TCR signaling of intermediate strength, thus escaping the fate of apoptosis and further differentiating into Foxp3+ Treg cells [19].

Treg cells can also be induced from peripheral naïve T cells in a *Foxp3* enhancer CNS1-dependent manner upon exposure to tumor growth factor (TGFβ) [20]. In the periphery, Treg cells display various expression levels of homing receptors such as adhesion molecules and chemokine receptors, leading to the heterogeneity of

the Treg localization and consequently the compartmentalization of Treg-mediated immune responses [21]. After settlement within secondary lymph nodes, Treg cells can be activated by cognate antigen at a concentration much lower than that required for activating naïve T cells. Meanwhile, proliferation of Treg cells is also contained and fine-tuned by cell death mechanisms to maintain homeostasis. Downregulation of anti-apoptotic Bcl-2 in Treg cells plays an essential role during this process [22]. Treg cells can execute their suppressive function by either inhibiting the function of antigen-presenting cells (APC) or direct secretion of inhibitory cytokines [23].

B-Lineage Development

B cells arise from BLPs, which are composed of Ly6D+ CLPs. BLPs first differentiate into pre-pro-B cells, which then develop into pro-B cells through a series of recombination events and the induction of a B-lineage specific program of gene expression [24]. The rearrangement of immunoglobulin (Ig) genes is ordered. During the transition from the pre-pro-B to the pro-B cell stage, the diversity (Dh) and joining (Jh) recombine to generate a Dh-Jh segment [25]. Recombination activating gene 1 (RAG1) and recombination activating gene 2 (RAG2) mediate somatic recombination involving antigen receptor loci. This is followed by Vh-DhJh locus rearrangement leading to conformational changes involving the *Igh* locus. Specifically, the proximal and distal clusters of the variable (Vh) segments merge providing an equal playing field for the variable region repertoire [26]. The rearranged heavy chain associates with the surrogate light chains to give rise to the pre-BCR complex, which promotes differentiation towards the small pre-B stage while counteracting the activity of RAG1 and RAG2 [27]. Light chain rearrangement (either *Igκ* or *Igλ*) occurs in small pre-B cells and continues until the BCR passes both positive and negative selection [28-30]. A highly regulated and hierarchical gene expression program is required for B cell lineage commitment. These involve the E-protein E2A, early B cell factor 1 (EBF1), paired box 5 (Pax5) and forkhead box protein O1 (FoxO1). Depletion of E2A or EBF1 expression results in B cell developmental [31]. Recent studies have provided insight into the transcriptional circuitry that promotes the specification towards the B cell lineage. The E2A proteins activate the expression of FOXO1, which in turn,

induce the expression of EBF1. FOXO1 and EBF1 then act in a positive feed-forward loop to orchestrate a B-lineage specific program of gene expression.

B Cell Differentiation in Periphery

After completing the aforementioned developmental program within the bone marrow, immature B cells exit the bone marrow, migrate through the circulation, and localize in lymph nodes, Peyer's patches and the spleen [32]. Follicular (FO) B cells constitute the majority of the peripheral B cell pool where they interact with T cells upon antigen stimulation to mount an immune response [33].

When stimulated with foreign antigens, naïve B cells within B cell follicles initiate their proliferation and terminal differentiation program. This proliferation leads to generation of secondary follicles termed germinal centers (GCs). In GCs the majority of cells are activated B cells undergoing clonal expansion, somatic hypermutation (SHM), and class-switch recombination (CSR), ultimately leading to the production of high-affinity antibodies [34]. The GC can be further divided into 2 anatomical sub-compartments, a dark zone (DZ) and a light zone (LZ). The DZ and LZ differ not only in cellular components and densities, but also phenotypically. In the LZ, B cells are spread among a network of follicular dendritic cells (FDCs), on which antigen deposits. Hence this is the compartment where positive selection for high-affinity BCR variants takes place [35]. In contrast, the DZ is composed almost entirely of B cells, which have a higher percentage of cells in the G2/M phase when compared to their LZ counterparts. In addition, DZ B cells also show higher expression of chemokine receptor CXCR4, while two surface markers CD83 and CD86, display a higher level of expression on the surface of LZ B cells. Combining these markers, it is now possible to distinguish between DZ and LZ B cells by flow

cytometry. DZ B cells are associated with $CXCR4^{hi}CD86^{lo}$ expression, while LZ cells display $CXCR4^{lo}CD86^{hi}$ [36,37].

Within the DZ of the GC, B cells undergo a combination of affinity maturation processes, including CSR and SHM, both of which require the expression of activation-induced cytidine deaminase (AID) [38]. CSR is required for the generation of antibodies associated with distinct effector functions by changing the expression from *Igh* constant *Cμ* region to other *Igh* constant (C) regions such as *Cγ*, *Cε* and *Cα*, leading to the production of IgG, IgE and IgA, respectively. CSR itself doesn't alter the antigen specificity of BCR. Instead, SHM is responsible for changing BCR specificity. During SHM, point mutations are introduced to the V region of the immunoglobulin loci. Accumulation of these point mutations engenders B cells expressing high-affinity BCRs (immunoglobulin in a membrane-bound form) on their surface. Post-SHM B cells are able to secrete high-affinity antibodies against invading antigens [39].

After completing the affinity maturation reactions within GCs, B cells exit the GC phase and select between two mutually exclusive terminal fates: antibody-secreting plasma cells (PCs) and resting memory B cells. Several master transcriptional regulators have been identified to be critical for the generation of PCs, including *Xbp-1*, *Blimp-1* and *Irf-4* [40-42]. However, no such factors have been discovered for memory B cell formation.

Long-lived PCs generated in adaptive immune responses can be found in the red pulp of spleen and bone marrow weeks after primary antigen challenge. These

long-lived PCs constitutively secrete protective antibodies, forming the first line of protection against reinfection. When these pre-existing antibodies are not sufficient to combat the reinfection, cognate memory B cells can be re-activated very quickly and a reactive humoral memory response is organized. Such memory response is characterized by its faster recruitment and greater magnitude. Furthermore, the antibodies secreted during the memory response frequently also display higher affinity with a switched effector isotype [43-45].

E-proteins and ID proteins in Lymphoid Development

The differentiation of HSCs into lineage-committed populations is orchestrated by an ensemble of transcriptional regulators. Prominent among these are the E2A proteins. The E2A proteins belong to the family of E proteins, which include E12, E47, HEB, E2-2, and Daughterless. Tcf3, Tcf4, and Tcf12 encode E2A, E2-2 and HEB respectively. E12 and E47 are two isoforms of the E2A protein due to alternative splicing [46,47]. The E2A protein can specifically bind to the canonical E-box site embedded in the enhancers through formation of homodimers or as heterodimers with HEB or E2-2. E2A proteins are critical for maintenance of the HSC pool as they are shown to regulate cell cycle progression and self-renewal activity of HSCs. E2A deficiency led to impairment of the HSC pool and a wide ensemble of progenitor populations including long-term HSC, MPPs, and erythroid progenitors were dramatically reduced [48]. E2A, together with other transcription factors such as Ikaros, promote the developmental progression from HSCs to LMPPs. In lineage-committed cells, the E2A proteins also play essential roles and E2A activity is indispensable for establishing a diverse BCR or TCR repertoire [49-51].

During B cell development the E2A proteins induce the expression of EBF and FOXO1, which form a positive feed-forward loop to initiate a lineage specific gene expression program [52,53]. Within the thymus, the E2A proteins promote β-rearrangement of TCR during the DN2 and DN3 stages. E2A activity is also essential to the initiation of T cell lineage commitment. The E2A proteins are required for activating gene expression involved in Notch and pre-TCR signaling pathways and

their collaboration with Bcl11b and GATA3 is also critical for regulating T cell development [54].

The E2A proteins also perform critical roles during the terminal differentiation of lymphocytes within peripheral lymphoid organs. Upon activation of naïve B cells by foreign antigens, E2A expression is induced to establish germinal centers and activate class-switch recombination (CSR). Previous studies revealed that E2A proteins directly regulate the expression of AID. Consistent with these findings a deficiency in E2A activity leads to perturbation of CSR [55,56].

The activity of E-proteins is under strict control at several levels. One of these, the inhibitor of DNA binding (ID) proteins, can form non-DNA-binding heterodimers with E-proteins through the helix-loop-helix (HLH) dimerization domain preventing their E-box-binding activities [57]. Four ID proteins (ID1 to ID4) have been identified till now. Among them, ID2 and ID3 are particularly important in the immune system. Both ID2 and ID3 are induced in the DN3 stage upon pre-TCR signaling, plausibly acting to regulate TCR β-rearrangement [58,59]. *Id2*$^{-/-}$ mice display a NK cell deficiency, which can be rescued by deletion of *E2a*, confirming the critical role for E-Id protein interactions during NK cell development [60,61]. ID3 has been shown to execute important functions during the differentiation and activation of various peripheral T cell populations. *Id3* deletion led to defect in the generation of Treg cells along with increased interleukin 17 (IL-17)-producing helper T cells (T_H17) cells differentiation [62]. Recently, it was revealed that ID3 was involved in regulating the secretion of interleukin 9 (IL-9) by T_H9 cells [63, 64].

In sum, it is now clear how distinct combinations of transcriptional regulators orchestrate lineage specific programs of gene expression. In this thesis I will describe our studies that have revealed critical roles for the Id-E protein axis in Treg, TFH and germinal center B cells.

Chapter II:

Id2 and Id3 maintain the regulatory T cell pool

nature immunology

Id2 and Id3 maintain the regulatory T cell pool to suppress inflammatory disease

Masaki Miyazaki[1,6], Kazuko Miyazaki[1,6], Shuwen Chen[1,6], Manami Itoi[2], Marina Miller[3], Li-Fan Lu[1], Nissi Varki[4], Aaron N Chang[5], David H Broide[3] & Cornelis Murre[1]

Regulatory T (T_{reg}) cells suppress the development of inflammatory disease, but our knowledge of transcriptional regulators that control this function remains incomplete. Here we show that expression of *Id2* and *Id3* in T_{reg} cells was required to suppress development of fatal inflammatory disease. We found that T cell antigen receptor (TCR)-driven signaling initially decreased the abundance of Id3, which led to the activation of a follicular regulatory T (T_{FR}) cell–specific transcription signature. However, sustained lower abundance of Id2 and Id3 interfered with proper development of T_{FR} cells. Depletion of Id2 and Id3 expression in T_{reg} cells resulted in compromised maintenance and localization of the T_{reg} cell population. Thus, Id2 and Id3 enforce T_{FR} cell checkpoints and control the maintenance and homing of T_{reg} cells.

Homeostasis of the immune system requires careful control mechanisms at mucosal barriers, sites exposed to abundant foreign antigens. Immune system cells must provide protection against a broad range of invading pathogens but also ensure tolerance to self antigens and innocuous non-self antigens[1–3]. Failure of the immune system to enforce tolerance readily leads to the development of autoimmune disease and allergies, including asthma and atopic dermatitis. Allergy is characterized by the expression of T_H2 cell cytokines, high concentrations of serum immunoglobulin E (IgE) and eosinophilia[4,5]. T_{reg} cells are prominent among the cell types that suppress spontaneous inflammation and are characterized by expression of the transcription factor Foxp3 (refs. 6–11). Absence of *Foxp3* in mice and *FOXP3* in humans rapidly results in the development of multiorgan autoimmunity, inflammatory bowel disease and allergy. T_{reg} cells develop in the thymus (tT_{reg} cells) as well as in the peripheral organs (pT_{reg} cells)[1–3]. pT_{reg} cells act primarily to control the development of mucosal inflammation[12]. T_{reg} cells are also essential in regulation of humoral immunity; loss of T_{reg} cells leads to elevated concentrations of autoantibodies, hyper-IgE syndrome, increased numbers of follicular helper T (T_{FH}) cells and spontaneous development of germinal centers (GCs)[13]. Recent studies have identified a subset of T_{reg} cells named T_{FR} cells that control GC reactions, characterized by the expression of *Cxcr5*, *Bcl6*, *Pdcd1* and *Prdm1* (refs. 14–16).

Members of the helix-loop-helix (HLH) family regulate many developmental trajectories in the thymus[17]. These include E proteins as well as Id proteins. E proteins function as transcriptional activators or repressors with the ability to bind specific DNA sequences termed E-box sites. Four E proteins have been identified and characterized: E12, E47, HEB and E2-2. E12 and E47 are encoded by the *Tcf3* locus and are generated by differential splicing[18]. HEB and E2-2 are related to the *Tcf3* gene products but diverge substantially in the N-terminal transactivation domains. DNA-binding activity of E proteins is regulated by the Id proteins[19,20]. Four Id proteins named Id1, Id2, Id3 and Id4 contain an HLH dimerization domain but lack the basic DNA-binding region. Interactions between Id proteins and E proteins suppress DNA-binding activity of E proteins. Id2 and Id3 are particularly important in modulating the developmental progression of T lineage cells[21–26].

Here we found that depletion of *Id2* and *Id3* expression in T_{reg} cells resulted in the early onset of fatal T_H2 cell–mediated inflammatory disease. We found that upon TCR-mediated signaling in T_{reg} cells, expression of *Id2* and *Id3* declined, leading to higher binding activity of E proteins and induction of a T_{FR} cell–specific program of gene expression, including *Cxcr5* and *Il10*. Loss of *Id2* and *Id3* in T_{reg} cells resulted in compromised T_{reg} cell homeostasis, increased susceptibility to cell death upon stimulation and aberrant tissue localization. Taken together, we propose that Id2 and Id3 maintain the T_{reg} cell pool and act as gatekeepers to enforce multiple checkpoints during T_{FR} cell differentiation.

RESULTS

Id2 and *Id3* expression in T_{reg} cells

As a first approach to explore potential roles for *Id2* and *Id3* in T_{reg} cells, we analyzed their expression patterns using *Id2*-YFP and *Id3*-GFP reporter mice[26,27]. We found that the thymic T_{reg} cell population can be segregated into $Id2^+Id3^+$ as well as $Id2^-Id3^+$ compartments (**Fig. 1a**). In maturing T_{reg} cells, which first express CD69 and then upregulate CD62L, *Id2* expression declined, leading to an increase

[1]Department of Molecular Biology, University of California, San Diego, La Jolla, California, USA. [2]Department of Immunology and Microbiology, Meiji University of Integrative Medicine, Hiyoshi-cho, Kyoto, Japan. [3]Department of Medicine, University of California, San Diego, La Jolla, California, USA. [4]Department of Pathology, University of California, San Diego, La Jolla, California, USA. [5]Center for Computational Biology, Institute for Genomic Medicine, University of California, San Diego, La Jolla, California, USA. [6]These authors contributed equally to this work. Correspondence should be addressed to C.M. (murre@biomail.ucsd.edu).

Received 11 September 2013; accepted 22 May 2014; published online 29 June 2014; doi:10.1038/ni.2928

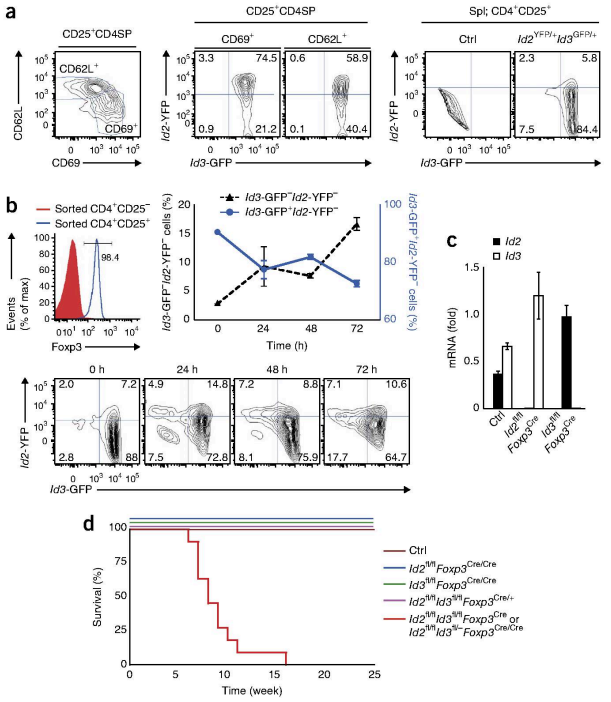

Figure 1 Ablation of *Id2* and *Id3* expression in T_{reg} cells leads to the early onset of fatal inflammatory disease. (**a**) Flow cytometric analysis of CD69 versus CD62L expression gated on the CD4+CD25+ T_{reg} cell population derived from the thymus (CD4+CD25+CD8−TCRβ^{hi} (left). CD4SP, CD4+CD8−. GFP versus YFP expression, gated on CD69+CD62L− or CD69−CD62L+ T_{reg} cells derived from the thymus (middle). GFP versus YFP expression in CD4+CD25+ T_{reg} cells isolated from the spleens (Spl) of control and *Id2*$^{YFP/+}$*Id3*$^{GFP/+}$ mice (right). Numbers in quadrants indicate percent cells in each compartment. (**b**) Flow cytometric analysis of Foxp3 expression on sorted CD4+CD25+ and CD4+CD25− T cells (left; number indicates the percentage of Foxp3+ cells gated on the CD4+CD25+ T cells); sorted CD4+CD25+ T_{reg} cells from *Id2*$^{YFP/+}$*Id3*$^{GFP/+}$ mouse (CD45.2) were cocultured with CD4+CD25− T cells (CD45.1) and stimulated with anti-CD3ε plus anti-CD28 in the presence of T cell–depleted splenocytes (APCs). Flow cytometric analysis of GFP versus YFP expression gated on CD45.2+CD45.1−CD4+TCRβ+CD25+ cells for the indicated time points (bottom). Percentage of *Id3*-GFP+*Id2*-YFP− cells and *Id3*-GFP−*Id2*-YFP− cells (middle). (**c**) Quantitative real-time PCR analysis of *Id2* and *Id3* transcript levels in sorted CD4+TCRβ+CD25+YFP+ T_{reg} cells derived from the lymph nodes of *Id2*$^{+/+}$*Id3*$^{+/+}$*Foxp3*^{Cre} (Ctrl), *Id2*$^{fl/fl}$*Foxp3*^{Cre} or *Id3*$^{fl/fl}$*Foxp3*^{Cre} mice. (**d**) Survival plot of *Id2*$^{fl/fl}$*Id3*$^{fl/fl}$*Foxp3*^{Cre} and *Id2*$^{fl/fl}$*Id3*$^{fl/-}$*Foxp3*$^{Cre/Cre}$, *Id2*$^{fl/fl}$*Foxp3*$^{Cre/Cre}$, *Id3*$^{fl/fl}$*Foxp3*$^{Cre/Cre}$, *Id2*$^{fl/fl}$*Id3*$^{fl/fl}$*Foxp3*$^{Cre/+}$ and littermate control (Ctrl) mice, monitored during a 25-week period. Data are representative of two experiments (**a**,**b**; error bars in **b**, s.d.; $n = 3$ technical replicates), one experiment (**c**; error bars, s.d.; $n = 3$ technical replicates) and one experiment (**d**; $n = 11$ independent biological replicates per group).

of the Id2−Id3+ compartment (**Fig. 1a**). In the peripheral lymphoid organs, the majority of T_{reg} cells consisted of Id2−Id3+ cells (**Fig. 1a**). To examine the dynamics of *Id2* and *Id3* expression upon stimulation, sorted T_{reg} cells carrying the *Id2*-YFP and *Id3*-GFP reporters were activated *in vitro* by exposure to anti-CD3e and anti-CD28 in the presence of non–T_{reg} cells as well as antigen-presenting cells (APCs) (**Fig. 1b**). The most pronounced change occurred in *Id3* expression, which declined substantially upon exposure to TCR-mediated signaling (**Fig. 1b**). Thus, the majority of T_{reg} cells isolated from peripheral organs expressed abundant Id3 but lacked Id2, but upon *in vitro* stimulation, Id3 expression declined in a fraction of cells, leading to Id2^{lo}Id3^{lo} and Id2^{int}Id3^{lo} T_{reg} cell populations.

Id2 and *Id3* expression suppresses fatal inflammation

To evaluate the roles of *Id2* and *Id3* in T_{reg} cell function, we crossed *Id2*$^{loxP/loxP}$ (*Id2*$^{fl/fl}$) and *Id3*$^{fl/fl}$ mice with *Foxp3*^{Cre} mice[23,28,29]. The *Foxp3*^{Cre} mice used throughout this study carried an internal ribosomal entry site followed by a sequence encoding a Cre-YFP functional fusion protein located downstream of the *Foxp3* termination codon[29]. The *Foxp3* locus is X chromosome–linked, and consequently gender-based differences in excision of the *loxP*-flanked alleles impact the population of T_{reg} cells present in these mice. Here will refer to male mice carrying the *Foxp3-Cre-YFP* allele as *Foxp3*^{Cre} mice and to female mice as *Foxp3*$^{Cre/Cre}$ or *Foxp3*$^{Cre/+}$ mice. Mice deficient for *Id2* or *Id3* alone in T_{reg} cells did not show evidence of inflammatory disease (**Supplementary Fig. 1** and data not shown). To examine whether *Id2* and *Id3* compensate for each other, we sorted T_{reg} cells from *Id2*$^{fl/fl}$*Foxp3*^{Cre} mice as well as *Id3*$^{fl/fl}$*Foxp3*^{Cre} mice. We isolated RNA from the sorted populations and examined it by real-time PCR for *Id2* and *Id3* expression. In the absence of *Id2* expression, the abundance of *Id3* increased, whereas in T_{reg} cells deficient for *Id3* expression, abundance of *Id2* increased, as compared to controls (**Fig. 1c**).

Next, we generated *Id2*$^{fl/fl}$*Id3*$^{fl/fl}$*Foxp3*^{Cre} as well as *Id2*$^{fl/fl}$*Id3*$^{fl/fl}$*Foxp3*$^{Cre/Cre}$ mice. *Id2*$^{fl/fl}$*Id3*$^{fl/fl}$*Foxp3*^{Cre} and *Id2*$^{fl/fl}$*Id3*$^{fl/fl}$*Foxp3*$^{Cre/Cre}$ mice were born with Mendelian frequencies and were healthy up to 4 weeks of age. However, 6–8-week-old mice with no sex bias developed dermatitis with swelling and fur loss across the eyelids, and the majority of *Id2*$^{fl/fl}$*Id3*$^{fl/fl}$*Foxp3*^{Cre} and *Id2*$^{fl/fl}$*Id3*$^{fl/fl}$*Foxp3*$^{Cre/Cre}$ mice died within ten weeks (**Fig. 1d** and **Supplementary Fig. 2a**). Neither *Id2*$^{fl/+}$*Id3*$^{fl/fl}$*Foxp3*^{Cre} nor *Id2*$^{fl/fl}$*Id3*$^{fl/+}$*Foxp3*^{Cre} mice displayed early morbidity (data not shown). Approximately one-third of *Id2*$^{fl/fl}$*Id3*$^{fl/fl}$*Foxp3*^{Cre} and *Id2*$^{fl/fl}$*Id3*$^{fl/fl}$*Foxp3*$^{Cre/Cre}$ mice showed intense dermatitis with scaling and fur loss throughout the body but not in the skin of the tail (data not shown). Similar to the case with human atopic dermatitis, *Id2*$^{fl/fl}$*Id3*$^{fl/fl}$*Foxp3*^{Cre} mice displayed dermatitis as evidenced by compulsive scratching of the face and back (**Supplementary Video 1**).

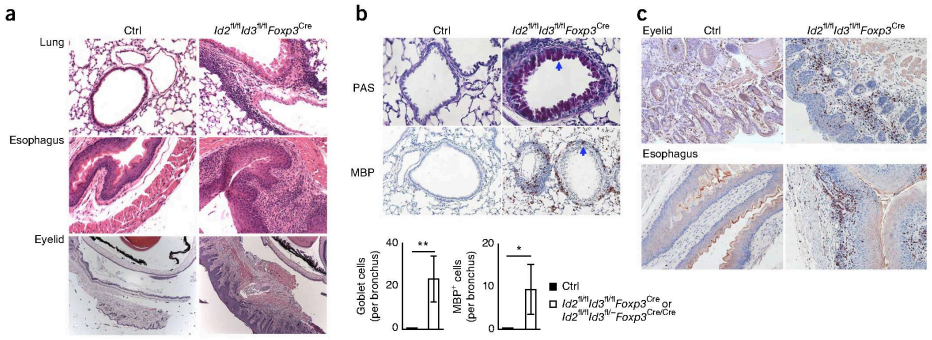

Figure 2 Spontaneous inflammation in the lung, eyelid, skin and esophagus in mice depleted for the expression of *Id2* and *Id3* in T_{reg} cells. (**a**) Hematoxylin and eosin (H&E) staining of the lung, esophagus and eyelid derived from control (Ctrl; female $Id2^{fl/fl}Id3^{fl/fl}Foxp3^{Cre/+}$) and $Id2^{fl/fl}Id3^{fl/fl}Foxp3^{Cre}$ mice. Original magnification: ×200 (lung), ×200 (esophagus) and ×50 (eyelid). (**b**) Periodic acid Schiff (PAS) staining and MBP immunostaining of lungs of indicated genotypes (top; arrows indicate muous-producing goblet cell (PAS staining) and MBP-positive eosinophil). Original magnification: ×400 (PAS) and ×200 (MBP). Quantification of PAS-stained epithelial cells per bronchus or MBP-positive eosinophils in peribronchial area (bottom). (**c**) MBP staining of eyelid and esophagus. Original magnification: ×200 (eyelid) and ×200 (esophagus). Data are representative of six experiments (**a**), two experiments (**b**; mean ± s.d. ($n = 4$ biological replicates) and two experiments (**c**). $^*P < 0.05$, $^{**}P < 0.01$ (two-tailed unpaired Student's *t* test).

$Id2^{fl/fl}Id3^{fl/fl}Foxp3^{Cre}$ and $Id2^{fl/fl}Id3^{fl/fl}Foxp3^{Cre/Cre}$ mice also showed splenomegaly and lymphadenopathy of subcutaneous lymph nodes accompanied by increasing cell numbers, whereas the size of mesenteric lymph nodes (MLNs) was comparable to that of littermate control mice (**Supplementary Fig. 2a**,**b**). As the *Foxp3* locus is located on the X chromosome, half of the T_{reg} cells in heterozygous female mice that carry one copy of $Foxp3^{Cre}$ express normal amounts of *Id2* and *Id3* (ref. 30). We found that heterozygous female $Id2^{fl/fl}Id3^{fl/fl}Foxp3^{Cre/+}$ mice lacked dermatitis across the eyelids, lacked detectable splenomegaly and lymphadenopathy, and had normal percentages of naive $CD4^+$ and $CD8^+$ T cells (**Supplementary Fig. 2c**,**d** and data not shown). Histological analysis of tissue samples from $Id2^{fl/fl}Id3^{fl/fl}Foxp3^{Cre}$ and $Id2^{fl/fl}Id3^{fl/fl}Foxp3^{Cre/Cre}$ mice revealed leukocytic infiltrates in the lung, esophagus and eyelids, with an associated reactive hyperplasia of the adjacent mucosal epithelial cells (**Fig. 2a**). The inflammatory infiltrates in the eyelid were localized to the subepithelial area and there was no inflammation in the lachrymal gland (**Supplementary Fig. 3a**). The inflammatory infiltrates in the lungs were peribronchial and perivascular, accompanied by production of mucus in the bronchial mucosal goblet cells (**Fig. 2b**). Many of the peribronchial and perivascular infiltrates of inflammatory cells in the lungs of $Id2^{fl/fl}Id3^{fl/fl}Foxp3^{Cre}$ and $Id2^{fl/fl}Id3^{fl/fl}Foxp3^{Cre/Cre}$ mice displayed expression of major basic protein (MBP), indicative of eosinophils, accompanied by infiltrating B cells and T cells (**Fig. 2b** and **Supplementary Fig. 3b**). In a similar fashion, inflammatory infiltrates across subepithelial regions of eyelids and the esophagus of $Id2^{fl/fl}Id3^{fl/fl}Foxp3^{Cre}$ as well as $Id2^{fl/fl}Id3^{fl/fl}Foxp3^{Cre/Cre}$ mice were composed primarily of eosinophils (**Fig. 2c**). We also found considerable eosinophilic infiltration in the hilar lymph nodes as well in the pancreas but not across the pancreatic islands (**Supplementary Fig. 3c**,**d**). We did not observe esophagitis in *Foxp3* mutant mice, which indicated that pathologies associated with depletion of *Id2* and *Id3* expression differ from that observed in mice lacking Foxp3 (**Supplementary Fig. 3e**). Notably, the larger bronchioles were filled with denuded epithelial cells and cell debris in dying $Id2^{fl/fl}Id3^{fl/fl}Foxp3^{Cre}$ and $Id2^{fl/fl}Id3^{fl/fl}Foxp3^{Cre/Cre}$ mice (**Supplementary Fig. 3a**).

In a minor fraction of mice (<20%), other organs such as liver, kidney, stomach, pancreas and colon displayed low levels of inflammation (data not shown). Notably, three of five $Id2^{fl/fl}Id3^{fl/fl}Foxp3^{Cre}$ mice that survived beyond 12 weeks of age showed evidence of focal pneumonia, characterized by areas in the lung that were filled with eosinophilic foamy macrophages, and had scarring and increased deposition of collagen surrounding the bronchioles (**Supplementary Fig. 4**). We also observed mild to moderate colitis with an increase in numbers of mucosal MBP-expressing eosinophils (**Supplementary Fig. 4**).

Consistent with the pathology in the lung, we found an increase in the total number of eosinophils and lymphocytes in the bronchial alveolar lavage (BAL) fluid and markedly elevated numbers of eosinophils, neutrophils, T cells and B cells in the lung derived from $Id2^{fl/fl}Id3^{fl/fl}Foxp3^{Cre}$ and $Id2^{fl/fl}Id3^{fl/fl}Foxp3^{Cre/Cre}$ mice (**Fig. 3a**,**b**). The increase in eosinophil cellularity in the lung was closely associated with elevated numbers of type 2 innate lymphoid cells (ILC2) (**Fig. 3b**)[31–33]. In addition, we observed substantially increased numbers of eosinophils, basophils and neutrophils in the lymph nodes and spleen derived from $Id2^{fl/fl}Id3^{fl/fl}Foxp3^{Cre}$ and $Id2^{fl/fl}Id3^{fl/fl}Foxp3^{Cre/Cre}$ mice as compared to littermate control mice (**Fig. 3c**). These observations indicate that the absence of *Id2* and *Id3* expression in T_{reg} cells leads to spontaneous T_H2 cell–mediated fatal airway inflammation in the lungs as well as inflammation of the eyelids, the skin and the esophagus.

Id2 and *Id3* suppress T_H2-mediated inflammation

To determine how depletion of *Id2* and *Id3* expression in T_{reg} cells leads to inflammatory disease, we examined the lymphoid organs. We noticed increased numbers of T cells and B cells in the spleen and subcutaneous LNs, in which we observed lower percentages of $CD62L^{hi}CD44^{lo}$ naive $CD4^+$ and $CD8^+$ T cells as well as a significant increase in the percentages of T_{FH} cells, GC B cells and IgG1 class–switched B cells (**Fig. 4a**,**b** and data not shown). We observed

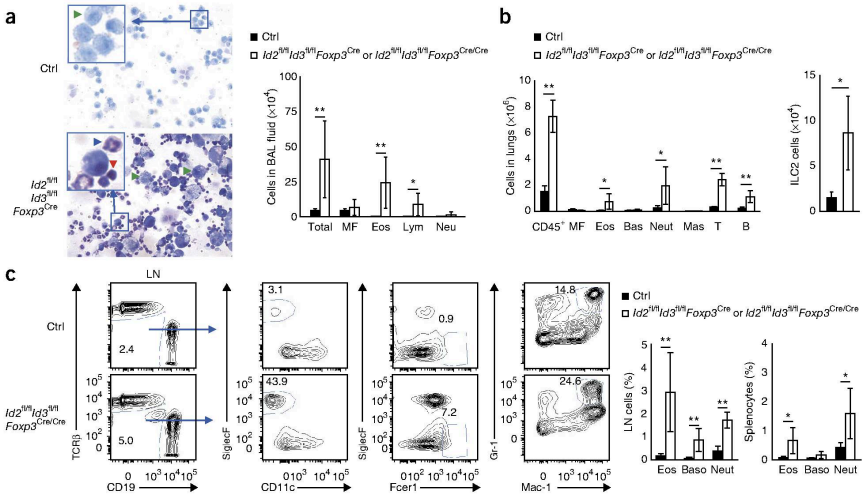

Figure 3 T_H2 cell–mediated inflammation in the lungs of mice depleted for *Id2* and *Id3* expression in T_{reg} cells. (**a**) May-Giemsa staining images of cells (left) and cell numbers (right) in BAL fluid derived from 6–8-week-old control (Ctrl) or $Id2^{fl/fl}Id3^{fl/fl}Foxp3^{Cre}$ mice (left). Green, red and blue arrowheads indicate macrophages (MF), lymphocytes (Lym) and eosinophils (Eos), respectively; Neu, neutrophil. Insets show magnification of boxed areas. Original magnification, ×40 (×120 in insets). (**b**) Numbers of hematopoietic cells (CD45+), macrophages (MF), eosinophils (Eos), basophils (Bas), neutrophils (Neu), mast cells (Mas), T cells (T) and B cells (B) isolated from the left lobes of the lungs derived from $Id2^{fl/fl}Id3^{fl/fl}Foxp3^{Cre}$ mice (left). Numbers of type 2 innate lymphoid cells (ILC2; CD45+Lineage−CD25+IL7R+Sca1^{hi}Thy1.2^{hi}) isolated from the left lobes of the lungs derived from $Id2^{fl/fl}Id3^{fl/fl}Foxp3^{Cre}$ mice (right). (**c**) Flow cytometric analysis of CD19 versus TCRβ expression of cells derived from the LNs isolated from 6–8-week-old control ($Id2^{fl/fl}Id3^{fl/fl}Foxp3^{Cre/+}$) or $Id2^{fl/fl}Id3^{fl/fl}Foxp3^{Cre/Cre}$ mice. Adjacent panels indicate CD11c versus SiglecF, Fcer1 versus SiglecF and Mac-1 versus Gr-1 expression, gated on the TCRβ−CD19− compartment derived from 6–8-week-old control ($Id2^{fl/fl}Id3^{fl/fl}Foxp3^{Cre/+}$) or $Id2^{fl/fl}Id3^{fl/fl}Foxp3^{Cre/Cre}$ lymphocytes isolated from subcutaneous LNs. Numbers in plots indicate percent CD19−TCRβ−, CD11c−SiglecF+, Fcer1+SiglecF− and Mac-1+Gr-1+ cells. Right, percentages of eosinophils (SiglecF+CD11c−), basophils (Baso; Fcer1^{hi}SiglecF−) and neutrophils (Neut; Mac-1^{hi}Gr-1^{hi}) in subcutaneous LN cells and splenocytes. Data are representative of four experiments (**a**,**c**; mean ± s.d.; in **a**, $n = 8$ independent biological replicates; in **b**, control $n = 5$, $Id2^{fl/fl}Id3^{fl/fl}Foxp3^{Cre}$ $n = 4$ independent biological replicates; in **c**, control $n = 6$, $Id2^{fl/fl}Id3^{fl/fl}Foxp3^{Cre}$ $n = 9$ independent biological replicates). $^*P < 0.05$, $^{**}P < 0.01$ (two-tailed unpaired Student's *t* test).

a substantial increase in T_H2 cell–mediated production of cytokines, such as interleukin 4 (IL-4), IL-5 and IL-13 in the lymph nodes and spleen derived from $Id2^{fl/fl}Id3^{fl/fl}Foxp3^{Cre}$ mice (**Fig. 4c**). Consistent with the markedly increased numbers of T_{FH} cells and GC B cells, and the augmented expression of T_H2 cell cytokines, 6–8-week-old $Id2^{fl/fl}Id3^{fl/fl}Foxp3^{Cre}$ mice exhibited a spontaneous increase in IgM, IgG1 and IgE serum concentrations but not in IgG2b, IgG3 and IgA (**Fig. 4d**). Titers of anti-nuclear antibodies in serum isolated from $Id2^{fl/fl}Id3^{fl/fl}Foxp3^{Cre}$ mice, however, were comparable to those in the littermate control (data not shown). These data indicate that expression of *Id2* and *Id3* in T_{reg} cells is required to suppress spontaneous GC development and T_H2 cell–mediated inflammatory disease.

Id2 and *Id3* modulate CXCR5 and Foxp3 expression

The T_{reg} population can be segregated into distinct functional subsets, including effector T_{reg} (eT_{reg}) cells[34]. Previously, low *Id3* expression has been observed in the Blimp-1+ eT_{reg} cell population[35]. Consistent with these observations, we found that a fraction of ICOS+ eT_{reg} cells displayed low *Id3* expression and Id2^{lo}Id3^{lo} T_{reg} cells expressed more CXCR5 (**Fig. 5a**). In line with this, T_{reg} cells that lacked Id2 and Id3 expression exhibited increased expression of CXCR5, PD-1, ICOS, CXCR3, CXCR4 and CTLA-4 but decreased CD62L expression as compared to Id-sufficient T_{reg} cells (**Fig. 5b** and **Supplementary Fig. 5a–c**)[36]. T_{reg} cells derived from healthy heterozygous female $Id2^{fl/fl}Id3^{fl/fl}Foxp3^{Cre/+}$ mice also displayed increased expression of CXCR5 and PD-1, but expression of CXCR3, CXCR4, CD62L and CTLA-4 was comparable to that in wild-type T_{reg} cells (**Fig. 5c,d** and **Supplementary Fig. 5a–c**). $Id2^{fl/fl}Id3^{fl/fl}Foxp3^{Cre}$ mice displayed significantly reduced expression of Foxp3 protein (**Fig. 5e**). We observed this downregulation of Foxp3 even in heterozygous female $Id2^{fl/fl}Id3^{fl/fl}Foxp3^{Cre/+}$ mice, although abundance of *Foxp3* transcript in T_{reg} cells isolated from $Id2^{fl/fl}Id3^{fl/fl}Foxp3^{Cre/+}$ mice did not differ from that for $Id2^{+/+}Id3^{+/+}Foxp3^{Cre/+}$ mice (**Supplementary Fig. 5d,e**). These data indicate that loss of *Id2* and *Id3* expression in T_{reg} cells leads to decreased abundance of Foxp3 and increased proportions of CXCR5+PD-1+ T_{reg} cells.

Recent studies have indicated that T_{reg} cells generated in the thymus (tT_{reg} cells) abundantly express Helios or Neuropilin-1 (Nrp1)[37,38]. We found that the proportions of Helios+ T_{reg} cells were comparable between 4-week-old $Id2^{fl/fl}Id3^{fl/fl}Foxp3^{Cre}$ mice versus control mice but reduced in 8–9-week-old $Id2^{fl/fl}Id3^{fl/fl}Foxp3^{Cre}$ as compared to control mice. These data indicate that *Id2* and *Id3* maintain the Helios+ T_{reg} cell pool (**Fig. 5f**). Recent observations also have indicated a critical role for Nrp1 expression in maintaining stability of T_{reg} cells in inflammatory sites[39]. We found that Nrp1 expression was

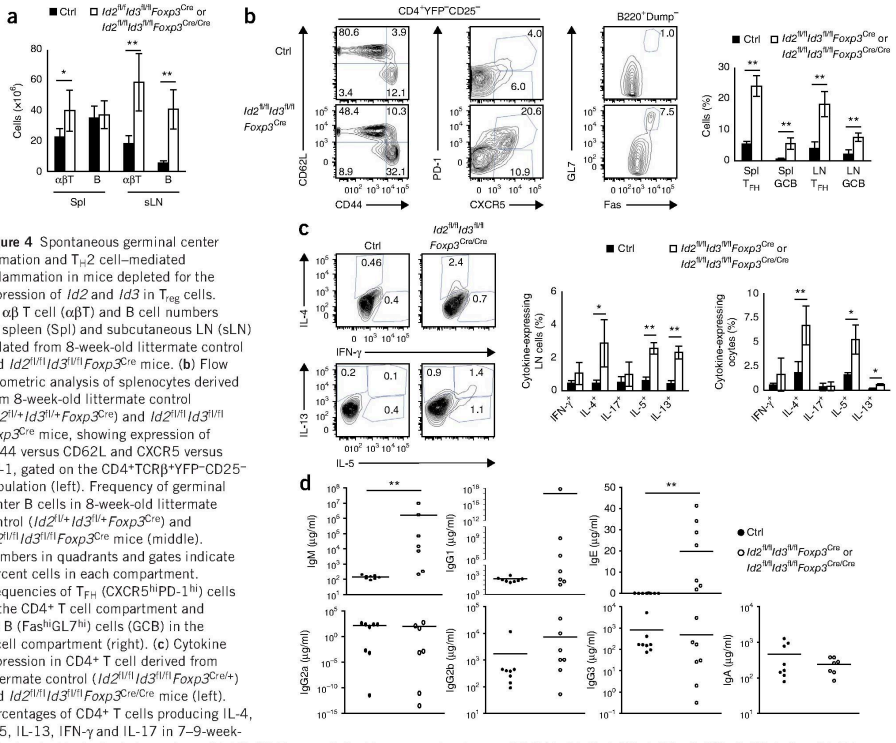

Figure 4 Spontaneous germinal center formation and T_H2 cell–mediated inflammation in mice depleted for the expression of *Id2* and *Id3* in T_{reg} cells. (**a**) αβ T cell (αβT) and B cell numbers for spleen (Spl) and subcutaneous LN (sLN) isolated from 8-week-old littermate control and $Id2^{fl/fl}Id3^{fl/fl}Foxp3^{Cre}$ mice. (**b**) Flow cytometric analysis of splenocytes derived from 8-week-old littermate control ($Id2^{fl/+}Id3^{fl/+}Foxp3^{Cre}$) and $Id2^{fl/fl}Id3^{fl/fl}Foxp3^{Cre}$ mice, showing expression of CD44 versus CD62L and CXCR5 versus PD-1, gated on the $CD4^+TCR\beta^+YFP^-CD25^-$ population (left). Frequency of germinal center B cells in 8-week-old littermate control ($Id2^{fl/+}Id3^{fl/+}Foxp3^{Cre}$) and $Id2^{fl/fl}Id3^{fl/fl}Foxp3^{Cre}$ mice (middle). Numbers in quadrants and gates indicate percent cells in each compartment. Frequencies of T_{FH} ($CXCR5^{hi}PD\text{-}1^{hi}$) cells in the $CD4^+$ T cell compartment and GC B ($Fas^{hi}GL7^{hi}$) cells (GCB) in the B cell compartment (right). (**c**) Cytokine expression in $CD4^+$ T cell derived from littermate control ($Id2^{fl/fl}Id3^{fl/fl}Foxp3^{Cre/+}$) and $Id2^{fl/fl}Id3^{fl/fl}Foxp3^{Cre/Cre}$ mice (left). Percentages of $CD4^+$ T cells producing IL-4, IL-5, IL-13, IFN-γ and IL-17 in 7–9-week-old mice for the indicated genotypes (right). (**d**) Enzyme-linked immunosorbent assay (ELISA) of IgM, IgG1, IgG2a, IgG2b, IgG3, IgA and IgE in serum derived from 6–9-week-old mice for the indicated genotypes. Data are representative of four experiments (**a**; mean ± s.d.; $n = 8$ biological replicates), three independent experiments (**b**; mean ± s.d.; control $n = 4$, $Id2^{fl/fl}Id3^{fl/fl}Foxp3^{Cre}$ $n = 5$ biological replicates), two experiments (**c**; mean ± s.d.; $n = 4$ biological replicates), one experiment (**d**; mean ± s.d.; control $n = 8$, $Id2^{fl/fl}Id3^{fl/fl}Foxp3^{Cre}$ $n = 7$ biological replicates) $^*P < 0.05$, $^{**}P < 0.01$ (two-tailed unpaired Student's *t* test).

substantially reduced in T_{reg} cells derived from $Id2^{fl/fl}Id3^{fl/fl}Foxp3^{Cre}$ mice or $Id2^{fl/fl}Id3^{fl/fl}Foxp3^{Cre/+}$ mice (**Fig. 5f** and **Supplementary Fig. 5f**). These data indicate that the expression of a subset of genes associated with T_{reg} cell function, including CXCR5, PD-1, Foxp3 and Nrp1, are directly affected by loss of *Id2* and *Id3* expression.

Id2 and *Id3* expression affects T_{reg} cell localization

Data described above indicate that loss of *Id2* and *Id3* expression leads to the abnormal proportions of T_{reg} cells that express CXCR5. To explore the possibility that aberrant expression of CXCR5 affects localization and/or homing of T_{reg} cells, we examined the localization of T_{reg} cells in spleens from control or $Id2^{fl/fl}Id3^{fl/fl}Foxp3^{Cre}$ and $Id2^{fl/fl}Id3^{fl/fl}Foxp3^{Cre/Cre}$ mice. Increased numbers of $Foxp3^+$ cells were localized to the B cell area in the spleens derived from $Id2^{fl/fl}Id3^{fl/fl}Foxp3^{Cre}$ mice versus control mice (**Supplementary Fig. 6**). T_{reg} cells depleted for Id2 and Id3 expression also appeared to home more deeply into the B cell follicles across LNs (**Supplementary Fig. 6**). To examine how depletion of Id2 and Id3 expression affects T_{reg} localization across the lung tissues, we analyzed T_{reg} cells derived from 4-week-old and 7–8-week-old $Id2^{fl/fl}Id3^{fl/fl}Foxp3^{Cre}$ mice. Whereas the $Foxp3^+$ pool was not significantly affected in the lungs derived from healthy 4-week-old $Id2^{fl/fl}Id3^{fl/fl}Foxp3^{Cre}$ mice, the percentage of Foxp3 T_{reg} cells localized across the lungs in 7–8-week-old $Id2^{fl/fl}Id3^{fl/fl}Foxp3^{Cre}$ mice was significantly decreased (**Supplementary Fig. 7a**). To compare the abilities of T_{reg} cells deficient for *Id2* and *Id3* expression to home to the lymphoid organs versus lung tissues, we transferred T_{reg} cells isolated from heterozygous female $Id2^{fl/fl}Id3^{fl/fl}Foxp3^{Cre/+}$ mice into wild-type CD45.1 recipient mice. We found that the homing potential of T_{reg} cells depleted for *Id2* and *Id3* expression was reduced in the lung, as compared to the lymph nodes or spleen (**Supplementary Fig. 7b**).

Roles of *Id2* and *Id3* in T_{reg}-mediated immunosuppression

To determine whether the development of fatal T_H2 cell–mediated inflammation upon depletion of *Id2* and *Id3* expression in T_{reg} cells was caused by loss of suppressive functions of T_{reg} cells, we examined the *in vitro* suppressive function of T_{reg} cells sorted from 4-week-old $Id2^{fl/fl}Id3^{fl/fl}Foxp3^{Cre}$ or $Foxp3^{Cre}$ mice. We found that T_{reg} cells

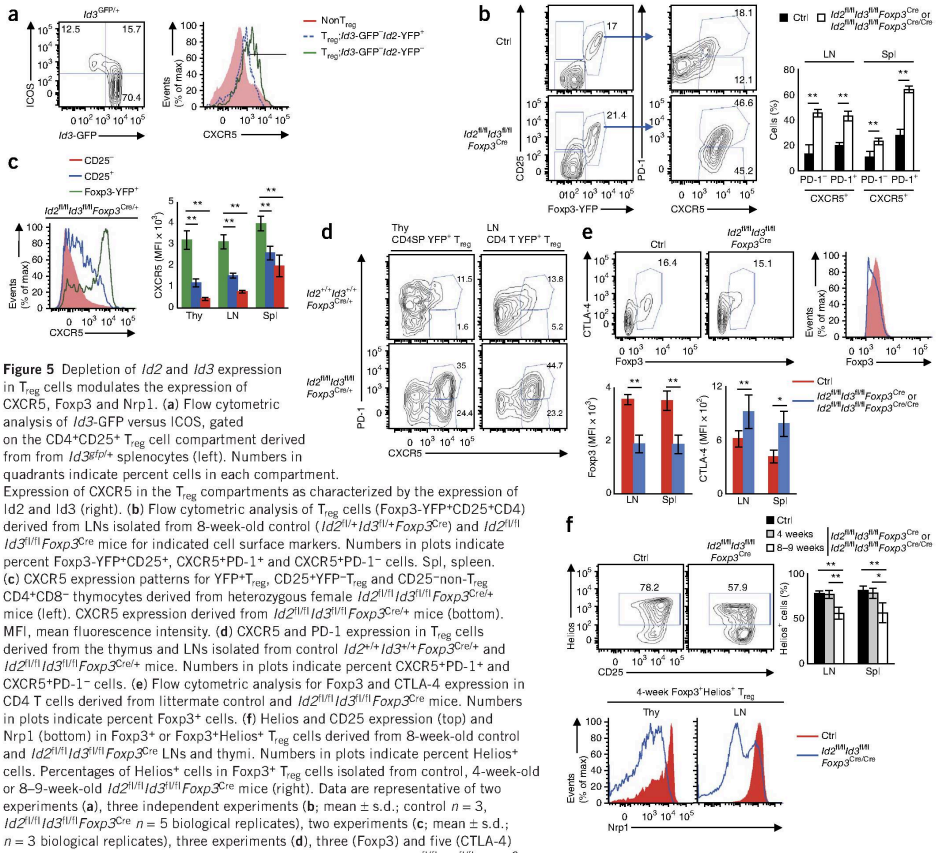

Figure 5 Depletion of *Id2* and *Id3* expression in T_{reg} cells modulates the expression of CXCR5, Foxp3 and Nrp1. (**a**) Flow cytometric analysis of *Id3*-GFP versus ICOS, gated on the CD4$^+$CD25$^+$ T_{reg} cell compartment derived from from *Id3*$^{gfp/+}$ splenocytes (left). Numbers in quadrants indicate percent cells in each compartment. Expression of CXCR5 in the T_{reg} compartments as characterized by the expression of Id2 and Id3 (right). (**b**) Flow cytometric analysis of T_{reg} cells (Foxp3-YFP$^+$CD25$^+$CD4) derived from LNs isolated from 8-week-old control (*Id2*$^{fl/+}$*Id3*$^{fl/+}$*Foxp3*^{Cre}) and *Id2*$^{fl/fl}$ *Id3*$^{fl/fl}$*Foxp3*^{Cre} mice for indicated cell surface markers. Numbers in plots indicate percent Foxp3-YFP$^+$CD25$^+$, CXCR5$^+$PD-1$^+$ and CXCR5$^+$PD-1$^-$ cells. Spl, spleen. (**c**) CXCR5 expression patterns for YFP$^+$$T_{reg}$, CD25$^+YFP^-$$T_{reg}$ and CD25$^-$non-T_{reg} CD4$^+$CD8$^-$ thymocytes derived from heterozygous female *Id2*$^{fl/fl}$*Id3*$^{fl/fl}$*Foxp3*$^{Cre/+}$ mice (left). CXCR5 expression derived from *Id2*$^{fl/fl}$*Id3*$^{fl/fl}$*Foxp3*$^{Cre/+}$ mice (bottom). MFI, mean fluorescence intensity. (**d**) CXCR5 and PD-1 expression in T_{reg} cells derived from the thymus and LNs isolated from control *Id2*$^{+/+}$*Id3*$^{+/+}$*Foxp3*$^{Cre/+}$ and *Id2*$^{fl/fl}$*Id3*$^{fl/fl}$*Foxp3*$^{Cre/+}$ mice. Numbers in plots indicate percent CXCR5$^+$PD-1$^+$ and CXCR5$^+$PD-1$^-$ cells. (**e**) Flow cytometric analysis for Foxp3 and CTLA-4 expression in CD4 T cells derived from littermate control and *Id2*$^{fl/fl}$*Id3*$^{fl/fl}$*Foxp3*^{Cre} mice. Numbers in plots indicate percent Foxp3$^+$ cells. (**f**) Helios and CD25 expression (top) and Nrp1 (bottom) in Foxp3$^+$ or Foxp3$^+$Helios$^+$ T_{reg} cells derived from 8-week-old control and *Id2*$^{fl/fl}$*Id3*$^{fl/fl}$*Foxp3*^{Cre} LNs and thymi. Numbers in plots indicate percent Helios$^+$ cells. Percentages of Helios$^+$ cells in Foxp3$^+$ T_{reg} cells isolated from control, 4-week-old or 8–9-week-old *Id2*$^{fl/fl}$*Id3*$^{fl/fl}$*Foxp3*^{Cre} mice (right). Data are representative of two experiments (**a**), three independent experiments (**b**; mean ± s.d.; control $n = 3$, *Id2*$^{fl/fl}$*Id3*$^{fl/fl}$*Foxp3*^{Cre} $n = 5$ biological replicates), two experiments (**c**; mean ± s.d.; $n = 3$ biological replicates), three experiments (**d**), three (Foxp3) and five (CTLA-4) experiments (**e**; mean ± s.d.; Foxp3 $n = 3$, CTLA-4 control $n = 7$, *Id2*$^{fl/fl}$*Id3*$^{fl/fl}$*Foxp3*^{Cre} $n = 9$ biological replicates), and three experiments (**f**; mean ± s.d.; $n = 4$ biological replicates). $^*P < 0.05$, $^{**}P < 0.01$ (two-tailed unpaired Student's *t* test).

depleted for *Id2* and *Id3* expression displayed normal *in vitro* immunosuppressive function (**Supplementary Fig. 8**).

To examine whether T_{reg} cells depleted for *Id2* and *Id3* expression have the ability to suppress T cell–mediated inflammation *in vivo*, we injected sorted CD4$^+$CD25$^-$CD45RB^{hi} T cells (T_{conv} cells) derived from CD45.1 mice into *Rag1*$^{-/-}$ recipient mice with or without purified T_{reg} cells isolated from 4-week-old *Id2*$^{fl/fl}$*Id3*$^{fl/fl}$*Foxp3*^{Cre} or *Foxp3*^{Cre} mice (**Fig. 6a**). As expected, *Rag1*$^{-/-}$ recipient mice transferred with T_{conv} cells alone showed severe colitis accompanied by body-weight loss (**Fig. 6a**,**b**). Cotransfer of T_{reg} cells isolated from *Id2*$^{fl/fl}$*Id3*$^{fl/fl}$*Foxp3*^{Cre} mice resulted in partially impaired suppressive activity (**Fig. 6a**,**b**). As expected, we found a large fraction of CD45.1$^-$Foxp3$^+$ T_{reg} cells in the MLNs of recipient mice but fewer Id-deficient T_{reg} cells in the MLNs of recipient mice (**Fig. 6c**). These findings are consistent with the notion that expression of *Id2* and *Id3* is required to maintain the T_{reg} pool. Overall these data indicate that T_{reg} cells depleted for *Id2* and *Id3* expression have the ability to suppress, albeit partially, T cell–mediated inflammation in a transfer colitis model.

Id2 and *Id3* maintain T_{reg} cell homeostatic potential

To assess directly the roles of *Id2* and *Id3* under noninflammatory conditions, we analyzed heterozygous female *Id2*$^{fl/fl}$*Id3*$^{fl/fl}$*Foxp3*$^{Cre/+}$ mice carrying the IRES-YFP reporter as described above. As inactivation of the X chromosome can occur on either allele, 50% of the T_{reg} cells in heterozygous female *Foxp3*$^{Cre\text{-}YFP/+}$ mice expressed the *Foxp3*$^{Cre\text{-}YFP}$ marker, whereas the rest of the T_{reg} cell population lacked expression of *Foxp3*$^{Cre\text{-}YFP}$. This setting allows for a direct functional comparison of T_{reg} cells that are deficient for *Id2* and *Id3* expression versus wild-type cells under noninflammatory conditions. In the thymi derived from female *Id2*$^{fl/fl}$*Id3*$^{fl/fl}$*Foxp3*$^{Cre/+}$ mice, the YFP$^+$/CD25$^+$ ratio of the CD4$^+$ T cell population was comparable to that of *Id2*$^{+/+}$*Id3*$^{+/+}$ *Foxp3*$^{Cre/+}$ mice, whereas the YFP$^+$/CD25$^+$ ratio in the spleen and LNs

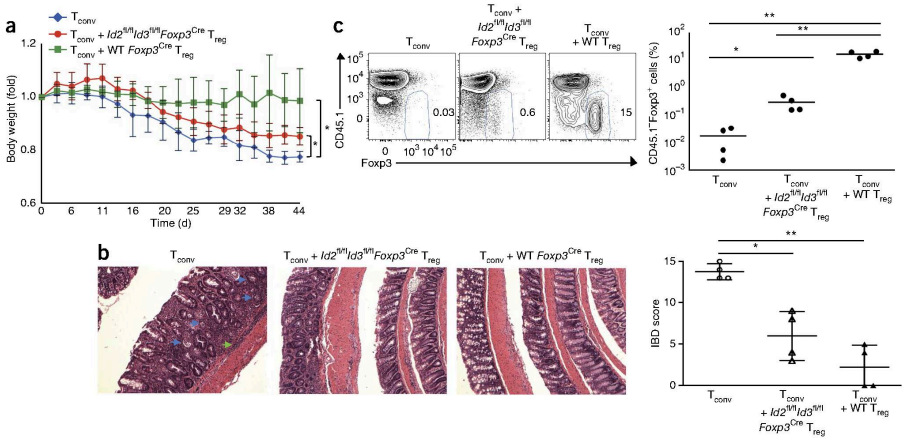

Figure 6 Impaired homeostasis of T_{reg} cells deleted for *Id2* and *Id3* expression after transfer into *Rag1*$^{-/-}$ mice. (**a**) Body weight in indicated populations of mice after CD4$^+$CD25$^-$CD45RB^{hi} T cell (T_{conv}) from CD45.1 mice were intravenously injected into *Rag1*$^{-/-}$ recipient mice with or without CD4$^+$CD25$^+$Foxp3-YFP$^+$ T cell (T_{reg}) from 4-week-old *Id2*$^{fl/fl}$*Id3*$^{fl/fl}$*Foxp3*^{Cre} or wild-type *Foxp3*^{Cre} mice (CD45.2) ($n = 4$ each group). WT, wild type. (**b**) H&E staining of large intestine (left). Blue and green arrowheads indicate crypt abscess and infiltration of inflammatory cells in the submucosal muscle layer, respectively. IBD score[50] in large intestine on day 44 after transfer (right). Original magnification, ×100 (**c**) Flow cytometric analysis of Foxp3 and CD45.1 expression gated on CD4$^+$TCRβ$^+$ cells in mesenteric LNs (left) and analysis of CD45.1$^-$Foxp3$^+$ cells (right). Data are representative of one experiment (**a**–**c**; error bars, s.d.; $n = 4$ independent biological replicates). $^*P < 0.05$, $^{**}P < 0.01$ (two-tailed unpaired Student's *t* test).

was substantially reduced (**Fig. 7a**). Similarly, the fraction of YFP$^+$ cells as compared to the proportion of Foxp3$^+$ cells was substantially lower in spleen and LNs, indicating that the Id-sufficient Foxp3$^+$ population outcompeted the Id-deficient population (**Fig. 7a**). We did not detect obvious differences in CD25, Annexin-V or Ki67 expression in *Id2*- and *Id3*-deficient YFP$^+$ T_{reg} cells derived from *Id2*$^{fl/fl}$*Id3*$^{fl/fl}$*Foxp3*$^{Cre/+}$ versus *Foxp3*$^{Cre/+}$ mice (data not shown). Notably, we found that when cultured in the presence of anti-CD3 and anti-CD28, the fraction of T_{reg} cells depleted for *Id2* and *Id3* expression (YFP$^+$ cells) among Foxp3$^+$ populations declined progressively over time and was accompanied by elevated numbers of apoptotic cells and decreased numbers of Ki67$^+$ cells at 24 h (**Fig. 7b**). These observations indicate that in the absence of *Id2* and *Id3*, T_{reg} cells are more susceptible to cell death upon TCR stimulation. Collectively, these data indicate that *Id2* and *Id3* expression is required to maintain the peripheral T_{reg} cell pool.

Id2 and *Id3* regulate T_{FR} cell–specific transcription signatures

As a first approach to identify critical target genes affected by the depletion of *Id2* and *Id3* in T_{reg} cells, we isolated by cell sorting YFP$^+$ T_{reg} cells from subcutaneous LNs derived from 3-week-old *Id2*$^{fl/fl}$*Id3*$^{fl/fl}$*Foxp3*^{Cre} or *Id2*$^{fl/+}$*Id3*$^{fl/+}$*Foxp3*^{Cre} mice. 792 genes were differentially expressed (greater than twofold; fragments per kilobase of exons per million fragments mapped; FPKM) in YFP$^+$ T_{reg} cells derived from *Id2*$^{fl/fl}$*Id3*$^{fl/fl}$*Foxp3*^{Cre} mice when compared to those in *Id2*$^{fl/+}$*Id3*$^{fl/+}$*Foxp3*^{Cre} mice (**Fig. 8a**). Hierarchical clustering showed that a large fraction of transcripts that were differentially expressed were associated with genes encoding for metabolic process, transcription, T cell lymphocyte activation, cytokine/chemokine inflammation, cell cycle and cell death by Gene Ontology (GO) analysis (**Supplementary Fig. 9**). Prominent among the putative targets were *Cxcr5, Ikzf3, Cebpa, Hif1a, Pparg, Il10, Il10ra, Ccr2, Nrp1* and *Ccr6* (**Fig. 8a**–**c** and **Supplementary Fig. 10a**). However, expression of genes encoding transcriptional regulators, such as *Tbx21, Irf4, Gata3, Stat3, Prdm1* and *Sh2d1a*, was not affected (data not shown). Similarly, cytokine genes including *Il2, Il4, Il5, Il13, Ifng, Il17* and *Il21* were not modulated upon depletion of *Id2* and *Id3* expression in the T_{reg} cell pool (data not shown). Similar to the case in T_{FR} cells, we found elevated expression of *Gzma*, *Il10* and *Ctla4*. On the other hand, expression of *Bcl6* and *Prdm1* was not altered[15] (**Fig. 8a**,**b** and **Supplementary Fig. 10a**).

To identify target genes directly affected by depletion of *Id2* and *Id3* expression rather than genes affected by inflammatory disease, we isolated RNA from YFP$^+$ T_{reg} cells from heterozygous female *Id2*$^{fl/fl}$*Id3*$^{fl/fl}$*Foxp3*$^{Cre/+}$ and *Id2*$^{+/+}$*Id3*$^{+/+}$*Foxp3*$^{Cre/+}$ mice and examined it by real-time PCR. We found that ablation of *Id2* and *Id3* expression in the T_{reg} cell pool in healthy mice affected *Cxcr5, Ikzf3, Hif1a, Myb, Apoe, Il10, Il10ra, Ccr2, E2f2, Nrp1* and *Il18r1* transcript abundance (**Fig. 8c**). In contrast, *Ikzf4, Ccr6, Cebpa, Pparg1* and *S1pr1* transcript abundance was not altered in T_{reg} cells depleted of *Id2* and *Id3* (data not shown). To determine whether the differences in transcript abundance directly relate to transcription factor occupancy across putative enhancer elements, we inspected previous genome-wide studies for E2A occupancy as well as deposition of monomethylation of histone H3K4 (H3K4me1) in CD4$^-$CD8$^-$double-negative (DN3) thymocytes, pro-B cells and T cell lymphomas[26,40]. Notably, E2A-bound sites were closely associated with putative enhancer regions across the *Cxcr5, IL10, Hif1a, Ikzf3, Myb, Il10ra, Nrp1, E2f2* and *Bmp7* loci, which indicated that this ensemble of loci is directly regulated by E proteins (**Fig. 8d** and **Supplementary Fig. 10b**). These data indicate that a subset of genes associated with T_{FR} cells, including *Il10* and *Cxcr5*, but not *Bcl6* and *Prdm1*, are directly regulated by the expression of *Id2* and *Id3* in T_{reg} cells to orchestrate the developmental progression of the T_{FR} cell population (**Supplementary Fig. 10c**).

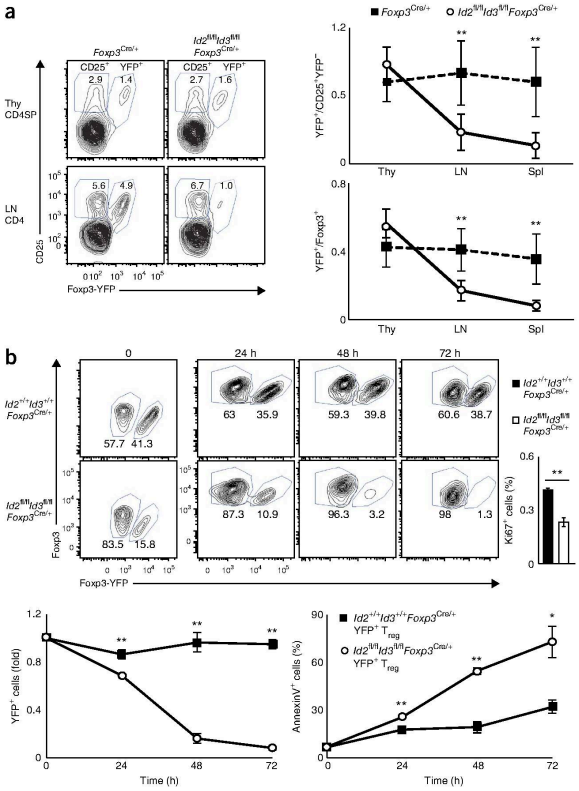

Figure 7 Id2 and Id3 modulate the homeostasis and survival of T_{reg} cells. (**a**) Flow cytometric analysis for YFP and CD25 expression on cells isolated from thymocytes (Thy) and LNs (LN) derived from *Id2*$^{+/+}$*Id3*$^{+/+}$*Foxp3*$^{Cre/+}$ or *Id2*$^{fl/fl}$*Id3*$^{fl/fl}$*Foxp3*$^{Cre/+}$ mice (left; cells were gated on the CD4$^+$CD8$^-$TCRβ^{hi}, CD4$^+$CD8$^-$ or CD4$^+$ populations). Numbers in plots indicate percent YFP$^+$CD25$^+$ and YFP$^-$CD25$^+$ cells. Ratios of YFP$^+$ T_{reg} cells versus CD25$^+$YFP$^-$ T_{reg} cells and YFP$^+$Foxp3$^+$ T_{reg} versus Foxp3$^+$ T_{reg} cells in indicated tissues (right). (**b**) Flow cytometric analysis of the Foxp3$^+$CD4$^+$ population in splenocytes derived from heterozygous female *Id2*$^{+/+}$*Id3*$^{+/+}$*Foxp3*$^{Cre/+}$ or *Id2*$^{fl/fl}$*Id3*$^{fl/fl}$*Foxp3*$^{Cre/+}$ mice cultured and stimulated with anti-CD3ε plus anti-CD28 antibodies in the presence of human IL-2 (top left). Numbers indicate the fraction of YFP$^+$Foxp3$^+$ and YFP$^-$Foxp3$^+$ cells. Percentages of Ki67$^+$ cells in the YFP$^+$ T_{reg} cell populations analyzed 24 h after stimulation for the indicated genotypes (top right). Ratios of YFP$^+$ cells for the indicated time points as compared to the zero time point (bottom left). Percentages of annexin-V$^+$ cells gated on the YFP$^+$ T_{reg} cell population (right). Data are representative of three independent experiments (**a**; mean ± s.d.; *Id2*$^{+/+}$*Id3*$^{+/+}$*Foxp3*$^{cre/+}$ $n = 5$, *Id2*$^{fl/fl}$*Id3*$^{fl/fl}$*Foxp3*$^{cre/+}$ $n = 7$ biological replicates) and one experiment (**b**; mean ± s.d.; $n = 3$ technical replicates). $^*P < 0.05$, $^{**}P < 0.01$ (two-tailed unpaired Student's *t* test).

DISCUSSION

Here we demonstrated that expression of the antagonist HLH proteins, Id2 and Id3, in T_{reg} cells is required for suppression of early onset inflammation at mucosal barriers. How does depletion of Id2 and Id3 expression in T_{reg} cells lead to the development of severe inflammation? Our data indicate that expression of Id2 and Id3 is essential to maintain the T_{reg} cell population. In 3–4-week-old mice that lacked expression of Id2 and Id3, we observed T_{reg} cells in near wild-type numbers. However, in 7–8-week-old mice, the T_{reg} cell population depleted for expression of Id2 and Id3 was severely reduced across the lung tissues. Homing of T_{reg} cells to the lung in transfer experiments was also compromised in the absence of *Id2* and *Id3* expression. Finally, we found that activated T_{reg} cells depleted for expression of *Id2* and *Id3* displayed decreased viability and impaired proliferation upon stimulation. Collectively, these data indicate that Id2 and Id3 coordinate the survival, expansion and homing of T_{reg} cells under inflammatory conditions.

In addition to the roles of Id2 and Id3 in suppressing T_H2 cell–mediated inflammation, our observations also point to a role for Id2 and Id3 in T_{FR} cell development. How may Id2 and Id3 regulate T_{FR} differentiation? We suggest that *Id2* and *Id3* expression enforces distinct T_{FR} checkpoints. Upon TCR-mediated signaling, *Id2* and *Id3* levels readily decline permitting increased E-protein binding activity and the induction of a T_{FR}-specific transcription signature, including the activation of Cxcr5 and IL-10 expression. We propose that abundance of Id2 and/or Id3 is elevated and required again in differentiating T_{FR} cells to indirectly modulate Bcl-6 and Blimp-1 protein abundance, which ultimately leads to the development of a mature T_{FR} cell population.

There are interesting parallels between the roles of E and Id proteins in development of T_{FR} cells and T_{FH} cells. Differentiation of T_{FH} cells is characterized by distinct developmental stages. First, upon activation, effector T_{FH} cells induce the expression of CXCR5 to migrate to the border that separates the T cell areas from the B cell follicles. Followed by ICOS-ICOSL interaction with B cells, T_{FH} cells continue to differentiate, acquire Bcl-6 expression and migrate to GCs[41,42]. Two critical factors control the early developmental progression of naive CD4$^+$ T cells toward the effector T_{FH} cell type: *Id3* and a heterodimeric complex involving the basic HLH protein Ascl2 and E proteins to activate the expression of CXCR5 and other critical target genes[26,43,44]. Based on these observations, we suggest that a common genetic circuitry that involves the E-Id protein module controls the homing of both T_{FR} cells and T_{FH} cells.

In sum, higher *Id2* and *Id3* expression enforces the early T_{FR} cell checkpoint, whereas at intermediate developmental stages the abundance of E protein versus Id protein controls developmental progression toward a fully mature T_{FR} cell fate. We note this property of Id proteins and E proteins is not unique to T_{reg} cells. Previous studies have demonstrated critical roles for E and Id proteins acting as

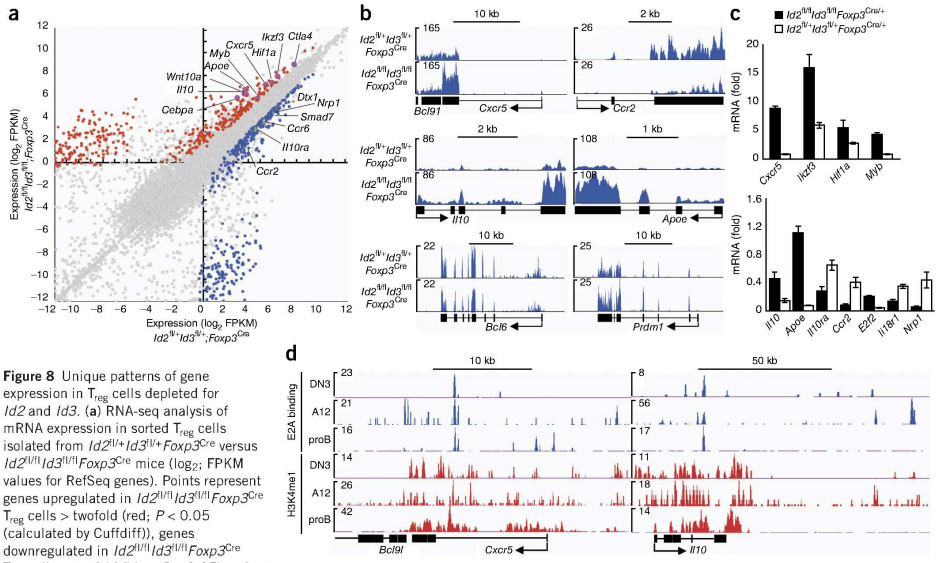

Figure 8 Unique patterns of gene expression in T_{reg} cells depleted for *Id2* and *Id3*. (**a**) RNA-seq analysis of mRNA expression in sorted T_{reg} cells isolated from $Id2^{fl/+}Id3^{fl/+}Foxp3^{Cre}$ versus $Id2^{fl/fl}Id3^{fl/fl}Foxp3^{Cre}$ mice (log_2; FPKM values for RefSeq genes). Points represent genes upregulated in $Id2^{fl/fl}Id3^{fl/fl}Foxp3^{Cre}$ T_{reg} cells > twofold (red; $P < 0.05$ (calculated by Cuffdiff)), genes downregulated in $Id2^{fl/fl}Id3^{fl/fl}Foxp3^{Cre}$ T_{reg} cells > twofold (blue; $P < 0.05$) and not significantly changed (gray) as compared to control cells. Selected genes are labeled. (**b**) RNA-seq analysis at *Cxcr5*, *Ccr2*, *Il10*, *Apoe*, *Bcl6* and *Prdm1* loci, presented in reads per million reads aligned (RPM). Arrows indicate transcription start site and direction of transcription. (**c**) Quantitative real-time PCR analysis of genes in sorted Foxp3-YFP+ T_{reg} cells derived from LNs isolated from heterozygous female $Id2^{+/+}Id3^{+/+}Foxp3^{Cre/+}$ or $Id2^{fl/fl}Id3^{fl/fl}Foxp3^{Cre/+}$ mice, presented normalized by the abundance of *Hprt1* transcript. (**d**) E2A occupancy (E2A binding) and deposition of H3K4me1 across the *Cxcr5* and *Il10* loci in DN3, A12 and proB cells. Numbers in plots indicate total tags observed. DN3 cells; $Rag2^{-/-}$ thymocytes, A12 cells; $E2a^{-/-}$ E47-reconstituted T cell line, pro-B cells; $Rag2^{-/-}$ bone marrow B cells. Arrows indicate transcriptional start site and direction of transcription. Data are representative of three experiments (**a**,**b**), one experiment (**c**; mean ± s.d.; $n = 3$ technical replicates) and one experiment (**d**).

gatekeepers at the pre-TCR, TCR and B cell antigen receptor checkpoints[21,23,45–47]. During the developmental progression of the $CD8^+$ and T_{FH} cell lineages, the Id proteins also control key developmental transitions[27,48,49]. Each of these checkpoints involves the regulation of Id protein expression by antigen receptor–mediated signaling. Thus, a picture is now emerging in which antigen receptors directly connect to the E protein and Id protein machinery to orchestrate the developmental transitions of cells that comprise the adaptive immune system under healthy as well as inflammatory conditions.

METHODS

Methods and any associated references are available in the online version of the paper.

Accession codes. Gene Expression Ominibus: GSE57682.

Note: Any Supplementary Information and Source Data files are available in the online version of the paper.

ACKNOWLEDGMENTS

We thank A. Bortnick for critical reading of the manuscript, S. Kuan, B. Lin and Z. Ye for help with Illumina DNA sequencing, B. Ren for access to the Illumina Hi-Seq instrumentation, A. Goldrath (University of California San Diego) for *Id2*-YFP mice, Y. Zhuang for $Id3^{fl/fl}$ mice (Duke University), A. Lasorella (Columbia University) for $Id2^{fl/fl}$ mice, Y. Zheng (Salk Institute) for Foxp3-deficient organs, C. Katayama, M. Suzukawa, L. Deng, P. Rosenthal, T. Katakai, A. Beppu and A. Coddington for technical advice, J. Lee (Mayo Clinic) for providing the MBP antibodies, and members of the University of California, San Diego Histology Core for performing histology. This work was supported by US National Institutes of Health (AI 38425, AI 70535 and AI 7211 to D.H.B. and CA054198, CA78384 and 1P01AI102853 to C.M.).

AUTHOR CONTRIBUTIONS

M.Miy., K.M. and S.C. performed the majority of experiments. K.M. performed RNA-seq analysis. M.I. performed immunostaining of spleen and lymph nodes. N.V. contributed to the analysis of pathology. M.Mil. contributed to the analysis of lung tissue. L.-F.L. suggested key experiments and edited the manuscript. A.N.C. analyzed RNA-seq data. M.Miy. and C.M. wrote the manuscript. D.H.B. and C.M. supervised the study.

COMPETING FINANCIAL INTERESTS

The authors declare no competing financial interests.

1. Josefowicz, S.Z., Lu, L.F. & Rudensky, A.Y. Regulatory T cells: mechanisms of differentiation and function. *Annu. Rev. Immunol.* **30**, 531–564 (2012).
2. Sakaguchi, S., Yamaguchi, T., Nomura, T. & Ono, M. Regulatory T cells and immune tolerance. *Cell* **133**, 775–787 (2008).
3. Vignali, D.A.A., Collison, L.W. & Workman, C.J. How regulatory T cells work. *Nat. Rev. Immunol.* **8**, 523–532 (2008).
4. Locksley, R.M. Asthma and allergic inflammation. *Cell* **140**, 777–783 (2010).
5. Rothenberg, M.E. & Hogan, S.P. The eosinophil. *Annu. Rev. Immunol.* **24**, 147–174 (2006).
6. Sakaguchi, S. *et al.* Immunologic self-tolerance maintained by activated T cells expressing Il2-receptor alpha-chains (CD25). Breakdown of a single mechanism of self-tolerance causes various autoimmune diseases. *J. Immunol.* **155**, 1151–1164 (1995).

7. Bennett, C.L. *et al.* The immune dysregulation, polyendocrinopahty, X-linked syndrome (IPEX) is caused by mutations of Foxp3. *Nat. Genet.* **27**, 20–21 (2001).
8. Wildin, R.S. *et al.* X-linked neonatal diabetes, emteropathy and endocrinopathy syndrome is the human equivalent of mouse scurfy. *Nat. Genet.* **27**, 18–20 (2001).
9. Hori, S., Nomura, T. & Sakaguchi, S. Control of regulatory T cell development by the transcription factor Foxp3. *Science* **299**, 1057–1061 (2003).
10. Fontenot, J.D., Gavin, M.A. & Rudensky, A.Y. Foxp3 programs the development and function of CD4+CD25+ regulatory T cells. *Nat. Immunol.* **4**, 330–336 (2003).
11. Khattri, R., Cox, T., Yasayko, S.A. & Ramsdell, F. An essential role for Scurfin in CD4+CD25+ T regulatory cells. *Nat. Immunol.* **4**, 337–342 (2003).
12. Josefowicz, S.Z. *et al.* Extratymically generated regulatory T cells control mucosal Th2 inflammation. *Nature* **482**, 395–399 (2012).
13. Wing, J.B. & Sakaguchi, S. Foxp3+ T_{reg} cells in humoral immunity. *Int. Immunol.* **26**, 61–69 (2014).
14. Chung, Y. *et al.* Follicular regulatory T cells expressing Foxp3 and Bcl-6 suppress germinal center reactions. *Nat. Med.* **17**, 983–988 (2011).
15. Linterman, M.A. *et al.* Foxp3 follicular regulatory T cells control the germinal center response. *Nat. Med.* **17**, 975–982 (2011).
16. Sage, P.T., Francisco, L.M., Carman, C.V. & Sharpe, A.H. The receptor PD-1 controls follicular regulatory T cells in the lymph nodes and blood. *Nat. Immunol.* **14**, 152–161 (2013).
17. Murre, C. Helix-loop-helix proteins and lymphocyte development. *Nat. Immunol.* **6**, 1079–1086 (2005).
18. Murre, C., McCaw, P.S. & Baltimore, D. A new DNA binding and dimerization motif. *Cell* **56**, 777–783 (1989).
19. Benezra, R., Davis, R.L., Lockshon, D., Turner, D.L. & Weintraub, H. The protein Id: A negative regulator of helix-loop-helix DNA binding proteins. *Cell* **61**, 49–59 (1990).
20. Yokota, Y. *et al.* Development of peripheral lymphoid organs and natural killer cells depends on the helix-loop-helix protein Id2. *Nature* **397**, 702–706 (1999).
21. Rivera, R.R., Johns, C.P., Quan, J., Johnson, R.S. & Murre, C. Thymocyte selection is regulated by the helix-loop-helix inhibitor protein, Id3. *Immunity* **12**, 17–26 (2000).
22. Verykokakis, M., Boos, M.D., Bendelac, A. & Kee, B.L. SAP protein-dependent natural killer T-like cells regulate the development of CD8(+) T cells with innate lymphocyte characteristics. *Immunity* **33**, 203–215 (2010).
23. Jones-Mason, M.E. *et al.* E protein transcription factors are required for the development of CD4(+) lineage T cells. *Immunity* **36**, 348–361 (2012).
24. Li, H., Dai, M. & Zhuang, Y.A. T cell intrinsic role of Id3 in a mouse model for primary Sjogren's syndrome. *Immunity* **21**, 551–560 (2004).
25. Maruyama, T. *et al.* Control of the differentiation of regulatory T cells and T_H17 cells by the DNA-binding inhibitor Id3. *Nat. Immunol.* **12**, 86–95 (2011).
26. Miyazaki, M. *et al.* The opposing roles of the transcription factor E2A and its antagonist Id3 that orchestrate and enforce the naive fate of T cells. *Nat. Immunol.* **12**, 992–1001 (2011).
27. Yang, C.Y. *et al.* The transcriptional regulators Id2 and Id3 control the formation of distinct memory CD8+ T cell subsets. *Nat. Immunol.* **12**, 1221–1229 (2011).
28. Niola, F. *et al.* Id proteins synchronize stemness and anchorage to the niche of neural stem cells. *Nat. Cell Biol.* **14**, 477–487 (2012).
29. Rubtsov, Y.P. *et al.* Regulatory T cell-derived interleukin-10 limits inflammation at environmental interfaces. *Immunity* **28**, 546–558 (2008).
30. Liston, A., Lu, L.F., O'Carroll, D., Tarakhovsky, A. & Rudensky, A.Y. Dicer-dependent microRNA pathway safeguards regulatory T cell function. *J. Exp. Med.* **205**, 1993–2004 (2008).
31. Nussbaum, J.C. *et al.* Type 2 Innate lymphoid cells control eosinophil homeostasis. *Nature* **502**, 245–248 (2013).
32. Monticelli, L.A., Sonnenberg, G.F. & Artis, D. Innate lymphoid cells: critical regulators of allergic inflammation and tissue repair in the lung. *Curr. Opin. Immunol.* **24**, 284–289 (2012).
33. Chang, Y.J. *et al.* Innate lymphoid cells mediate influenza-induced airway hyper-reactivity independently of adaptive immunity. *Nat. Immunol.* **12**, 631–638 (2011).
34. Cretney, E., Kallies, A. & Nutt, S.L. Differentiation and function of Foxp3+ effector regulatory T cells. *Trends Immunol.* **34**, 74–80 (2013).
35. Cretney, E. *et al.* The transcription factors, Blimp-1 and IRF4 jointly control the differentiation and function of effector regulatory T cells. *Nat. Immunol.* **12**, 304–311 (2011).
36. Smigiel, K.S. *et al.* CCR7 provides localized access to IL-2 and defines homeostatically distinct regulatory T cell subsets. *J. Exp. Med.* **211**, 121–136 (2014).
37. Thornton, A.M. *et al.* Expression of Helios, an Ikaros transcription factor family member, differentiates thymic-derived from peripherally induced Foxp3+ T regulatory cells. *J. Immunol.* **184**, 3433–3441 (2010).
38. Weiss, J.M. *et al.* Neuropilin 1 is expressed on thymus-derived natural regulatory T cells, but not mucosa-generated induced Foxp3+ Treg cells. *J. Exp. Med.* **209**, 1723–1742 (2012).
39. Delgoffe, G.M. *et al.* Stability of regulatory T cells is maintained by a neuropilin-1-semaphorin-4a axis. *Nature* **501**, 252–256 (2013).
40. Lin, Y.C. *et al.* A global network of transcription factors, involving E2A, EBF1, and Foxo1, that orchestrates B cell fate. *Nat. Immunol.* **11**, 635–643 (2010).
41. Xu, H. *et al.* Follicular T-helper cell recruitment governed by bystanding B cells and ICOS-driven motility. *Nature* **496**, 523–527 (2013).
42. Choi, Y.S. *et al.* ICOS receptor instructs T follicular helper cell versus effector cell differentiation via induction of the transcriptional repressor Bcl6. *Immunity* **34**, 932–946 (2011).
43. Liu, X. *et al.* Transcription factor achaete-scute homologue 2 initiates follicular T-helper-cell development. *Nature* **507**, 513–518 (2014).
44. Murre, C. *et al.* Interactions between heterologous helix-loop-helix proteins generate complexes that bind specifically to a common DNA sequence. *Cell* **58**, 537–544 (1989).
45. Bain, G. *et al.* Thymocyte maturation is regulated by the activity of the helix-loop-helix protein, E47. *J. Exp. Med.* **190**, 1605–1616 (1999).
46. Engel, I., Johns, C., Bain, G., Rivera, R.R. & Murre, C. Early thymocyte development is regulated by modulation of E2A protein activity. *J. Exp. Med.* **194**, 733–745 (2001).
47. Quong, M. *et al.* Receptor editing and marginal zone B cell development are regulated by the helix-loop-helix protein, E2A. *J. Exp. Med.* **199**, 1101–1112 (2004).
48. Masson, F. *et al.* Id2-mediated inhibition of E2A represses memory CD8+ T cell differentiation. *J. Immunol.* **190**, 4585–4594 (2013).
49. Knell, J. *et al.* Id2 influences differentiation of killer cell lectin-like receptor G1(hi) short-lived CD8+ effector T cells. *J. Immunol.* **190**, 1501–1509 (2013).
50. Burich, A. *et al. Helicobacter*-induced inflammatory bowel disease in IL-10- and T cell-deficient mice. *Am. J. Physiol. Gastrointest. Liver Physiol.* **281**, G764–G778 (2001).

ONLINE METHODS

Mice. C57BL/6, *Id3*$^{fl/fl}$, Id2$^{fl/fl}$ *Id3*$^{-/-}$, *Foxp3*$^{Cre\text{-}YFP}$ and *Id3*$^{GEP/+}$ *Id2*$^{YFP/+}$ mice were bred and housed in specific pathogen–free conditions in accordance with the Institutional Animal Care and Use Guidelines of the University of California, San Diego.

Flow cytometry. Single-cell suspensions from thymus, lymph nodes and spleen were stained with the following: FITC-, PE-, APC-, APC-Cy7–, Pacific Blue-, Alexa Fluor 700–, Alexa Fluor 780–, PerCP-Cy5.5-, PE-Cy7– or biotin-labeled monoclonal antibodies were purchased from BD PharMingen including CD11c (HL3), CD44 (IM7), CXCR5 (2G8), CD95 (Jo-2), GL-7 (GL7), SiglecF (E50-2440), IL-5 (TRFK5). CD8 (53-6.7), CD19 (ID3), CD38 (90), CD62L (MEL-14), CD44 (IM7), B220 (RA3-6B2), Mac1 (M1/70), Gr1 (RB6-8C5), Nk1.1 (PK136), Ter119 (TER119), TCRβ (H57), TCRγδ (GL3), PD-1 (J43), ICOS (7E.17G9), CXCR4 (2B11), IL-4 (11B11), IL-13 (eBio13A), IL-17 (eBio17B7), IFN-γ (XMG1.2), FOXP3 (FJK-16s) and TBR2 (Dan11mag) were purchased from eBioscience. FcεR1 (MAR-1), CD3ε (2C11), CD4 (GK1.5), CD8 (53-6.7), CD11b (M1/70), CD25 (PC61), CD122 (TMb1), CTLA4 (UC10-4B9), CCR6 (29-2L17), Helios (22F6) and PD-1 (RMP1-30) were obtained from BioLegend. Anti-Nrp1 (AF566) was purchased from R&D Systems. Biotinylated antibodies were labeled with streptavidin-conjugated Qdot-665 or Qdot-605 (Invitrogen). Clone 2.4 G2 anti-CD32:CD16 (eBioscience) was used to block Fc receptors. Dead cells were removed from analysis and sorting by staining with propidium iodide (PI) (Sigma-Aldrich). Isolation of lung single cells was performed as described[51]. Mouse T_{reg} cell staining kit (eBioscience) was used for intracellular Foxp3, CTLA4 and Helios staining. Samples were collected on a LSRII (BD Biosciences) and were analyzed with FlowJo software (Tree Star). Cells were sorted on a FACSAria (BD). For intracellular staining of IFN-γ, IL-4, IL-5, IL-13 and IL-17, isolated cells from spleen and lymph nodes were treated with phorbol 12-myristate 13-acetate (PMA) plus ionomycin (4 h) and Golgi stop (2 h). After culture, cells were stained with anti-CD4, CD8, TCRβ and CD3ε. Intracellular staining was performed with the BD Biosciences Cytofix/Cytopermkit.

RNA sequencing. Total RNA was isolated using the RNeasy-Mini Kit (Qiagen) and was processed for deep sequencing as described previously with slight modifications. Briefly, mRNA was purified from total RNA using Dynabeads mRNA purification kit (Invitrogen). The mRNA was then subjected to first-strand cDNA synthesis using a combination of random hexamers and oligo(dT). Second-strand synthesis was performed using dUTP instead of dTTP. The double-stranded cDNA was sonicated using S220 Focused-ultrasonicator (Covaris). Sonicated cDNA was next ligated to adaptors and size-selected. The size-selected cDNA was treated with uracil-N-glycosylase and then multiplex-amplified by PCR. cDNA libraries were sequenced with a HiSeq 2000 sequencer (Illumina). Sequence reads from each cDNA library were analyzed with Galaxy (http://galaxyproject.org/). They were mapped to mouse genome build NCBI37 mm9 using TopHat. The expression values were obtained using Cufflink and Cuffdiff. GO analyses were performed using Homer (http://homer.salk.edu/homer/index.html). Visualization files were generated using Homer and read pile-ups visualized using the University of California Santa Cruz Genome Browser.

Histology and immunostaining. Tissues were fixed in 4% paraformaldehyde (Electron Microscopy Sciences). Fixed tissues were embedded in paraffin and sliced, followed by hematoxylin and eosin (H&E) staining, periodic acid Schiff (PAS) staining and MBP staining. For MBP immunostaining, we used a monoclonal antibody directed against MBP[51]. For quantification of MBP$^+$ or PAS$^+$ cells, we chose five bronchioles and count positive cells in one mouse. For Foxp3 staining, spleen and lymph nodes were embedded in optimal cutting temperature (OCT) compound and snap-frozen. 5-μm serial sections were stained with anti-CD45R (B220; supernatant isolated from the medium of cultured hybridomas) or anti-Foxp3 (FJK-16s). Secondary antibody used was donkey anti-rat IgG Alexa Fluor 488 (Molecular Probes). The images were captured by Olympus Provis AX80 microscopy. The digital images were acquired using RETIGA EXi (Nippon Rooper). Image process was done by Photoshop (Adobe). IBD scores were calculated as described[50].

Enzyme-linked immunosorbent assay. Serum IgM, IgG1, IgG2a, IgG2b, IgG3 and IgA were done as described[52]. For IgE, ELISA was performed using Mouse IgE Standard Set Module (BioLegend).

RNA isolation and reverse transcriptase PCR. First, cDNA was obtained from purified YFP$^+$ or CD25$^+$ T_{reg} cells from *Id2*$^{+/+}$*Id3*$^{+/+}$*Foxp3*$^{Cre/+}$ or *Id2*$^{fl/fl}$*Id3*$^{fl/fl}$*Foxp3*$^{Cre/+}$ mice. Total RNA was isolated from sorted cells with RNeasy kit (Quagen), followed by reverse transcription with the SuperScript III RT-PCR system (Invitrogen) and quantitative real-time reverse transcription (RT)-PCR.

***In vitro* and *in vivo* suppression and *in vitro* stimulation.** For *in vitro* suppression assay, YFP$^+$ T_{reg} cells and responder CD4$^+$CD25$^-$ T cells were purified by sorting. 2×10^4 Responder CD4$^+$ T cells were cocultured with T_{reg} cells at indicated ratios and were stimulated with soluble anti-CD3 antibody (1 μg/ml) in the presence of T cell–depleted splenocytes treated with mitomycin C (1×10^5) in 96-well plates for 72 h. Cells were pulsed with [^{3}H]thymidine deoxyribose (1 μCi/well) for the last 12 h. *In vivo* suppression assay was performed as described[53]. For *in vitro* stimulation, total lymphocytes were cultured *in vitro* and stimulated with anti-CD3ε (0.5 μg/ml) plus anti-CD28 (1 μg/ml) antibodies in the presence of human IL-2 (100 U/ml) as described[30].

Statistical analysis. *P* values were calculated with the two-tailed Student's *t*-test for two-group comparison as applicable with Microsoft Excel software. The statistical significance level was 0.05.

51. Suzukawa, M. *et al.* Sialyltransferase ST3Gal-III regulates SiglecF ligand formation and eosinophilic lung inflammation in mice. *J. Immunol.* **190**, 5939–5948 (2013).
52. Smith, K.G.C. *et al.* bcl-2 transgene expression Inhibits apoptosis in the germinal center and reveals differences in the selection of memory B cells and bone marrow antibody-forming cells. *J. Exp. Med.* **191**, 475–484 (2000).
53. Miyazaki, K. *et al.* The role of the basic helix-loop-helix transcription factor Dec1 in the regulatory T cells. *J. Immunol.* **185**, 7330–7339 (2010).

This chapter, in full, is a reprint of the material as it appears in *Nature Immunology* (2014). Miyazaki M, Miyazaki K, Chen S, Itoi M, Miller M, Lu LF, Varki N, Chang AN, Broide DH, Murre C. *Id2 and Id3 maintain the regulatory T cell pool to suppress inflammatory disease.* Shuwen Chen is one of the primary authors.

Chapter III:

The E-Id protein axis modulates the activities of the PI3K-AKT-mTORC1-Hif1a and c-myc/p19Arf pathways to suppress innate variant TFH cell development, thymocyte expansion, and lymphomagenesis

The E–Id protein axis modulates the activities of the PI3K–AKT–mTORC1–Hif1a and c-myc/p19Arf pathways to suppress innate variant T_{FH} cell development, thymocyte expansion, and lymphomagenesis

Masaki Miyazaki,[1,8] Kazuko Miyazaki,[1,8] Shuwen Chen,[1] Vivek Chandra,[1] Keisuke Wagatsuma,[2] Yasutoshi Agata,[2] Hans-Reimer Rodewald,[3] Rintaro Saito,[4] Aaron N. Chang,[5] Nissi Varki,[6] Hiroshi Kawamoto,[7] and Cornelis Murre[1]

[1]Department of Molecular Biology, University of California at San Diego, La Jolla, California 92093, USA; [2]Department of Biochemistry and Molecular Biology, Shiga University of Medical School, Shiga 520-2192, Japan; [3]Division of Cellular Immunology, German Cancer Research Center, D-69120 Heidelberg, Germany; [4]Department of Medicine, University of California at San Diego, La Jolla, California 92093, USA; [5]Center for Computational Biology, Institute for Genomic Medicine, University of California at San Diego, La Jolla, California 92093, USA; [6]Department of Pathology, University of California at San Diego, La Jolla, California 92093, USA; [7]Department of Immunology, Institute for Frontier Medical Sciences, Kyoto University, Kyoto 606-8507, Japan

It is now well established that the E and Id protein axis regulates multiple steps in lymphocyte development. However, it remains unknown how E and Id proteins mechanistically enforce and maintain the naïve T-cell fate. Here we show that Id2 and Id3 suppressed the development and expansion of innate variant follicular helper T (T_{FH}) cells. Innate variant T_{FH} cells required major histocompatibility complex (MHC) class I-like signaling and were associated with germinal center B cells. We found that Id2 and Id3 induced *Foxo1* and *Foxp1* expression to antagonize the activation of a T_{FH} transcription signature. We show that Id2 and Id3 acted upstream of the Hif1a/Foxo/AKT/mTORC1 pathway as well as the c-myc/p19Arf module to control cellular expansion. We found that mice depleted for *Id2* and *Id3* expression developed colitis and αβ T-cell lymphomas. Lymphomas depleted for *Id2* and *Id3* expression displayed elevated levels of *c-myc*, whereas *p19Arf* abundance declined. Transcription signatures of *Id2*- and *Id3*-depleted lymphomas revealed similarities to genetic deficiencies associated with Burkitt lymphoma. We propose that, in response to antigen receptor and/or cytokine signaling, the E–Id protein axis modulates the activities of the PI3K–AKT–mTORC1–Hif1a and c-myc/p19Arf pathways to control cellular expansion and homeostatic proliferation.

[*Keywords*: Id proteins; T-cell quiescence; T-cell lymphoma,; tumor suppressor; FOXO/mTORC1 pathway; c-Myc/p19Arf]

Supplemental material is available for this article.

Received November 4, 2014; revised version accepted January 8, 2015.

The differentiation of T-lineage cells is initiated in the thymus. Soon after arriving in the thymus, T-cell progenitors initiate TCRβ locus rearrangement, undergo limited expansion, and initiate a T-lineage-specific program of gene expression. This developmental stage is characterized by the lack of expression of the coreceptors CD4 and CD8 and is commonly referred to as the double-negative (DN) stage. Once a functional TCRβ chain has been generated and the pre-TCR is assembled and expressed, DN cells undergo rapid expansion and give

[8]**These authors contributed equally to this work.**
Corresponding author: murre@biomail.ucsd.edu
Article is online at http://www.genesdev.org/cgi/doi/10.1101/gad.255331.114. Freely available online through the *Genes & Development* Open Access option.

rise to $CD4^+CD8^+$ double-positive (DP) cells (Carpenter and Bosselut 2010). Upon reaching the DP compartment, thymocytes exit the cell cycle, initiate TCRα locus rearrangement, and undergo positive and negative selection (Singer et al. 2008; Kreslavsky et al. 2010). The lymphoid populations can be segregated into adaptive or innate immune cells. The selection process permits the developmental progression of a selected group of adaptive T-lineage cells that have acquired a TCR with moderate affinity for major histocompatibility complex (MHC) class II (CD4 single positive [CD4SP]) or class I (CD8SP) associated with self-antigens (Klein et al. 2014). On the other hand, innate T-lineage cells are selected by CD1 for invariant natural killer T (iNKT) cells and by MHC-related protein MR1 for mucosal-associated invariant T lymphocytes (MAIT) (Bendelac et al. 2007; Gold and Lewinsohn 2013)

Adaptive B and T cells express an enormously diverse antigen receptor repertoire. They maintain a naïve lymphoid cell state until they encounter invading pathogens, upon which they expand and differentiate into effector cells. Innate lymphoid cells (ILCs) carry germline-encoded receptors or express a limited antigen receptor repertoire and have the potential to rapidly induce cytokine expression (Cerutti et al. 2013; Verykokakis et al. 2014). The innate lymphoid system is comprised of multiple cell types, including natural killer (NK), lymphoid tissue inducer (LTi), type 2 ILCs, and innate-like B and T cells (Diefenbach et al. 2014). The innate-like B- and T-cell compartment consists of marginal zone B cells, iNKT cells, MAIT cells, and subsets of γδ T cells. ILCs act primarily by modulating the activities of adaptive immune cells.

It is now established that a large majority of developmental trajectories in the thymus involve regulation by members of the helix–loop–helix (HLH) family (Rothenberg 2014). These include E proteins as well as Id proteins. Four E proteins have been identified and characterized. They include E12, E47, HEB, and E2-2. E12 and E47 are encoded by the E2A locus and are generated by differential splicing. E protein DNA-binding activity is regulated by the Id gene products, named Id1–4. Id proteins contain an HLH dimerization domain but lack the basic DNA-binding region. They function predominantly by antagonizing the DNA-binding activities of E proteins (Benezra et al. 1990; Lazorchak et al. 2005; Miyazaki et al. 2014).

E protein levels are abundant in T-cell progenitors, where they activate TCRβ V(D)J locus rearrangement and induce the expression of genes encoding for members of the Notch and pre-TCR signaling cascade (Ikawa et al. 2006; Agata et al. 2007). E47 expression declines in resting DP cells and decreases further upon maturating beyond the TCR checkpoint (Engel et al. 2001; Miyazaki et al. 2011). High E2A expression prevents developmental progression, whereas decreasing E2A and HEB levels promote positive selection (Rivera et al. 2000; Jones and Zhuang 2007). HEB acts in the DP compartment to promote the development of NKT cells (D'Cruz et al. 2010). The traversal of these checkpoints in response to pre-TCR, γδ TCR, and αβ TCR signals is facilitated by the induction of Id3 expression. Beyond the pre-TCR, γδ TCR, and αβ TCR checkpoints, Id3 expression is required to maintain the naïve state (Verykokakis et al. 2010, 2014; Miyazaki et al. 2011; Li et al. 2013). The combined activities of Id2 and Id3 are required to promote efficient developmental progression of CD8SP cells (Jones-Mason et al. 2012).

Here we examined how Id2 and Id3 act mechanistically beyond the TCR checkpoint to orchestrate T-cell fate. We found that the activation of *Id3* and *Id2* expression in DP cells is sequential and that Id2 and Id3 suppressed the development and expansion of innate variant follicular helper T (T_{FH})-like cells acting in turn to promote the ectopic development of germinal center (GC) B cells. The innate T_{FH}-like cells carried a highly restricted antigen receptor repertoire indicative of a self-renewing population. We identified a genetic network involving the Id–E protein, AKT–FOXO–mTOR, and Myc–p19Arf modules, which orchestrate a self-renewal-specific program of gene expression. Finally, mice depleted for *Id2* and *Id3* in T cells developed colitis as well as T-cell lymphoma. Collectively, these data point to a regulatory circuitry that underpins the mechanism by which Id2 and Id3 act to antagonize an innate variant T_{FH}-specific program of gene expression, maintain thymocyte quiescence, and suppress the development of lymphoma.

Results

Expression patterns of Id2 and Id3 in positively selected thymocytes

Previous studies have demonstrated that *Id3* expression is induced at the pre-TCR checkpoint and further elevated during the positive selection process, whereas *Id2* expression is low in positively selected DP cells but elevated in CD4SP or CD8SP cells (Bain et al. 2001; Engel et al. 2001; Miyazaki et al. 2011; Jones-Mason et al. 2012). To examine in greater detail how *Id2* and *Id3* expression is regulated during positive selection, we used *Id2*-YFP and *Id3*-GFP reporter mice (Yang et al. 2011a). Positively selected cells, identified as $CD5^+CD69^-$ or $CD69^+TCR\beta^-$ DP cells, expressed higher levels of *Id3* but did not display significant levels of *Id2*-YFP (Fig. 1A). *Id2* expression was only detectable in $TCR\beta^+$ DP cells (Fig. 1A). The majority of mature $CD62L^+$ CD4SP or CD8SP cells displayed abundant levels of *Id2* and *Id3* expression (Fig. 1A). Collectively, these data indicate that the induction of *Id2* and *Id3* expression during positive selection is sequential: *Id3* expression is activated by TCR signaling in positively selected cells, whereas *Id2* expression is induced at a later stage by a separate pathway, which remains to be revealed.

Development of T_{FH}-like cells and GC formation in primary and peripheral lymphoid organs derived from $Id2^{fl/fl}Id3^{fl/fl}IL7R^{Cre}$ mice

Previous studies have demonstrated key roles of E and Id proteins in enforcing and modulating the pre-TCR and TCR checkpoints (Bain et al. 1999; Engel et al. 2001; D'Cruz et al. 2010; Miyazaki et al. 2011; Jones-Mason

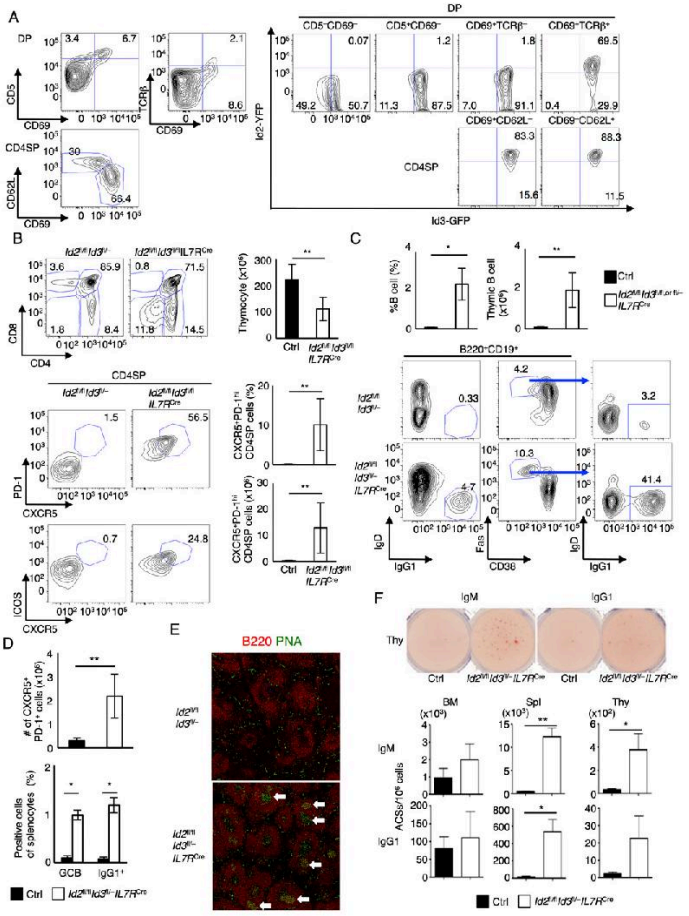

Figure 1. Development of CXCR5$^+$PD-1$^+$ αβ T cells and IgG1 class-switched B cells in thymi derived from *Id2*$^{fl/fl}$*Id3*$^{fl/fl}$*IL7R*^{Cre} mice. (*A*) Flow cytometric analysis of CD69 versus CD5 expression and CD69 versus TCRβ expression gated on CD4$^+$CD8$^+$ DP cells (*top left*); CD69 versus CD62L expression gated on CD4SP (CD4$^+$CD8$^-$TCRβ$^+$) cells (*bottom left*); and GFP versus YFP expression gated on CD5$^-$CD69$^-$, CD5$^+$CD69$^-$, CD69$^+$TCRβ$^-$, CD69$^+$TCRβ$^+$ (DP), and CD69$^+$CD62L$^-$ and CD69$^-$CD62L$^+$ (CD4SP) cells (*right*). Numbers in quadrants indicate percentages of cells in each compartment. Data are representative of two independent experiments. (*B*, *top left*) Flow cytometric analysis of CD4 versus CD8 expression in total thymocytes derived from 5-wk-old *Id2*$^{fl/fl}$*Id3*$^{fl/fl}$*IL7R*^{Cre} and *Id2*$^{fl/fl}$*Id3*$^{fl/-}$ control mice. (*Top right*) The graph shows the number of total thymocytes of 5-wk-old *Id2*$^{fl/fl}$*Id3*$^{fl/fl}$*IL7R*^{Cre} and *Id2*$^{fl/fl}$*Id3*$^{fl/-}$ control mice. The *bottom* panels show the expression of CXCR5 and PD-1 (*middle*) and CXCR5 and ICOS (*bottom*) gated on CD4SP (CD4$^+$CD8$^-$TCRβ$^+$) cells. The absolute number and frequency of gated cells are shown in adjacent panels. Numbers in plots refer to CXCR5$^+$PD-1$^-$ and CXCR5$^+$ICOS$^+$ cells. Data represent the mean ± SD from two independent experiments analyzing four 5-wk-old mice. (*C*) The *top* graphs show the percentage and absolute number of B cells (B220$^+$CD19$^+$) in thymi derived from 5-wk-old *Id2*$^{fl/fl}$*Id3*$^{fl/fl}$*IL7R*^{Cre} and littermate control mice. Flow cytometric analysis of IgG1 versus IgD expression and CD38 versus Fas expression gated on the B220$^+$CD19$^+$ population. The *bottom right* panel shows IgG1 and IgD expression gated on the CD38$^-$Fas^{hi} cells. Data represent the mean ± SD from two independent experiments analyzing four 5-wk-old mice. (*D*) The absolute number of CXCR5$^+$PD-1$^+$ CD4T cells and frequency of GC (Fas$^+$GL7$^+$) B cells and IgG1 class-switched (IgG1$^+$IgD$^-$) B cells in spleens derived from 5-wk-old *Id2*$^{fl/fl}$*Id3*$^{fl/fl}$*IL7R*^{Cre} mice. Data represent the mean ± SD from two independent experiments analyzing four 5-wk-old mice. (*E*) Representative immunofluorescence staining with anti-B220 antibody and PNA in spleens derived from 5-wk-old *Id2*$^{fl/fl}$*Id3*$^{fl/fl}$*IL7R*^{Cre} mice. Arrows indicate PNA$^+$ GCs. (*F*) Representative ELISPOT wells using thymocytes (*top*) and the frequency of IgM- or IgG1-secreting cells in bone marrow (BM), spleen (Spl), and thymus (Thy) derived from 6-mo-old *Id2*$^{fl/fl}$*Id3*$^{fl/fl}$*IL7R*^{Cre} and littermate control mice (*middle* and *bottom*) are shown. (*E*) Data are representative of two independent experiments with three mice each. (*) $P < 0.05$; (**) $P < 0.01$ (Student's *t*-test).

et al. 2012). To evaluate the roles of Id2 and Id3 throughout thymocyte development, we used $Id2^{fl/fl}Id3^{fl/fl}IL7R^{Cre}$ mice to ablate Id2 and Id3 expression in common lymphoid progenitors (CLPs) (Schlenner et al. 2010; Jones-Mason et al. 2012; Niola et al. 2012). Consistent with previous observations, the CD8SP compartment was virtually absent in $Id2^{fl/fl}Id3^{fl/fl}IL7R^{Cre}$ mice (Fig. 1B; Jones-Mason et al. 2012). Additionally, $Id2^{fl/fl}Id3^{fl/fl}IL7R^{Cre}$ mice displayed an increase in the total number of DN cells that expressed TCRβ (Supplemental Fig. 1A). Since a previous study showed aberrant development of T_{FH}-like cells in thymi derived from *Id3*-null mutant mice, we examined $Id2^{fl/fl}Id3^{fl/fl}IL7R^{Cre}$ mice for CXCR5, PD-1, and ICOS expression (Miyazaki et al. 2011). We found that a large fraction of CD4SP and DN TCRβ$^+$ as well as iNKT cells expressed CXCR5, PD-1, and ICOS in thymi derived from 5-wk-old $Id2^{fl/fl}Id3^{fl/fl}IL7R^{Cre}$ mice (Fig. 1B; Supplemental Fig. 1A,B). CXCR5$^+$PD-1$^+$ T_{FH}-like cells were detectable in $Id3^{-/-}$, $Id3^{fl/-}CD4^{Cre}$, and $Id3^{fl/fl}IL7R^{Cre}$ mice but not in $Id2^{fl/fl}IL7R^{Cre}$ mice (Supplemental Fig. 1C,D). The T_{FH}-like populations were accompanied by increased numbers of B220$^+$CD19$^+$ thymic B cells, $Fas^{hi}CD38^-$ GC B cells, and IgG1 class-switched cells (Fig. 1C). We found that the segregation of cortical and medullary regions was completely abolished, and B220$^+$ cells were observed throughout the thymi derived from 5-wk-old $Id2^{fl/fl}Id3^{fl/fl}IL7R^{Cre}$ mice (Supplemental Fig. 1E). In addition, we noted spontaneous GCs in the spleens derived from $Id2^{fl/fl}Id3^{fl/fl}IL7R^{Cre}$ mice, accompanied by fewer naïve CD4 T cells and an increased number of T_{FH} cells (Fig. 1D,E; Supplemental Fig. 2A,B). The elevated number of T_{FH} cells was associated with the development of GC B cells, IgG1 class-switched B cells, plasma blasts, and plasma cells (Fig. 1D; Supplemental Fig. 2C). Furthermore, substantial numbers of IgM- and IgG1-secreting cells were detected in thymi and spleens, but not in the bone marrow, derived from 4- to 6-mo-old $Id2^{fl/fl}Id3^{fl/fl}IL7R^{Cre}$ mice (Fig. 1F). Taken together, these data indicate that *Id2* and *Id3* suppress the development and/or selection of T_{FH}-like cells and GC B cells in primary and peripheral lymphoid organs.

Development of innate T_{FH}-like cells in $Id2^{fl/fl}Id3^{fl/fl}IL7R^{Cre}$ mice

To examine in greater detail the phenotypes associated with the development of T_{FH}-like cells, CD4SP cells were analyzed for the expression of markers associated with maturation and migration. In line with previous studies, we found that TCRβ^{hi} DP and CD4SP thymocytes displayed aberrant CCR7, CXCR4, CD62L, and CD69 expression in $Id2^{fl/fl}Id3^{fl/fl}IL7R^{Cre}$ mice (Fig. 2A; Jones-Mason et al. 2012). The level of CD44 expression displayed by $Id2^{fl/fl}Id3^{fl/fl}IL7R^{Cre}$ CD4SP thymocytes was distinct from that observed for splenic CD4$^+$ T cells, suggesting that the CD4SP cells in the thymus were not derived from recirculating CD4$^+$ T cells (Fig. 2B). Previous studies have demonstrated that a fraction of CD4SP cells derived from $Id3^{-/-}$ thymi aberrantly expressed PLZF or Eomes (Verykokakis et al. 2010, 2013; Miyazaki et al. 2011; Li et al. 2013; D'Cruz et al. 2014). The fraction of thymocytes expressing PLZF was increased in the thymi and spleens derived from $Id2^{fl/fl}Id3^{fl/fl}IL7R^{Cre}$ mice, while Eomes expressors were mostly lacking (Fig. 2C). Since PLZF is the transcription factor that is expressed in innate T cells such as iNKT cells, we examined whether the innate T_{FH}-like population was distinct from that of iNKT cells. We found that only a small fraction of CXCR5$^+$ CD4SP cells represented iNKT cells and that the majority of CXCR5$^+$ CD4SP cells expressed PLZF (Fig. 2D,E). Furthermore, we found significantly increased numbers of IL-4- but not IFN-γ-producing CD4SP cells (Fig. 2F). Taken together, these data indicate that depletion of *Id2* and *Id3* expression at an early developmental stage results in the development of an innate T_{FH}-like population in the thymus.

Rapidly expanding innate T_{FH}-like cells in $Id2^{fl/fl}Id3^{fl/fl}IL7R^{Cre}$ mice

To obtain further insight into the mechanism that underpins the roles of Id2 and Id3 in thymocyte development, $Id2^{fl/fl}Id3^{fl/fl}IL7R^{Cre}$ thymi were examined for abnormalities upon aging. We found that at 2 wk after birth, thymi derived from $Id2^{fl/fl}Id3^{fl/fl}IL7R^{Cre}$ mice displayed a complete block in positive selection, with a pronounced defect during the CD69$^+$TCRβ$^-$-to-CD69$^+$TCRβ^{hi} transition (Fig. 3A). For comparison, we analyzed DP cells derived from $TCR\alpha^{-/-}$ mice for CD5 or CD69 expression. We found that DP cells derived from $TCR\alpha^{-/-}$ thymi did not display either CD69 or CD5 expression (Supplemental Fig. 3A). These data suggest that DP thymocytes that have received a TCR signal required Id2 and Id3 expression to fully differentiate into the TCRβ^{hi} stage. However, unlike the complete block in positive selection observed in 2-wk-old mice, we found that in adult (4- to 8-wk-old) mice, CD4SP cells in $Id2^{fl/fl}Id3^{fl/fl}IL7R^{Cre}$ mice readily were detectable and continued to expand (Fig. 3B, top; Supplemental Fig. 3B). A significant fraction of the expanding CD4SP populations displayed CXCR5 and PD-1 expression (Fig. 3B, bottom; Supplemental Fig. 3B). The expanding CD4SP population showed relatively high levels of Ki67 expression and BrdU incorporation, whereas proliferating cells in the control CD4SP compartment were barely detectable (Fig. 3C,D). Likewise, DN TCRβ$^+$ cells derived from $Id2^{fl/fl}Id3^{fl/fl}IL7R^{Cre}$ mice displayed a substantial increase in the fraction of BrdU$^+$ cells (Supplemental Fig. 3C). Annexin V expression was not affected in these populations (Supplemental Fig. 3D). We also observed a substantial increase in cell size across the CD4SP but not in the DP compartment in $Id2^{fl/fl}Id3^{fl/fl}IL7R^{Cre}$ thymocytes (Fig. 3E). Over time, the majority of thymocytes expressed CXCR5 and PD-1 associated with large cell size (Supplemental Fig. 3E). Sections of thymi derived from 6-mo-old $Id2^{fl/fl}Id3^{fl/fl}IL7R^{Cre}$ mice showed effacement of the cortico–medullary junction due to proliferation of neoplastic cells with large, hyperchromatic, irregular nuclei and scant cytoplasm (Fig. 3F).

To determine whether the expanding population was derived from a small fraction of selected thymocytes, the

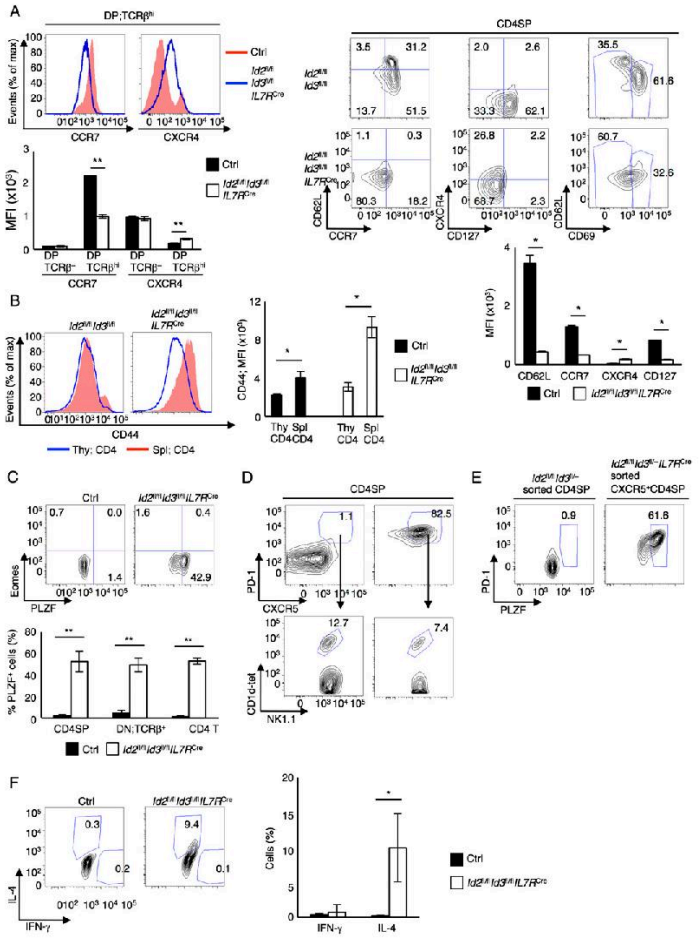

Figure 2. Id2 and Id3 suppress the development of PLZF-expressing non-iNKT αβ T cells. (*A*, *left*) Flow cytometric analysis of CCR7 and CXCR4 gated on TCRβ$^+$ DP cells derived from 6-wk-old *Id2*$^{fl/fl}$*Id3*$^{fl/fl}$*IL7R*^{Cre} and littermate control mice. (*Bottom left*) The graph shows CCR7 and CXCR4 expression in CD69$^-$TCRβ$^-$ and TCRβ$^+$ DP cells presented as mean fluorescence intensity (MFI). Flow cytometric analysis of CCR7 versus CD62L, CD127 versus CXCR4, and CD69 versus CD62L gated on CD4SP cells derived from 6-wk-old *Id2*$^{fl/fl}$*Id3*$^{fl/fl}$*IL7R*^{Cre} and littermate control mice. Numbers adjacent to the outlined areas or in quadrants indicate the percentage of cells in the population that was examined. (*Bottom right*) The graph shows the CD62L, CCR7, CXCR4, and CD127 expression in CD4SP cells, presented as MFI. Data are representative of one experiment with 6-wk-old mice (mean ± SD; $n = 3$). (*B*) Flow cytometric analysis of CD44 expression in CD4SP thymocytes (blue) and splenic CD4 T cells (red) derived from 6- to 8-wk-old *Id2*$^{fl/fl}$*Id3*$^{fl/fl}$*IL7R*^{Cre} and *Id2*$^{fl/fl}$*Id3*$^{fl/fl}$ control mice. The *right* panel shows the expression of CD44 in CD4SP thymocytes and splenic CD4 T cells, presented as MFI. Data are representative of one experiment with 6-wk-old mice (mean ± SD; $n = 4$). (*C*, *top*) Flow cytometric analysis of PLZF versus Eomes expression gated on CD4SP cells derived from *Id2*$^{fl/fl}$*Id3*$^{fl/fl}$*IL7R*^{Cre} and control thymus. (*Bottom*) The graph shows the percentage of PLZF-expressing cells in CD4SP, DN;TCRβ$^+$ in the thymus and CD4 T cells in the spleen. Numbers in quadrants indicate the percentages of cells. Data are representative of three independent experiments with 6-wk-old mice (mean ± SD; $n = 4$ biological replicates). (*D*) Representative flow cytometric analysis of CXCR5 versus PD-1 expression gated on CD4SP cells and CD1d-tet versus TCRβ expression gated on CXCR5$^+$PD-1$^+$ CD4SP cells derived from 8-wk-old thymus. (*E*) Flow cytometric analysis of PLZF and PD-1 expression in sorted CXCR5$^+$ CD4SP cells (CD4$^+$CD8$^-$TCRβ$^+$CD1d-tet$^-$CXCR5$^+$) from *Id2*$^{fl/fl}$*Id3*$^{fl/-}$*IL7R*^{Cre} thymus and sorted control CD4SP cells. Numbers indicate PLZF$^+$ cells. (*F*, *top*) Cytokine expression in CD4SP cells derived from *Id2*$^{fl/fl}$*Id3*$^{fl/fl}$*IL7R*^{Cre} and control thymi. (*Bottom*) The graph shows the percentage of IFN-γ$^+$ and IL-4$^+$ cells in CD4SP cells. Data are representative of three independent experiments with 6-wk-old mice (mean ± SD; $n = 3$ biological replicates). (*) $P < 0.05$; (**) $P < 0.01$ (Student's *t*-test).

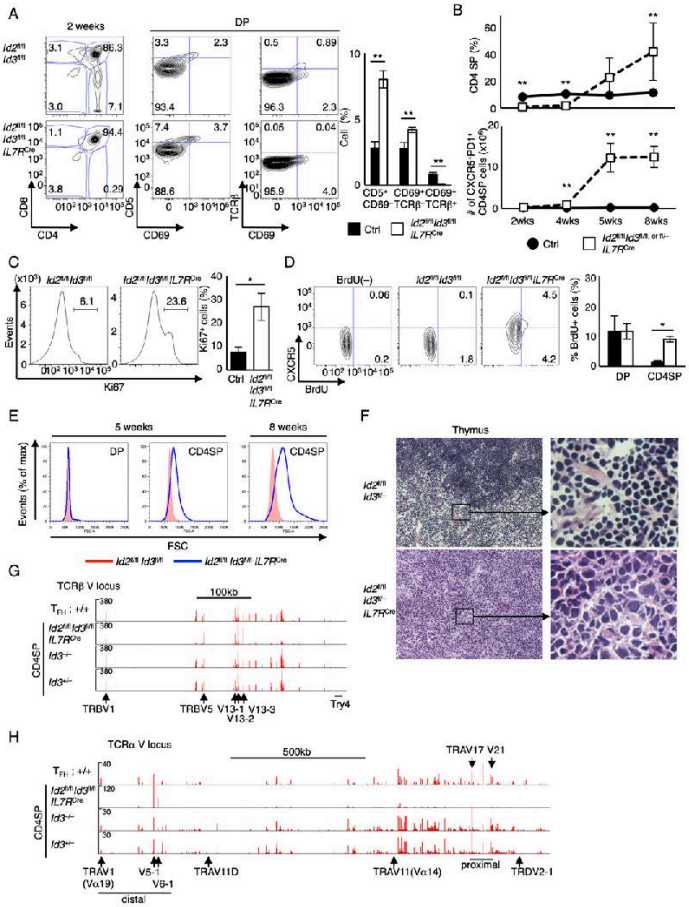

Figure 3. An expanding population of CXCR5$^+$ cells in thymi derived from $Id2^{fl/fl}Id3^{fl/fl}IL7R^{Cre}$ mice. (*A*) Flow cytometric analysis of CD4 versus CD8 expression in total thymocytes and CD69 versus CD5 expression and CD69 versus TCRβ expression gated on DP cells derived from 2-wk-old $Id2^{fl/fl}Id3^{fl/fl}IL7R^{Cre}$ or littermate control mice. The graph shows the frequency of CD5$^+$CD69$^-$, CD69$^+$TCRβ$^-$, and CD69$^+$TCRβ$^+$ cells in the DP compartment. Numbers adjacent to the outlined areas or in quadrants indicate the percentages of cells in the population. Data are representative of one experiment with 2-wk-old mice (mean ± SD; $n = 5$ [Ctrl] and 3 [$Id2^{fl/fl}Id3^{fl/fl}IL7R^{Cre}$] biological replicates). (*B*) The frequency of CD4SP cells (*top*) and the number of CXCR5$^+$PD-1$^+$ CD4SP cells (*bottom*) are plotted. Data were derived from five independent experiments (mean ± SD; $n = 5$ or 3 [2-wk], 3 [4-wk], and 4 [5- or 8-wk] biological replicates). (*C*) Intracellular staining of Ki67 in CD4SP cells derived from 8-wk-old $Id2^{fl/fl}Id3^{fl/fl}IL7R^{Cre}$ or littermate control mice. Numbers *above* lines indicate percentages of Ki67-expressing cells. The graph shows the frequency of Ki67-expressing cells derived from 6- to 8-wk-old $Id2^{fl/fl}Id3^{fl/fl}IL7R^{Cre}$ or littermate control mice. Data were derived from two independent experiments (mean ± SD; $n = 4$ biological replicates). (*D*) Flow cytometric analysis of BrdU incorporation and CXCR5 expression gated on CD4SP (TCRβ$^+$CD25$^-$) cells derived from 8-wk-old $Id2^{fl/fl}Id3^{fl/fl}IL7R^{Cre}$ or littermate control mice. Mice were injected intraperitoneally with 1 mg of PBS (BrdU$^-$) or BrdU twice (24 h and 2 h prior to harvesting). Numbers in quadrants indicate BrdU-incorporated cells. The graph shows the frequency of BrdU$^+$ cells in DP and CD4SP cells. Data were derived from two independent experiments (mean ± SD; $n = 4$ biological replicates). (*E*) Flow cytometric analysis of cell size (FSC) in DP and CD4SP cells derived from 5- or 8-wk-old $Id2^{fl/fl}Id3^{fl/fl}IL7R^{Cre}$ or littermate control mice. Data were derived from two (5-wk) or four (8-wk) independent experiments. (*F*) Representative hematoxylin and eosin (H&E) staining of thymi derived from 6-mo-old $Id2^{fl/fl}Id3^{fl/fl}IL7R^{Cre}$ or littermate control mice. Original magnification, 200×. Data are representative of three independent experiments. (*G*,*H*) RNA-seq data for the TCRα V locus (*H*) and TCRβ V locus (*G*). mRNA was isolated from sorted CXCR5$^+$CD44^{hi} CD4 T cells from SRBC-immunized wild-type spleens (T_{FH}) and CD4SP thymocytes derived from 8-wk-old $Id2^{fl/fl}Id3^{fl/fl}IL7R^{Cre}$, $Id3^{-/-}$, and $Id3^{+/-}$ thymi and analyzed using RNA-seq. Numbers of reads are indicated for each of the tracks. (*G*,*H*) Two independent experiments with three mice each. (*) $P < 0.05$; (**) $P < 0.01$ (Student's *t*-test).

TCR repertoires were examined using RNA sequencing (RNA-seq). To this end, RNA was isolated from CD4SP cells from *Id3*$^{+/-}$, *Id3*$^{-/-}$, and *Id2*$^{fl/fl}$*Id3*$^{fl/fl}$*IL7R*^{Cre} thymi as well as wild-type T_{FH} cells. We found that Vβ and Vα transcripts associated with wild-type T_{FH} cells and CD4SP thymocytes isolated from *Id3*$^{+/-}$ and *Id3*$^{-/-}$ thymi displayed a similar polyclonal Vβ or Vα repertoire (Fig. 3G,H). On the other hand, CD4SP cells derived from *Id2*$^{fl/fl}$*Id3*$^{fl/fl}$*IL7R*^{Cre} mice were enriched for TRBV5, TRBV13-2, and TRBV13-3 as well as distally located TRAV5-1 and TRAV6-1 transcripts (Fig. 3G,H). We also observed a substantial enrichment for transcripts encoding 3′ Jα elements (Supplemental Fig. 4A). Vα and Vβ gene usage observed in *Id2*$^{fl/fl}$*Id3*$^{fl/fl}$*IL7R*^{Cre} CD4SP cells, however, was not invariant, as described for iNKT or MAIT cells, but rather differed between the various *Id2*$^{fl/fl}$*Id3*$^{fl/fl}$*IL7R*^{Cre} mice that were examined (Supplemental Fig. 4B–D; Le Bourhis et al. 2011). To exclude the possibility that the oligclonal TCRα and TCRβ repertoires were caused by aberrant TCR recombination at the DP stage, we examined the CD69^{-}TCRβ^{-} DP cells from *Id2*$^{fl/fl}$*Id3*$^{fl/fl}$*IL7R*^{Cre} mice for TCRβ and TCRα rearrangements. No obvious differences were detected for TCRβ and TCRα loci in *Id2*$^{fl/fl}$*Id3*$^{fl/fl}$*IL7R*^{Cre} DP cells as compared with control cells (Supplemental Fig. 5A,B). Collectively, these observations indicate that Id2 and Id3 suppress the oligoclonal expansion of innate variant T_{FH}-like populations.

Id2 and Id3 suppress the expansion of innate variant T_{FH}-like cells beyond the TCR checkpoint

To deplete *Id2* and *Id3* expression in T-lineage cells, *Id2*$^{fl/fl}$*Id3*$^{fl/fl}$*CD4-Cre* mice were generated. Similar to as described above for *Id2*$^{fl/fl}$*Id3*$^{fl/fl}$*IL7R*^{Cre} mice, at 2 wk after birth, positive selection was severely impaired in *Id2*$^{fl/fl}$*Id3*$^{fl/fl}$*CD4*^{Cre} thymi (Fig. 4A). However, 7-wk-old *Id2*$^{fl/fl}$*Id3*$^{fl/fl}$*CD4*^{Cre} mice displayed CD4SP, DN TCRβ^{hi}, and iNKT populations that expressed high levels of CXCR5, PD-1, ICOS, and PLZF expression (Fig. 4B; Supplemental Fig. 6A,B). Again, these populations were associated with elevated numbers of thymic B cells as well as IgG1 class-switched GC B cells (Supplemental Fig. 6C).

Since recent studies have demonstrated a critical role for *Id2* and *Id3* in regulatory T (T_{reg}) cells, it remained possible that the innate T_{FH}-like population developed because of systemic inflammatory conditions (Miyazaki et al. 2014). To exclude this possibility and investigate the role of *Id2* and *Id3* in thymocyte development beyond the TCR checkpoint, *Id2*$^{fl/fl}$*Id3*$^{fl/fl}$*dLck*^{Cre} mice were generated (Zhang et al. 2005). We found that Cre-mediated deletion in *dLck*^{Cre} mice was initiated beyond the CD69^{+}TCRβ^{+} DP stage (Fig. 4C; Supplemental Fig. 7A). We found that a substantial fraction of peripheral T_{reg} cells did not exhibit Cre activity, indicative of T_{reg} cells expressing wild-type levels of Id2 and Id3 in *dLck*^{Cre} mice (Supplemental Fig. 7A). As observed for *Id2*$^{fl/fl}$*Id3*$^{fl/fl}$*Il7R*^{Cre} and *Id2*$^{fl/fl}$*Id3*$^{fl/fl}$*CD4*^{Cre} mice, in thymi derived from *Id2*$^{fl/fl}$*Id3*$^{fl/fl}$*dLck*^{Cre} mice, we found increased percentages of CD4SP cells and iNKT cells that expressed CXCR5, PD-1, and PLZF and a variant but limited TCRVα and TCRVβ repertoire (Fig. 4D; Supplemental Fig. 7B–D). Again, we noted an increase in the percentages of thymic B cells and a significant relationship between the proportions of thymic B cells and CXCR5^{+}PD-1^{+} CD4SP cells (R^2 = 0.51893) (Fig. 4E). Notably, we detected transcripts initiated from the first exon of the *Id2* and *Id3* genes in sorted CXCR5^{-}PD-1^{-} CD4SP cells but not in sorted CXCR5^{+}PD-1^{+} CD4SP cells from identical *Id2*$^{fl/fl}$*Id3*$^{fl/fl}$*dLck*^{Cre} mice, consistent with the notion that the aberrant activation of CXCR5 and PD-1 expression was caused by depletion of *Id2* and *Id3* expression (Supplemental Figure 7E). Taken together, these data indicate that Id2 and Id3 expression is required to suppress the development and expansion of an innate variant T_{FH}-like population beyond the TCR checkpoint.

To determine how Id2- and Id3-depleted innate variant T_{FH}-like cells are selected, *β2m*$^{-/-}$*Id2*$^{fl/fl}$*Id3*$^{fl/fl}$*IL7R*^{Cre} mice were generated. We found that the development of the innate variant T_{FH} cell population required β2-microglobulin expression (Fig. 4F). Specifically, CD4SP and CD8SP thymocytes were barely detectable in thymi derived from 8- to 10-wk-old *β2m*$^{-/-}$*Id2*$^{fl/fl}$*Id3*$^{fl/fl}$*IL7R*^{Cre} mice (Fig. 4F). Likewise, CXCR5^{+}PD-1^{+} CD4SP cells, DN TCRβ^{+} cells, PLZF-expressing T cells, and thymic B cells were virtually absent in *β2m*$^{-/-}$*Id2*$^{fl/fl}$*Id3*$^{fl/fl}$*IL7R*^{Cre} thymi (Fig. 4F; Supplemental Fig. 8A). Depletion of *β2m* expression in *Id2*$^{fl/fl}$*Id3*$^{fl/fl}$*Il7R*^{Cre} mice also abolished the development of GC and IgG1 class-switched B cells (Fig. 4G; Supplemental Fig. 8A). Thymi derived from *Id2*$^{fl/fl}$*Id3*$^{fl/fl}$*β2m*$^{-/-}$*IL7R*^{Cre} mice showed a normal thymic cortex but abnormal medulla (Supplemental Fig. 8B). These data indicate that selection of Id2- and Id3-depleted innate variant T_{FH} cells requires β2-microglobulin expression and that this population is closely associated with the development of GCs even in the absence of immunization.

Gene expression signature of innate variant T_{FH}-like cells

To determine how Id2 and Id3 suppressed the oligoclonal expansion of an innate variant T_{FH}-like population, CD4SP cells derived from control and *Id2*$^{fl/fl}$*Id3*$^{fl/fl}$*IL7R*^{Cre} thymi were isolated and analyzed by RNA-seq. Two-thousand-three-hundred-seventy-nine genes were differentially expressed (greater than twofold, $P < 0.05$; 1291 up-regulated; 1088 down-regulated) in *Id*-depleted CD4SP cells (Fig. 5A). Prominent among those genes were *Cxcr5*, *Ccr10*, *Wnt10a*, *Gzma*, *Myb*, *Cebpb*, *Tgfbr3*, and *Smad7* (Fig. 5A). Gene ontology (GO) analysis revealed that a large fraction of differentially expressed transcripts encoded for proteins associated with metabolism, cytokine production, RNA metabolism, T-cell activation, and cell cycle progression (Fig. 5B). Furthermore, Kyoto Encyclopedia of Genes and Genomics (KEGG) pathway analysis revealed p53 and genes associated with the PI3K–AKT, MAPK, and Rap1 pathways as well as genes involved in the suppression of inflammatory bowel disease as being affected by depletion of Id2 and Id3 expression (Fig. 5B). Next, we compared the transcription signatures of Id2/Id3-depleted CD4SP thymocytes with *Id3*$^{-/-}$ CD4SP and

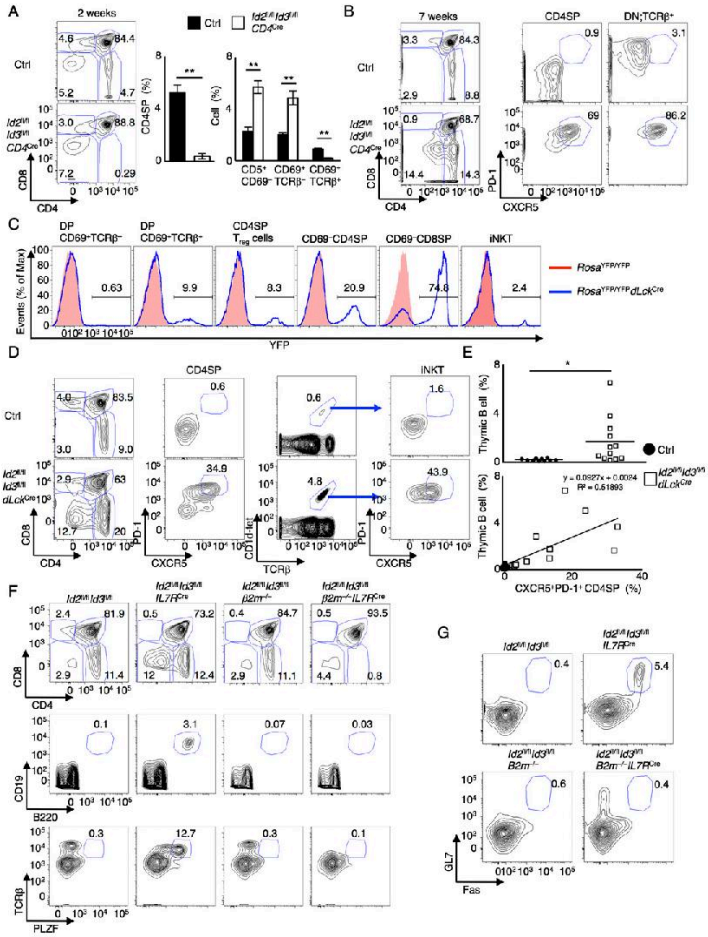

Figure 4. Id2 and Id3 suppress the expansion of innate αβ T cells beyond the TCR checkpoint. (*A*) Flow cytometric analysis of CD4 versus CD8 expression derived from 2-wk-old $Id2^{fl/fl}Id3^{fl/fl}CD4^{Cre}$ or littermate control mice. Numbers indicate the percentage of cells in each population. Graphs show the frequency of CD4SP cells in total thymocytes and $CD5^+CD69^-$, $CD69^+TCR\beta^{+/-}$ and $CD69^+TCR\beta^+$ cells gated on the DP compartment. Data are representative of one experiment with 2-wk-old mice (mean ± SD; $n = 5$ biological replicates). (*B*) Flow cytometric analysis of CD4 versus CD8 expression in total thymocytes and CXCR5 versus PD-1 expression gated on CD4SP cells ($CD4^+CD8^-TCR\beta^+CD1d\text{-}tet^-$) or $DN_3TCR\beta^+$ cells ($CD4^-CD8^-TCR\beta^+CD1d\text{-}tet^-$) derived from 7-wk-old $Id2^{fl/fl}Id3^{fl/fl}CD4^{Cre}$ or littermate control mice. Data were obtained from two independent experiments. (*C*) Representative flow cytometric analysis of YFP expression gated on each compartment derived from $Rosa^{YFP/YFP}$ (red) or $Rosa^{YFP/YFP}dLck^{Cre}$ (blue) mice. Numbers *above* the lines indicate percentages of YFP-expressing cells. Data were derived from two independent experiments. (*D*) Flow cytometric analysis of CD4 versus CD8 expression (*left*) and TCRβ versus CD1d-tet expression (*middle right*) in total thymocytes and CXCR5 versus PD-1 expression gated on CD4SP ($CD4^+CD8^-TCR\beta^+CD1d\text{-}tet^-$) cells (*middle left*) or iNKT ($CD1d\text{-}tet^+TCR\beta^+$) cells (*right*) derived from 10-wk-old $Id2^{fl/fl}Id3^{fl/fl}dLck^{Cre}$ or littermate control mice. Data were derived from four independent experiments. (*E*) Graphs show the frequencies of thymic B ($B220^+CD19^+$) cells and the correlation between thymic B cells and $CXCR5^+PD\text{-}1^+$ CD4SP cells. Data were derived from seven independent experiments. Ten-week-old to 16-wk-old mice were analyzed. (mean ± SD; $n = 10$ [Ctrl] and 12 [$Id2^{fl/fl}Id3^{fl/fl}dLck^{Cre}$] biological replicates). (*F*) Flow cytometric analysis of CD4 versus CD8 expression, B220 versus CD19 expression, and PLZF versus TCRβ expression in total thymocytes derived from $Id2^{fl/fl}Id3^{fl/fl}$, $Id2^{fl/fl}Id3^{fl/fl}IL7R^{Cre}$, $Id2^{fl/fl}Id3^{fl/fl}\beta2m^{-/-}$, and $Id2^{fl/fl}Id3^{fl/fl}\beta2m^{-/-}IL7R^{Cre}$ mice. (*G*) Fas and GL7 expression gated on $B220^+CD19^+$ splenic B cells derived from $Id2^{fl/fl}Id3^{fl/fl}$, $Id2^{fl/fl}Id3^{fl/fl}IL7R^{Cre}$, $Id2^{fl/fl}Id3^{fl/fl}\beta2m^{-/-}$, and $Id2^{fl/fl}Id3^{fl/fl}\beta2m^{-/-}IL7R^{Cre}$ mice. Numbers adjacent to the outlined areas indicate the percentage of cells in each population. Data are representative of three independent experiments. (*) $P < 0.05$; (**) $P < 0.01$ (Student's *t*-test).

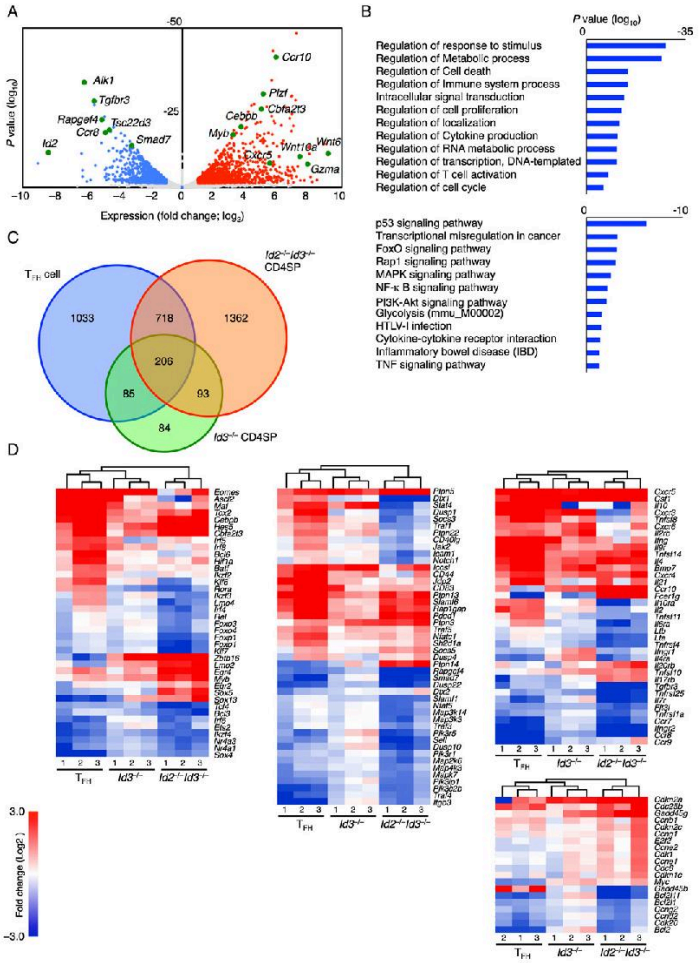

Figure 5. Transcription signature of innate T_{FH}-like cells. (*A*) Volcano plot of RNA-seq analysis of mRNA expression in sorted CD4SP thymocytes derived from 8-wk-old littermate control or $Id2^{fl/fl}Id3^{fl/fl}IL7R^{cre}$ mice. Red dots represent genes up-regulated in $Id2^{fl/fl}Id3^{fl/fl}IL7R^{Cre}$ CD4SP cells (more than twofold, $P < 0.05$, calculated by raw count value). Blue dots represent genes down-regulated in $Id2^{fl/fl}Id3^{fl/fl}IL7R^{Cre}$ CD4SP cells (more than twofold, $P < 0.05$). Gray dots represent genes whose expression was not significantly altered. (*B*) Clusters of genes whose expression was modulated in Id2- and Id3-depleted CD4SP thymocytes were identified using GO terms (*top*) and KEGG pathways (*bottom*). *P*-values are shown. (*C*) RNA-seq data of mRNA expression isolated from $CXCR5^{+}CD44^{hi}$ CD4T cells from SRBC-immunized wild-type spleen (T_{FH}) and CD4SP thymocytes derived from 8-wk-old $Id2^{fl/fl}Id3^{fl/fl}IL7R^{Cre}$ ($Id2^{-/-}Id3^{-/-}$ CD4SP), $Id3^{-/-}$ ($Id3^{-/-}$ CD4SP), and control thymi. Expression was normalized to control CD4SP cells. The Venn diagram shows quantification of genes significantly changed in T_{FH} cells, $Id3^{-/-}$ CD4SP cells, and $Id2^{fl/fl}Id3^{fl/fl}IL7R^{cre}$ CD4SP cells compared with control CD4SP cells. (*D*) Heat maps are presented to visualize differences in gene expression patterns for T_{FH} cells, CD4SP cells sorted from $Id3^{-/-}$ thymocytes, and CD4SP cells sorted from IL7R-Cre;Id2F/F;Id3F/F mice as compared with CD4SP control thymocytes. Bars *above* the heat maps indicate similarities between the different samples presented in each of the lanes. Differentially expressed genes are shown only for those that displayed greater than twofold differences ($P < 0.05$) as compared with control CD4SP thymocytes. The heat maps represent different ontology groups, including genes encoding for factors that regulate transcription (*left*), signal transduction (*middle*), and cell cycle (*bottom right*). (*Top right*) The heat map displays the KEGG pathway for chemokines, cytokines, and associated receptors.

peripheral T_{FH} cells. We found that 924 genes showed overlap between T_{FH} and *Id2*- and *Id3*-deficient CD4SP cells as compared with wild-type CD4SP thymocytes. Two-hundred-ninety-nine genes showed overlap between CD4SP cells isolated from $Id3^{-/-}$ and $Id2^{fl/fl}Id3^{fl/fl}IL7R^{Cre}$ thymi, whereas the expression of 1362 genes was modulated only in innate T_{FH}-like cells when compared with control CD4SP cells (Fig. 5C; Supplemental Fig. 9A). Transcription signatures derived from $Id3^{-/-}$ CD4SP cells showed an intermediate pattern when comparing T_{FH} and CD4SP cells derived from $Id2^{fl/fl}Id3^{fl/fl}IL7R^{Cre}$ thymi (Fig. 5C). The expression patterns of FcεR1 and IL-17rβ in control and mutant thymocytes were validated using flow cytometry (Supplemental Fig. 9B). Notably, genes associated with T_{FH} cell function were altered across the three populations, including *Maf*, *Batf*, *Foxo1*, *Foxp1*, *Sh2d1a*, *Cxcr5*, *Il4*, and *Il21* but not *Bcl6* and *Ascl2* (Fig. 5D; Ma et al. 2012; Wang et al. 2014; Xiao et al. 2014). As predicted, the expression levels of genes associated with an innate-specific program of gene expression were also elevated, including *Zbtb16* (*Plzf*), *Myb*, and *Egr2* (Kovalovsky et al. 2008; Hu et al. 2010; Seiler et al. 2012). Finally, consistent with an expanding population of *Id2*- and *Id3*-depleted CD4SP thymocytes, the expression patterns of genes associated with cell cycle regulation were affected (Fig. 5D). Taken together, these observations indicate that gene expression patterns of Id-depleted CD4SP thymocytes overlap, albeit partially, with that of T_{FH} and innate T-lineage cells.

A genetic circuitry links Id2 and Id3 and the AKT–FOXO–mTORC1 axis

In previous studies, we had identified a spectrum of target genes regulated by the Id–E protein module in T-lineage cells, including *Cxcr5*, *Il10*, *Hif1a*, *Ikzf3*, *Myb*, *Il10ra*, *E2f2*, and *Bmp7* (Miyazaki et al. 2014). Here we found additional target genes that are directly regulated by the E–Id protein axis, including *Foxo1*, *Foxo3*, *Foxp1*, *Slamf6*, *Il7r*, *Il6ra*, *Cxcr4*, *Tgfbr3*, *Wnt10a*, *Cdc25b*, *Gadd45b*, *Bcl2l1*, *Bcl2l11*, and *Rps6ka2* (Supplemental Fig. 9C; data not shown). To examine for molecular pathways or modules associated with depletion of *Id2* and *Id3* expression, transcription signatures derived from *Id*-depleted CD4SP thymocytes and E protein occupancy were linked into a common framework using Cytoscape software (Fig. 6A). Using this approach, we identified an ensemble of E protein targets—including Foxo1, Foxo3 and Foxp1—associated with the maintenance of a naïve and quiescent state. Additionally, a cluster of target genes was identified closely linked with an innate-like transcription signature, including *Myb*, *Plzf*, *Egr2*, and *Sox13* (Fig. 6A; Melichar et al. 2007; Kerdiles et al. 2009; Feng et al. 2011; Hedrick et al. 2012). Finally, we found that clusters of genes associated with the PI3K–AKT/FoxO/mTOR, NFκB/TNF, MAPK, Rap1, cytokine/chemokine, and p53/cell cycle pathways were targeted by the E and Id protein module (Fig. 6B).

To validate these findings, we examined activation of the mTOR and AKT pathways in developing thymocytes using flow cytometry. We found significant increases in phospho-S6 and phospho-4E-BP1 levels in *Id2*- and *Id3*-depleted PD-1^+ CD4SP cells derived from $Id2^{fl/fl}Id3^{fl/fl}dLck^{Cre}$ thymi as compared with control thymi (Fig. 6C). As predicted, phospho-S6 and phospho-4E-BP1 levels were not altered in PD-1^- CD4SP or DP cells derived from $Id2^{fl/fl}Id3^{fl/fl}dLck^{Cre}$ versus control mice (Fig. 6C). To determine whether the E–Id protein axis also regulates the activity of the mTORC pathway to control the expansion of innate γδ T cells, $Id3^{-/-}$ Vγ1.1^+ cells were examined for the expression of phospho-S6 and phospho-4E-BP1. Indeed, $Id3^{-/-}$ Vγ1.1^+ cells displayed significantly increased levels of phopho-S6 and phospho-4E-BP1 (Supplemental Fig. 10). In contrast, $Id3^{-/-}$ Vγ2^+ cells were not associated with elevated levels of phopho-S6 and phospho-4E-BP1 (Supplemental Fig. 10). Next, we examined the phosphorylation status of AKT (pAKT) in sorted control and Id-depleted CD4SP thymocytes. We found that resting control CD4SP cells lacked detectable levels of pAKT (Fig. 6D, left panel). However, activating TCR signaling readily elevated levels of pAKT (Fig. 6D, middle and right panels). Notably, *Id2*- and *Id3*-depleted CD4SP cells exhibited pAKT expression in the absence of TCR stimulation, and TCR-mediated signaling resulted in even higher levels of pAKT (Fig. 6D, bottom). Taken together, these data indicate that the E–Id protein axis modulates the PI3K–AKT–FOXO–mTORC1 pathway at multiple steps.

Id2 and Id3 suppress the development of αβ T-cell lymphomas

Previous studies have demonstrated that the development of Burkitt lymphoma is closely associated with mutations across the Id3 HLH region, that forced expression of Id2 in a murine model of BCR–ABL interferes with the development of chronic myeloid leukemia, and that Id3-deficient mice develop γδ T-cell lymphomas (Ko et al. 2008; Li et al. 2010; Schmitz et al. 2012). To determine whether the combined loss of *Id2* and *Id3* expression in T-lineage cells leads to the development of lymphoma, aged $Id2^{fl/fl}Id3^{fl/fl}IL7R^{Cre}$ mice were monitored for signs of distress. We found that a substantial fraction of 6- to 8-mo-old $Id2^{fl/fl}Id3^{fl/fl}IL7R^{Cre}$ mice exhibited ruffled fur, hunched posture, and rectal prolapse (data not shown). The majority of $Id2^{fl/fl}Id3^{fl/fl}IL7R^{Cre}$ or $Id2^{fl/fl}Id3^{fl/fl}dLck^{Cre}$ mice died within 1 yr (Fig. 7A). Histological analysis showed moderate to severe colitis in 6- to 8-mo-old $Id2^{fl/fl}Id3^{fl/fl}IL7R^{Cre}$, $Id2^{fl/fl}Id3^{fl/fl}CD4^{Cre}$, and $Id2^{fl/fl}Id3^{fl/fl}dLck^{Cre}$ mice (Fig. 7B; Supplemental Fig. 11A). In addition to colitis, we noted splenomegaly and large subcutaneous and/or mesenteric lymph nodes in 21 out of 41 8- to 14-mo-old $Id2^{fl/fl}Id3^{fl/fl}IL7R^{Cre}$, $Id2^{fl/fl}Id3^{fl/fl}CD4^{Cre}$, and $Id2^{fl/fl}Id3^{fl/fl}dLck^{Cre}$ mice (Fig. 7C). Four out of 21 $Id2^{fl/fl}Id3^{fl/fl}IL7R^{Cre}$, $Id2^{fl/fl}Id3^{fl/fl}CD4^{Cre}$, and $Id2^{fl/fl}Id3^{fl/fl}dLck^{Cre}$ mice also developed thymic lymphoma (Fig. 7C; Supplemental Fig. 11B). Histopathological analysis of the peripheral lymphoid organs displayed a disorganized architecture, such as blurring of the demarcation between red and white pulp in the spleen, with

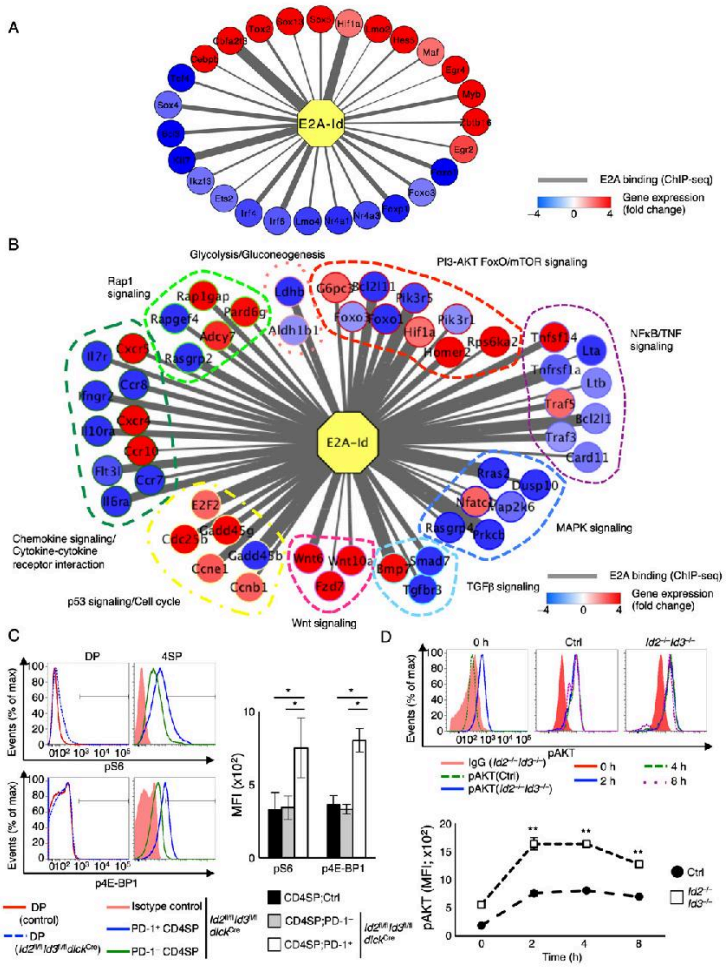

Figure 6. Id2, Id3, and the FOXO/mTOR axis. (*A*) Regulatory network that connects the activity of E proteins and an ensemble of transcriptional regulators in Id2- and Id3-depleted CD4SP thymocytes into a common framework. E2A ChIP-seq (chromatin immunoprecipitation [ChIP] combined with deep sequencing) data were derived from E2A-deficeint T-cell lymphoma cells transduced with E47 (Lin et al. 2010). The widths of the connectors reflect relative peak scores of E2A occupancy. Colors reflect higher (red) or lower (blue) gene expression levels in $Id2^{fl/fl}Id3^{fl/fl}IL7R^{Cre}$ CD4SP cells as compared with control CD4SP thymocytes. (*B*) Networks that link distinct pathways, as defined by KEGG analysis, to E2A occupancy. (*C*) Flow cytometric analysis of phosphorylation of S6 (pS6) and 4E-BP1 (p4E-BP1) in DP and CD4SP cells for the indicated populations derived from control and $Id2^{fl/fl}Id3^{fl/fl}dLck^{Cre}$ mice. The graph shows the level of phosphorylated S6 and 4E-BP1, presented as MFI. Data are representative of three independent experiments (mean ± SD; $n = 3$ biological replicates). (*D*) Flow cytometric analysis of phosphorylation of AKT. Sorted CD4SP cells ($CD4^+CD8^-TCR\beta^+CD1d\text{-}tet^-$) derived from the $Id2^{fl/fl}Id3^{fl/fl}IL7R^{Cre}$ thymus were stimulated with plate-coated anti-CD3ε (2 μg/mL) and anti-CD28 (5 μg/mL) antibodies and analyzed at the indicated time points for pAKT expression. (*) $P < 0.05$; (**) $P < 0.01$ (Student's *t*-test).

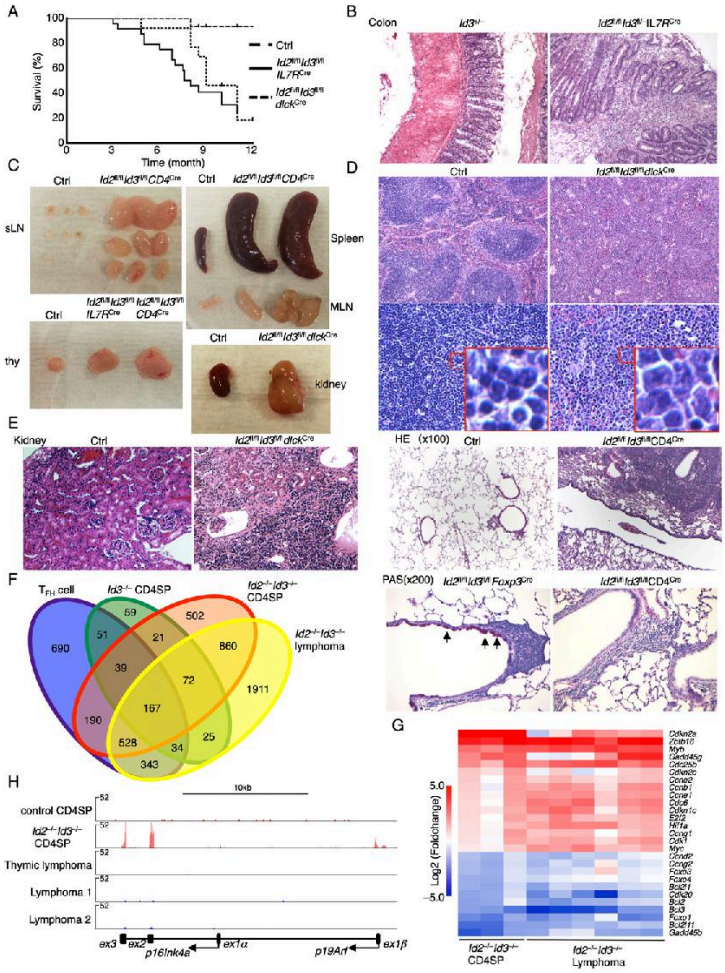

Figure 7. Id2 and Id3 suppress the development of T-cell lymphoma. (*A*) Kaplan-Meier curve of a survival plot of $Id2^{fl/fl}Id3^{fl/fl}IL7R^{Cre}$, $Id2^{fl/fl}Id3^{fl/fl}dLck^{Cre}$, and littermate control mice. ($Id2^{fl/fl}Id3^{fl/fl}IL7R^{Cre}$, $n = 24$; $Id2^{fl/fl}Id3^{fl/fl}dLck^{Cre}$, $n = 14$; control, $n = 16$). (*B*) Representative H&E staining of colons derived from 6-mo-old $Id3^{+/-}$ or $Id2^{fl/fl}Id3^{fl/-}IL7R^{Cre}$ mice. Original magnification, 100×. (*C*) Representative images of subcutaneous lymph nodes (sLN), thymi, spleens, mesenteric LNs (MLN), and kidneys derived from 8- to 12-mo-old control, $Id2^{fl/fl}Id3^{fl/fl}IL7R^{Cre}$, $Id2^{fl/fl}Id3^{fl/fl}CD4^{Cre}$, and $Id2^{fl/fl}Id3^{fl/fl}dLck^{Cre}$ mice are shown. (*D*) Representative H&E stainings of spleens derived from control and $Id2^{fl/fl}Id3^{fl/fl}dLck^{Cre}$ mice are displayed. Original magnifications: *top*, 100×; *bottom*, 400×. (*E*) Representative H&E stainings of kidneys (*left*) and lungs (*top right*) derived from control, $Id2^{fl/fl}Id3^{fl/fl}dLck^{Cre}$, and $Id2^{fl/fl}Id3^{fl/fl}CD4^{Cre}$ mice are shown. The kidney section was derived from metastasis of lymphoma cells as shown in *C*. (*Bottom right*) PAS stainings of the lungs from $Id2^{fl/fl}Id3^{fl/fl}Foxp3^{Cre}$ and $Id2^{fl/fl}Id3^{fl/fl}CD4^{Cre}$ mice are shown. Arrows indicate mucus-producing goblet cells. Original magnifications: kidney, 200×; lung (H&E), 100×; lung (PAS), 200×. (*F*) The Venn diagram shows overlaps among T_{FH} cells, $Id3^{-/-}$ CD4SP cells, $Id2^{-/-}Id3^{-/-}$ CD4SP cells, and $Id2^{-/-}Id3^{-/-}$ lymphoma cells as compared with control CD4SP cells, as shown in Figure 5C. (*G*) Heat map for selected significantly differentially expressed genes that are differentially expressed in *Id2*- and *Id3*-depleted CD4SP thymocytes as well as lymphomas. Clusters of genes associated with cell cycle and tumor suppression are indicated. (*H*) Visualized RNA-seq data across the *Cdkn2a* locus, presented in reads per million reads aligned (RPM). Arrows indicate transcription start site of *p19Arf* and *p16Ink4a* gene and direction of transcription.

infiltrating monomorphic lymphoid cells containing large polymorphic nuclei and scant cytoplasm (Fig. 7D; Supplemental Fig. 11C). The infiltrate in the lungs derived from $Id2^{fl/fl}Id3^{fl/fl}CD4^{Cre}$ mice was composed of neoplastic nucleated cells (Fig. 7E). We note that lymphocyte infiltration was not caused by inflammatory disease, since there was no evidence of elevated mucin levels in the bronchial epithelium (lack of periodic acid Schiff [PAS]-positive goblet cells) (Fig. 7E). The lymphomas that developed in lymph nodes and spleens were mainly composed of $TCR\beta^+CD3^+$ T-lineage cells associated with a $CD8^{low}CD4^-$, $CD8^-CD4^-$ or $CD8^-CD4^+$ phenotype (Supplemental Fig. 11E). As expected, a large fraction of these cells showed CXCR5 and PD-1 expression (Supplemental Fig. 11E). Finally, we found that lymphoma cells were highly malignant, as evidenced by metastasis across the liver (17 out of 21), kidney (three out of 10), and lung (10 out of 21) tissues (Fig. 7C,E; Supplemental Fig. 11B,D). Collectively, these observations indicate that depletion of Id2 and Id3 in T-lineage cells leads to increased levels of morbidity caused by the development of lymphoma and/or inflammatory disease.

The c-Myc and p19Arf axis and the development of Id2- and Id3-deficient lymphomas

To gain insight into the mechanism that underpins the development of lymphoma in *Id2*- and *Id3*-deficient mice, transcription signatures were analyzed from a set of lymphomas using RNA-seq. We found that *Id2*- and *Id3*-deficient lymphomas revealed transcription profiles that overlapped with those derived from *Id2*- and *Id3*-deficient CD4SP cells (Fig. 7F). Specifically, ~2100 genes were differentially expressed in *Id2*- and *Id3*-deficient lymphomas versus *Id2*- and *Id3*-depleted CD4SP cells (Supplemental Fig. 12A,B). The majority of isolated lymphomas expressed a limited TCR repertoire, arguing against polyclonal expansion (Supplemental Fig. 12C,D). We found that the differences in transcription profiles between lymphomas and CD4SP cells were closely associated with genes involved in metabolism, proliferation, and the immune response (Supplemental Fig. 12E). As predicted, we found substantial decreased levels of *Foxo1* and *Foxo3* as well as an elevated abundance of *c-Myc* and *Hif1a* (Fig. 7G). Conspicuous among the spectrum of aberrantly expressed genes was the *Cdkn2a* locus. Notably, *Cdkn2a* transcript abundance was high in $Id2^{fl/fl}Id3^{fl/fl}IL7R^{Cre}$ CD4SP cells but low in lymphoma cells (Fig. 7G). The *Cdkn2a* locus encodes for two tumor suppressors: *p16Ink4a* and *p19Arf*. *p19Arf* is activated by *c-Myc* and has been demonstrated to suppress lymphomagenesis (Kamijo et al. 1997; Zindy et al. 2003). We found that *p19Arf* but not *p16Ink4a* transcript abundance was elevated in the self-renewing innate variant T_{FH}-like population (Fig. 7H). In contrast, *p19Arf* transcript levels were virtually undetectable in Id-deficient lymphomas (Fig. 7H). Taken together, these data point to a regulatory circuitry that maintains thymocyte quiescence and provide a mechanism involving *c-myc* and *p19Arf* that underpins the development of T-cell lymphoma in *Id2*- and *Id3*-deficient T cells.

Discussion

Previous studies have demonstrated that positive selection is enforced by the E and Id protein module (Bain et al. 1999; Jones and Zhuang 2007; Jones-Mason et al. 2012). Here we examined how the Id proteins orchestrate thymocyte selection. Based on this analysis, we propose two key steps that involve Id2 and Id3 during the positive selection process. The first step involves the induction of *Id3* expression by TCR-mediated signaling. The second step involves the induction of *Id2* expression in cells that have already received a TCR signal. We demonstrate here that *Id2*- and *Id3*-depleted thymocytes were not able to pass this second step of selection, with the exception of a slowly expanding population of cells that was characterized by an innate-like transcription signature. Innate T cells, including iNKT, T-CD4T, and MAIT cells, are selected by a mechanism that is distinct from that of conventional CD4SP thymocytes (Li et al. 2005; Lee et al. 2010; Alonzo and Sant'Angelo 2011; Gold and Lewinsohn 2013). Specifically, iNKT and MAIT cells are MHC class I-like-restricted, involving innate TCR signaling. Additionally, iNKT and T-CD4 T cells are selected by DP thymocytes rather than by thymic epithelial cells. Hence, we propose that differences in TCR-mediated signaling—conventional or innate-mediated TCR signaling—affect the duration and/or periodicity of *Id3* and/or *Id2* transcription and that CD4 T cells selected by MHC class II in thymic epithelial cells but not innate CD4 T cells require *Id2* and *Id3* expression. Differences in the strength, periodicity, and timing of *Id2* and *Id3* expression would then instruct progenitors to commit to either the adaptive or innate T-cell lineage.

We found that *Id2*- and *Id3*-depleted positively selected thymocytes express a T_{FH}-like program of gene expression. Particularly intriguing was the decline of *Foxo1* and *Foxp1* abundance in *Id*-depleted CD4SP thymocytes. *Foxo1* and *Foxp1* are well-characterized suppressors of the T_{FH} cell fate (Hedrick et al. 2012; Wang et al. 2014; Xiao et al. 2014). These data bring into question how Id proteins and *Foxo1* and *Foxp1* are linked. We found E2A-bound sites across regulatory regions associated with the *Foxo1* and *Foxp1* loci. Hence, we suggest that in CD4SP thymocytes, the E proteins act as transcriptional repressors that interfere with *Foxo1* and *Foxp1* transcription. High levels of *Id2* and *Id3* antagonize the DNA-binding activity of E proteins, relieving *Foxo1* and *Foxp1* from E2A/HEB-mediated repression. Elevated levels of *Foxo1* and *Foxp1* in turn would prevent the premature activation of a T_{FH} lineage-specific program of gene expression (Supplemental Fig. 13A).

A notable feature of our findings is the development of an innate variant T_{FH} cell population in mice depleted for *Id2* and *Id3* expression. Are these cells genuine T_{FH} cells? We noted overlap but also significant differences in transcription signatures upon comparing T_{FH} and *Id*-depleted innate T_{FH} cells. Notably, *Bcl6* and *Ascl2* expression, closely associated with a T_{FH}-specific program of gene expression (Crotty 2014), were not modulated, at least transcriptionally, in *Id*-depleted CD4SP

thymocytes. Despite these differences, we found that *Id*-depleted innate variant T_{FH} cells secreted high levels of IL-4, required interaction with MHC class I-like molecules, and their presence was closely associated with the spontaneous development of GCs. Hence, we suggest that these cells represent a distinct subset of T_{FH} cells (Supplemental Fig. 13B).

A key aspect of the findings reported here involves a slowly expanding population of innate T_{FH}-like cells. How do Id2 and Id3 regulate thymocyte quiescence? We found that multiple pathways known to maintain lymphocyte quiescence were affected by depletion of *Id2* and *Id3* expression. Prominent among these was the FOXO–mTOR module. The roles for the FoxO proteins in maintaining thymocyte quiescence and acting as tumor suppressors are well documented (Paik et al. 2007; Kerdiles et al. 2009; Hedrick et al. 2012). Similarly, spontaneous activation of the mTORC1 pathway in *Tsc1*-deficient T cells leads to an increase in cell size and loss of quiescence, phenotypes that are equivalent to that described here for *Id2*- and *Id3*-depleted CD4SP thymocytes (Yang et al. 2011b). As mentioned previously, the entire ensemble of *Foxo* loci, including *Foxo1*, *Foxo3*, and *Foxo4*, appears to be controlled by the E–Id protein module. Likewise, the AKT–FOXO–mTOR pathway was activated in *Id2*- and *Id3*-depleted CD4SP thymocytes as well as in *Id3*-deficient innate γδ T cells. Multiple levels of regulation by the E–Id axis appear to be involved here: (1) modulation of Foxo transcript levels, (2) activation of the AKT pathway plausibly mediated by changes in the expression of an ensemble of PTPN phosphatases that are modulated upon depletion of Id2 and Id3, and (3) activation of the mTORC pathway in part by induction of Rps6ka2 expression. We suggest that this form of regulation is not restricted to innate variant T_{FH} and a subset of Vγ1.1 γδ T cells. Rather, we propose that the regulation of the PI3K–FOXO–mTOR pathway by the E–Id axis is a general mechanism that underpins the homeostasis of lymphoid progenitors and self-renewing committed B and T lymphoid cells.

Finally, we found that *c-Myc* and *p19Arf* levels were elevated in *Id*-depleted CD4SP thymocytes. *p19Arf* is a well-known tumor suppressor that is regulated by c-Myc (Lowe and Sherr 2003). Previous studies have demonstrated that c-myc expression is directly regulated by E proteins (Schwartz et al. 2006). Hence, we suggest that loss of Id expression leads to elevated c-Myc abundance, which in turn leads to the induction of *p19Arf* expression. We speculate that cellular expansion upon depletion of *Id2* and *Id3* expression is attenuated by the induction of *p19Arf* expression. This then would lead to a population that slowly self-renews. How do lymphomas develop in *Id2*- and *Id3*-depleted thymocytes? We speculate that, through mechanisms yet to be determined, *p19Arf* expression is inactivated in a single progenitor, releasing the brakes and ultimately leading to the development of a monoclonal αβ T-cell lymphoma (Supplemental Fig. 13C; von Boehmer 2004).

The mechanisms that underpin the development of αβ T-cell lymphomas in *Id2*- and *Id3*-depleted mice overlap with those observed in human Burkitt lymphoma and a murine model of Burkitt lymphoma (Sander et al. 2012; Schmitz et a. 2012). It is now established that the development of Burkitt lymphoma is closely associated with high levels of *c-Myc* expression and mutations localized across the HLH region of *Id3* (Love et al. 2012; Schmitz et al. 2012). Likewise, we found that *Id2*- and *Id3*-depleted murine T-cell lymphomas expressed relatively high levels of *c-Myc* expression. There are also similarities between the two sets of lymphomas as they relate to the PI3K pathway. Burkitt lymphomas are associated with increased PI3K signaling and display an activated AKT pathway (Sander et al. 2012; Schmitz et al. 2012). We found that Id-deficient CD4 T cells displayed decreased abundance of *Foxo1/3* expression as well as activated AKT and mTORC1 pathway. Upon examining transcription signatures in human T-cell lymphomas, we found that changes in *Id2*, *Foxo1*, and *Foxo3* abundance were significantly associated with the development of human T-cell lymphoma, (Supplemental Fig. 14; Piccaluga et al. 2007). Finally, since a very high fraction of aged mice display symptoms of inflammatory disease, it is conceivable that chronic inflammation contributes to the development of T-cell lymphoma in *Id2*- and *Id3*-deficient mice similarly to as described for viral infections associated with the development of human lymphomas.

Materials and methods

Mice

C57BL/6, $Id3^{f/f}$, $Id2^{f/f}$, $Id3^{-/-}$, $Id2^{YFP/+}$, $Id3^{GFP/+}$, $IL7R\alpha^{Cre}$, $CD4^{Cre}$, $dLck^{Cre}$, and $ROSA^{YFP/YFP}$ mice were bred and housed in specific pathogen-free conditions in accordance with the Institutional Animal Care and Use Guidelines of the University of California at San Diego.

Flow cytometry and cell sorting

Single-cell suspensions from the bone marrow, thymus, and spleen were stained with the following: FITC-labeled, PE-labeled, APC-labeled, APC-Cy7-labeled, Pacific Blue-labeled, Alexa Fluor 700-labeled, Alexa Fluor 780-labeled, PerCP-Cy5.5-labeled, PE-Cy7-labeled, or biotin-labeled monoclonal antibodies, which were purchased from BD PharMingen, including CD11c (HL3), CD44 (IM7), CXCR5 (2G8), IgG1 (A85-1), CD95 (Jo-2), CD138 (281-2), GL-7, Ki67 (B56), and phospho-AKT (M89-61). CD8 (53-6.7), CD19 (ID3), CD38 (90), CD62L (MEL-14), CD44 (IM7), CD69 (H1.2F3), CD127 (A7R34), B220 (RA3-6B2), Mac1 (M1/70), Gr1 (RB6-8C5), Nk1.1 (PK136), Ter119 (TER119), TCRβ (H57), TCRγδ (GL3), PD-1 (J43), ICOS (7E.17G9), IgD (11-26), CCR7 (4B12), CXCR4 (2B11), TBR2 (Dan11mag), phosph-S6 (supk43k), phosph-4E-BP1 (V3NTY24), and AnnexinV were purchased from eBioscience. FceR1 (MAR-1), CD3ε (2C11), CD4 (GK1.5), CD8 (53-6.7), CD11b (M1/70), CD24 (M169), CD25 (PC61), PD-1 (RMP1-30), and F4/80 (BM8) were obtained from Biolegend. CCR9 was purchased from R&D Systems. PLZF (clone D9) was obtained from Santa Cruz Biotechnology. PE-conjugated CD1d tetramer was generously provided by the National Institutes of Health Tetramer Core Facility (mCD1d/PBS57). Biotinylated antibodies were labeled with streptavidin-conjugated Qdot-665, or Qdot-605 (Invitrogen). Clone 2.4 G2 anti-CD32:CD16 (eBioscience) was used to block FcRs. Dead cells were removed

from analysis and sorting by staining with propidium iodide (PI) (Sigma-Aldrich). BrdU incorporation was performed using a BD BrdU flow kit. Annexin V staining was performed using an eBioscience Annexin V apoptosis detection kit APC. Treg cell staining kit (eBioscience) was used for intracellular staining of PLZF and Foxp3 and Eomes detection. Intracellular staining kit (eBioscience) was used for phosph-S6/4E-BP1 staining. BD Cytofix fixation buffer and BD Phosflow perm buffer III were used for phospho-AKT staining. Samples were collected on a LSRII (BD Biosciences) and were analyzed with FlowJo software (Tree Star). Cells were sorted on a FACSAria. For intracellular staining of IFN-γ and IL-4, MACS-purified CD4SP and DN TCRβ$^+$ cells from thymi were cultured in the presence of phorbol 12-myristate 13-acetate (PMA) plus ionomycin (4 h) and Golgi stop (2 h). After culture, cells were stained with anti-CD4, CD8, TCRβ, and CD3ε antibodies. Intracellular staining was performed with the BD Biosciences Cytofix/Cytopermkit.

RNA-seq analysis

Total RNA and the library preparations were described previously (Miyazaki et al. 2014). The strand-specific RNA-seq libraries were sequenced with a HiSeq 2500 sequencer (Illumina). Alignment and trimming of reads were performed using the OSA algorithm against the mm10 murine genome reference in Arraystudio (Omicsoft) (Hu et al. 2012). RNA transcripts were quantified using RSEM methods (http://deweylab.biostat.wisc.edu/rsem) as implemented in Arraystudio (Omicsoft). Abundance values (counts) were normalized and compared with calculated *P*-values using DESeq (http://www-huber.embl.de/users/anders/DESeq). Genes whose abundance values were <10 in all samples were removed. MultiExperiment Viewer software was used to generate heat maps and for hierarchical clustering. GO analyses and visualization files were generated using HOMER (http://biowhat.ucsd.edu/homer), and read pile-ups were visualized using the University of California at Santa Cruz Genome Browser.

Histology

Tissues were fixed in 4% paraformaldehyde (Electron Microscopy Sciences). Fixed tissues were embedded in paraffin and sliced, followed by haematoxylin and eosin (H&E) staining.

ELISPOT

Cells were cultured overnight at 37°C on 96-well MultiScreen-HA filter plates (Millipore) precoated with goat anti-murine Ig(H+L) capture antibodies (Southern Biotechnology Associates [SBA]). Spots were visualized with goat anti-murine IgM or IgG1 antibodies conjugated to HRP, and color was developed by 3-amino-9-ethyl carbazole (Sigma-Aldrich).

Statistical analyses

P-values were calculated with the two-tailed Student's test for two-group comparison, as applicable, with Microsoft Excel software.

Data access

RNA-seq data have been deposited at Gene Expression Omnibus under accession number GSE64779.

Acknowledgments

We thank the National Institutes of Health (NIH) Tetramer Facility for providing us with CD1d tetramers. We thank L. Deng and the University of California at San Diego Histology Core for performing the histology. We thank D. Broide, M. Suzukawa, C.Y. Yang, and C. Katayama for technical advice, and Rodrigo Hess for TCRα$^{-/-}$ thymi. We thank A. Goldrath (University of California at San Diego) for *Id2*-YFP mice, Yuan Zhuang (Duke University) for *Id3*$^{fl/fl}$ mice, A. Lasorella (Columbia University) for *Id2*$^{fl/fl}$ mice, and N. Kileen for *dLCK*^{Cre} mice. This work was partly funded by the National Resource for Network Biology (P41 GM103504) and the San Diego Center for Systems Biology (P50 GM085764). The studies were supported by grants awarded to H.-R.R. (European Research Council advanced grant no. 233074 and DFG-SFB 938-project L) and C.M. (NIH RO1CA078384 and 1PO1AI102853 and the Genomics Core associated with 1PO1AI102853).

References

Agata Y, Tamaki N, Sakamoto S, Ikawa T, Masuda K, Kawamoto H, Murre C. 2007. Regulation of T cell receptor β gene rearrangements and allelic exclusion by the helix–loop–helix protein, E47. *Immunity* **27:** 871–884.

Alonzo ES, Sant'Angelo DB. 2011. Development of PLZF-expressing innate T cells. *Curr Opin Immunol* **23:** 220–227.

Bain G, Quong MW, Soloff RS, Hedrick SM, Murre C. 1999. Thymocyte maturation is regulated by the activity of the helix–loop–helix protein, E47. *J Exp Med* **190:** 1605–1616.

Bain G, Cravatt CB, Loomans C, Alberola-Ila J, Hedrick SM, Murre C. 2001. Regulation of the helix–loop–helix proteins, E2A and Id3, by the Ras–ERK MAPK cascade. *Nat Immunol* **2:** 165–171.

Bendelac A, Savage PB, Teyton L. 2007. The biology of NKT cells. *Annu Rev Immunol* **25:** 297–336.

Benezra R, Davis RL, Lockshon D, Turner DL, Weintaub H. 1990. The protein Id: a negative regulator of helix–loop–helix DNA binding proteins. *Cell* **61:** 49–59.

Carpenter AC, Bosselut R. 2010. Decision checkpoints in the thymus. *Nat Immunol* **11:** 666–673.

Cerutti A, Cols M, Puga I. 2013. Marginal zone B cells: virtues of innate-like antibody-producing lymphocytes. *Nat Rev Immunol* **13:** 118–132.

Crotty S. 2014. T follicular helper cell differentiation, function and roles in disease. *Immunity* **41:** 529–542.

D'Cruz LM, Knell J, Fujimoto JK, Goldrath AW. 2010. An essential role for the transcription factor HEB in thymocyte survival, Tcra rearrangement and the development of natural killer T cells. *Nat Immunol* **11:** 240–249.

D'Cruz LM, Stradner MH, Yang CY, Goldrath AW. 2014. E and Id proteins influence invariant NKT cell sublineae differentiation and proliferation. *J Immunol* **192:** 2227–2236.

Diefenbach A, Colonna M, Koyasu S. 2014. Development, differentiation, and diversity of innate lymphoid cells. *Immunity* **41:** 354–365.

Engel I, Johns C, Bain G, Rivera RR, Murre C. 2001. Early thymocyte development is regulated by modulation of E2A protein activity. *J Exp Med* **194:** 733–745.

Feng X, Wang H, Takata H, Day TJ, Willen J, Hu H. 2011. Transcription factor Foxp1 exerts essential cell-intrinsic regulation of the quiescence of naive T cells. *Nat Immunol* **12:** 544–550.

Gold MC, Lewinsohn DM. 2013. Co-dependents: MR1-restricted MAIT cells and their antimicrobial function. *Nat Rev Microbiol* **11:** 14–19.

Hedrick SM, Hess Michelini R, Doedens AL, Goldrath AW, Stone EL. 2012. FOXO transcription factors throughout T cell biology. *Nat Rev Immunol* **12:** 649–661.

Hu T, Simmons A, Yuan J, Bender TP, Alberola-Ila J. 2010. The transcription factor c-Myb primes $CD4^+CD8^+$ immature thymocytes for selection into the iNKT lineage. *Nat Immunol* **11:** 435–441.

Hu J, Ge H, Newman M, Liu K. 2012. OSA: a fast and accurate alignment tool for RNA-seq. *Bioinformatics* **28:** 1933–1934.

Ikawa T, Kawamoto H, Goldrath AW, Murre C. 2006. E proteins and Notch signaling cooperate to promote T cell lineage specification and commitment. *J Exp Med* **203:** 1329–1342.

Jones ME, Zhuang Y. 2007. Acquisition of a functional T cell receptor during T lymphocyte development is enforced by HEB and E2A transcription factors. *Immunity* **27:** 860–870.

Jones-Mason ME, Zhao X, Kappes D, Lasorella A, Iavarone A, Zhuang Y. 2012. E protein transcription factors are required for the development of $CD4^+$ lineage T cells. *Immunity* **36:** 348–361.

Kamijo T, Zindy F, Roussel MF, Quelle DE, Downing JR, Ashmun RA, Grosveld G, Sherr CJ. 1997. Tumor suppression at the mouse INK4a locus mediated by the alternative reading frame product p19ARF. *Cell* **91:** 649–659.

Kerdiles YM, Beisner DR, Tinoco R, Dejean AS, Castrillon DH, DePinho RA, Hedrick SM. 2009. Foxo1 links homing and survival of naive T cells by regulating L-selectin, CCR7 and interleukin 7 receptor. *Nat Immunol* **10:** 176–184.

Klein L, Kyewski B, Allen PM, Hogquist KA. 2014. Positive and negative selection of the T cell repertoire: what thymocytes see (and don't see). *Nat Rev Immunol* **14:** 377–391.

Ko J, Patel N, Kawamoto H, Frank O, Rivera RR, Van Etten RA, Murre C. 2008. Suppression of E-protein activity interferes with the developmen of BCR-ABL-mediated myeloproliferative disease. *Proc Natl Acad Sci* **105:** 12967–12972.

Kovalovsky D, Uche OU, Eladad S, Hobbs RM, Yi W, Alonzo E, Chua K, Eidson M, Kim HJ, Im JS, et al. 2008. The BTB-zinc finger transcriptional regulator PLZF controls the development of invariant natural killer T cell effector functions. *Nat Immunol* **9:** 1055–1064.

Kreslavsky T, Gleimer M, von Boehmer H. 2010. αβ versus γδ lineage choice at the first TCR-controlled checkpoint. *Curr Opin Immunol* **22:** 185–192.

Lazorchak A, Jones ME, Zhuang Y. 2005. New insights into E-protein function in lymphocyte development. *Trends Immunol* **26:** 334–338.

Le Bourhis L, Guerri L, Dusseaux M, Martin E, Soudais C, Lantz O. 2011. Mucosal-associated invariant T cells: unconventional development and function. *Trends Immunol* **32:** 212–218.

Lee YJ, Jeon YK, Kang BH, Chung DH, Park CG, Shin HY, Jung KC, Park SH. 2010. Generation of $PLZF^+$ $CD4^+$ T cells via MHC class II-dependent thymocyte–thymocyte interaction is a physiological process in humans. *J Exp Med* **207:** 237–246.

Li W, Kim MG, Gourley TS, McCarthy BP, Sant'Angelo DB, Chang CH. 2005. An altermate pathway for CD4 T cell development: thymocyte-expressed MHC class II selects a distinct T cell population. *Immunity* **23:** 375–386.

Li J, Maruyama T, Zhang P, Konkel JE, Hoffman V, Zamarron B, Chen W. 2010. Mutation of inhibitory helix–loop–helix protein Id3 causes γδ T cell lymphoma. *Blood* **116:** 5615–5621.

Li J, Wu D, Jiang N, Zhuang Y. 2013. Combined deletion of Id2 and Id3 genes reveals multiple roles for E proteins in invariant NKT cell development and expansion. *J Immunol* **191:** 5052–5064.

Lin YC, Jhunjhunwala S, Benner C, Heinz S, Welinder E, Mannson R, Sigvardsson M, Hagman J, Espinoza CA, Dutkowski J, et al. 2010. A global network of transcription factors, involving E2A, EBF1 and Foxo1, that orchestrates B cell fate. *Nat Immunol* **11:** 635–643.

Love C, Sun Z, Jima D, Li G, Zhang J, Miles R, Richards KL, Dunphy CH, Choi WW, Srivastava G, et al. 2012. The genetic landscape of mutations in Burkitt lymphoma. *Nat Genet* **44:** 1321–1325.

Lowe SW, Sherr CJ. 2003. Tumor suppression by Ink4a–Arf: progress and puzzles. *Curr Opin Genet Dev* **13:** 77–83.

Ma CS, Deenick EK, Batten M, Tangye SG. 2012. The origins, function, and regulation of T follicular helper cells. *J Exp Med* **209:** 1241–1253.

Melichar HJ, Narayan K, Der SD, Hiraoka Y, Gardiol N, Jeannet G, Held W, Chambers CA, Kang J. 2007. Regulation of γδ versus αβ T lymphocyte differentiation by the transcription factor SOX13. *Science* **315:** 230–233.

Miyazaki M, Rivera RR, Miyazaki K, Lin YC, Agata Y, Murre C. 2011. The opposing roles of the transcription factor E2A and its antagonist Id3 that orchestrate and enforce the naive fate of T cells. *Nat Immunol* **12:** 992–1001.

Miyazaki K, Miyazaki M, Murre C. 2014. The establishment of B versus T cell identity. *Trends Immunol* **35:** 205–210.

Niola F, Zhao X, Singh D, Castano A, Sullivan R, Lauria M, Nam HS, Zhuang Y, Benezra R, Di Bernardo D, et al. 2012. Id proteins synchronize stemness and anchorage to the niche of neural stem cells. *Nat Cell Biol* **14:** 477–487.

Paik JH, Kollipara R, Chu G, Ji H, Xiao Y, Ding Z, Miao L, Tothova Z, Horner JW, Carrasco DR, et al. 2007. FoxOs are lineage-restricted redundant tumor suppressors and regulate endothelial cell homeostasis. *Cell* **128:** 309–323.

Piccaluga PP, Agostinelli C, Califano A, Rossi M, Basso K, Zupo S, Went P, Klein U, Zinzani PL, Baccarani M, et al. 2007. Gene expression analysis of peripheral T cell lymphoma, unspecified, reveals distinct profiles and new potential therapeutic targets. *J Clin Invest* **117:** 823–834.

Rivera RR, Johns CP, Quan J, Johnson RS, Murre C. 2000. Thymocyte selection is regulated by the helix-loop-helix inhibitor protein, Id3. *Immunity* **12:** 17–26.

Schlenner SM, Madan V, Busch K, Tietz A, Laufle C, Costa C, Blum C, Fehling HJ, Rodewald HR. 2010. Fate mapping reveals separate origins of T cells and myeloid lineages in the thymus. *Immunity* **32:** 426–436.

Schwartz R, Engel I, Fallahi-Sichani M, Petrie HT, Murre C. 2006. Gene expression patterns define novel roles for E47 in cell cycle progression, cytokine-meidaed signaling and T lineage development. *Proc Natl Acad Sci* **103:** 9976–9981.

Rothenberg EV. 2014. Transcriptional control of early T and B cell developmental choices. *Annu Rev Immunol* **32:** 283–321.

Sander S, Calado DP, Srinivasan L, Kochert K, Zang B, Rosolowski M, Rodig SJ, Holzman K, Stilgenbauer S, Siebert R, et al. 2012. Synergy between PI3K signaling and MYC in Burkitt lymphomagenesis. *Cancer Cell* **22:** 167–179.

Schmitz R, Young RM, Ceribelli M, Jhavar S, Xiao W, Zhang M, Wright G, Shaffer AL, Hodson DJ, Buras E, et al. 2012. Burkitt lymphoma pathogenesis and therapeutic targets from structural and functional genomics. *Nature* **490:** 116–120.

Seiler MP, Mathew R, Liszewski MK, Spooner CJ, Barr K, Meng F, Singh H, Bendelac A. 2012. Elevated and sustained expression of the transcription factors Egr1 and Egr2 controls NKT lineage differentiation in response to TCR signaling. *Nat Immunol* **13:** 264–271.

Singer A, Adoro S, Park JH. 2008. Lineage fate and intense debate: myths, models and mechanisms of $CD4^-$ versus CD8-lineage choice. *Nat Rev Immunol* **8:** 788–801.

Verykokakis M, Boos MD, Bendelac A, Kee BL. 2010. SAP protein-dependent natural killer T-like cells regulate the

development of CD8$^+$ T cells with innate lymphocyte characteristics. *Immunity* **33:** 203–215.

Verykokakis M, Krishnamoorth V, Iavarone A, Lasorella A, Sigvardsson M, Kee BL. 2013. Essential functions for ID proteins at multiple checkpoints in invariant NKT cell development. *J Immunol* **191:** 5973–5983.

Verykokakis M, Zook EC, Kee BL. 2014. ID'ing innate and innate-like lymphoid cells. *Immunol Rev* **261:** 177–197.

von Boehmer H. 2004. Selection of the T-cell repertoire: receptor-controlled checkpoints in T-cell development. *Adv Immunol* **84:** 201–238.

Wang H, Geng J, Wen X, Bi E, Kossenkov AV, Wolf AI, Tas J, Choi YS, Takata H, Day TJ, et al. 2014. The transcription factor Foxp1 is a critical negative regulator of the differentiation of follicular helper T cells. *Nat Immunol* **15:** 667–675.

Xiao N, Eto D, Elly C, Peng G, Crotty S, Liu YC. 2014. The E3 ubiquitin ligase Itch is required for the differentiation of follicular helper T cells. *Nat Immunol* **15:** 657–666.

Yang CY, Best JA, Knell J, Yang E, Sheridan AD, Jesionek AK, Li HS, Rivera RR, Lind KC, D'Cruz LM, et al. 2011a. The transcriptional regulators Id2 and Id3 control the formation of distinct memory CD8$^+$ T cell subsets. *Nat Immunol* **12:** 1221–1229.

Yang K, Neale G, Green DR, He W, Chi H. 2011b. The tumor suppressor Tsc1 enforces quiescence of naive T cells to promote immune homeostasis and function. *Nat Immunol* **12:** 888–897.

Zhang DJ, Wang Q, Wei J, Baimukanova G, Buchholz F, Stewart AF, Mao X, Killeen N. 2005. Selective expression of the cre recombinase in late-stage thymocytes using the distal promoter of the Lck gene. *J Immunol* **174:** 6725–6731.

Zindy F, Williams RT, Baudino TA, Rehg JE, Skapek SX, Cleveland JL, Roussel MF, Sherr CJ. 2003. Arf tumor suppressor promoter monitors latent oncogenic signals in vivo. *Proc Natl Acad Sci* **100:** 15930–15935.

This chapter, in full, is a reprint of the material as it appears in Genes & Development (2015). Miyazaki M, Miyazaki K, Chen S, Chandra V, Wagatsuma K, Agata Y, Rodewald HR, Saito R, Chang AN, Murre C. *The E-Id protein axis modulates the activities of the PI3K-AKT-mTORC1-Hif1a and c-myc/p19Arf pathways to suppress innate variant TFH cell development, thymocyte expansion, and lymphomagenesis*. Dr. Masaki Miyazaki is the primary author of this work.

Chapter IV:

The antagonist HLH protein Id3 acts to enforce the germinal center checkpoint in B-lineage cells

ABSTRACT

Previous studies have demonstrated that the Id proteins play critical roles in a wide spectrum of cells that comprise the adaptive and innate immune system. However, their roles, if any, in peripheral B-lineage development remain to be determined. Here, we found that Id3 expression is high in follicular B-lineage cells but declines upon differentiating into germinal center (GC) B cell. Whereas Id3 expression appeared non-essential for the developmental progression of early B cell progenitors, we found that the primary and memory responses were severely impaired in Id3-deficient mice. Specifically, we found that loss of Id3 expression resulted in impaired GC formation and class switch recombination. Based on these as well as previous observations we propose that Id3 acts to enforce the GC checkpoint.

INTRODUCTION

Germinal centers (GCs) are secondary structures that develop in peripheral lymphoid organs following immunization or antigen (Ag) stimulation. In GCs, B cells undergo class-switch recombination (CSR), somatic hypermutation (SHM), and additional affinity-based selection [65]. Upon B cell activation, CSR leads to the replacement of the immunoglobulin heavy chain (Igh) constant region (Cμ) with Cγ, Cα or Cε, thus enabling secretion of antibodies (Ab) with different effector functions [66]. SHM, an Ag-dependent secondary diversification process happening in peripheral B cells, introduces point mutations into the V region of the Igh locus, resulting in generation of higher-affinity Ab variants [67]. Both CSR and SHM depend crucially on the enzyme activation-induced deaminase (AID) expressed by GC B cells [68].

GC are composed of dark zones (DZ) and light zones (LZ) based on differences in cellular density and constituents. The sub-compartmentalization of GC into DZ and LZ segregates B cell proliferation from selection versus activation. In the LZ, B cells are spread across a network of follicular dendritic cells (FDC) to undergo selection upon interacting with Ag. In the DZ, B cells carry out additional rounds of clonal expansion and affinity maturation, including CSR and SHM. Upon completion of the affinity maturation process, B cells exit the GC cycle to differentiate either into Ab-secreting plasma cells (PC) or memory B cells.

E-proteins are members of the helix-loop-helix (HLH) family. E-proteins include E12, E47, E2-2 and Hela E-box binding protein (HEB). E12 and E47 are encoded by the E2a gene and arise through alternative splicing. B cell development in

E2A-deficient mice is blocked prior to the onset of Ig heavy chain locus rearrangements. The E2A gene products also regulate Igκ locus assembly as well as receptor editing. Whereas E47 is indispensable for the specification towards the B cell fate, E12 only appears to play a key role in receptor revision upon interacting with auto-antigen. Mechanistically, gradients of E12 and E47 are established in developing pre-B and immature-B cells to promote the deposition of H3K4me3 and H3 acetylation to recruit the RAG-proteins to its relevant target sites. In the peripheral organs E12 and E47 continue to play important roles including the developmental progression of follicular B cells.

Four proteins have been identified that antagonize the DNA binding activities of E-proteins: Id1, Id2, Id3 and Id4 69. The Id proteins play a wide spectrum of regulatory activities in developing cells that comprise the adaptive and innate immune system. They do not appear to play a key role in the developmental progression of early B progenitors. In the peripheral organs Id3 modulates the marginal zone versus follicular zone B cell development.

Here, we have examined potential roles for Id3 in activated B-lineage cells. We found that Id3 expression is high in follicular B-lineage cells but declines upon differentiating into GC B cells. Whereas Id3 expression appeared non-essential for the developmental progression of early B progenitors, we found that the primary and memory responses were severely impaired in Id3-deficient mice. Specifically, we found that loss of Id3 expression resulted in impaired GC formation and IgG1 CSR, and IgG1 secretion during the memory responses was almost completely abolished.

Based on these as well as previous observations we propose that Id3 acts to enforce the GC checkpoint.

RESULTS

E2a and *Id3* expression in B cells

As a first approach to explore potential roles for the E-Id protein axis in peripheral B-lineage cells derived from immunized mice, their expression profiles were analyzed using *E2a*-GFP and *Id3*-GFP reporter mice (Figure 1a). Specifically, E2a-GFP and Id3-GFP reporter mice were immunized with sheep red blood cells (SRBC). Two weeks post immunization GFP levels in the different B cell populations were examined in the peripheral B cell compartments using flow cytometry. Consistent with previous results follicular B cells displayed low levels of E2A expression (Figure 1b). E2A abundance increased in GCB cells and continued to be high throughout the GC cycle but declined in the plasma cell compartment. In contrast, *Id3* abundance was high in follicular B cells but decreased in both the light and dark zones and was barely detectable in the plasma cell compartment (Figure 1b). Interestingly, the $CD38^{+}IgG1^{+}$ compartment was associated with low levels of E2a expression but displayed high abundance of *Id3* expression reaching levels similar as detected in naïve follicular B cells. Thus, E2A and *Id3* expression in activated B-lineage cells was dynamic throughout the GC cycle with high levels of *Id3* expression associated with the naïve follicular B cells as well as memory-like cells and high levels of E2A abundance associated with the GC cycle (Figure 1c).

Role of *Id3* in GC differentiation

To assess the role of Id3 in B-lineage development, CD19-Cre; *Id3*$^{loxp/loxp}$ mice were generated. We found that early B cell development was not affected in the absence of Id3 expression (Figure 2). In contrast, the fraction of marginal zone (MZ) B cells in CD19-Cre; *Id3*$^{loxp/loxp}$ mice was reduced as compared to wild-type mice whereas the development of FoB cells was not altered upon depletion of Id3 expression (Figure 3).

To evaluate the role of *Id3* in the activated B cell compartment, control and CD19-Cre; *Id3*$^{loxp/loxp}$ mice were immunized with 4-hydroxy-3-nitrophenylacetyl and keyhole limpet hemocyanin (NP-KLH). Two weeks post immunization the mice were examined for GC formation using flow cytometry. Mice deficient for *Id3* expression showed a significant impairment in GC formation (Figure 4a). Likewise, IgG1 CSR was also perturbed in immunized CD19-Cre; *Id3*$^{loxp/loxp}$ mice (Figure 4a). In the absence of *Id3* expression B cells also displayed impaired differentiation into PC while the development of CD38^{+}IgG1^{+} "memory-like" B cells was not altered in mice depleted for *Id3* expression in B-lineage cells (Figure 4a). To examine the B cell response to specific antigens in the absence of *Id3* expression, we compared the percentages of NP^{+}IgG1^{+} B cells and NP^{+}IgG1^{+} PCs in control versus *Id3*-depleted B-lineage cells. Consistent with the aforementioned results, we found a lower fraction of NP-specific IgG1^{+} B cells and PCs in the spleen of *Id3*-depleted B-lineage cells as compared to control cells (Figure 4b). Next we assessed serum level of NP-reactive antibodies following immunization with NP-KLH. With serum titers of NP-specific IgM unchanged, serum titers of NP-reactive IgG1 were on average 2-fold lower in B

cells derived from CD19-Cre; *Id3*$^{loxp/loxp}$ mice versus serum isolated from control mice (Figure 4c). Consistent with the declined titers of serum IgG1, the number of NP-specific IgG1 antibody-secreting cells (ASCs) in the spleen of CD19-Cre; *Id3*$^{loxp/loxp}$ mice immunized with NP-KLH was reduced to half of that found in control mice immunized in the same way (Figure 2d). As described above the in vivo analysis indicates that *Id3* expression is essential for the developmental progression of mature B-lineage cells. To examine in greater detail how Id3 affects CSR ex vivo B cells derived from both control and CD19-Cre; *Id3*$^{loxp/loxp}$ mice were cultured in the presence of LPS and IL-4. Consistent with the data described above, B cells deficient for *Id3* produced much lower IgG1-switched cells following activation by either LPS+IL-4 or α-CD40+IL-4 (Figure 5a). To examine a potential role for *Id3* in SHM, both control and CD19-Cre; *Id3*$^{loxp/loxp}$ mice were immunized with SRBC. Two weeks post immunization GC B cells were isolated using cell sorting and examined for SHM activity. Specifically, the intronic region localized downstream of the *Igh* J-region 4 (J_H4) was amplified from genomic DNA isolated from purified GC B cells. We found that the number and frequency of AID-induced mutations were not altered upon depletion of *Id3* expression (Figure 5b). Collectively, these data indicated that *Id3* expression is essential to promote the developmental progression of follicular B cells towards the GC B cell fate and plays a critical role in promoting CSR.

_Id3_ expression is not essential to modulate cell cycle progression in the germinal centers of immunized mice

The data described above indicates that loss of *Id3* expression in B cells leads to impaired GC formation in immunized mice. To explore the possibility that the absence of *Id3* expression affects the distribution of GC cells across the DZ and LZ compartments, we examined the proportion of B cells in the different compartments, LZ and DZ, that comprise the GC in both control and CD19-Cre; $Id3^{loxp/loxp}$ mice that were immunized with SRBC. The DZ and LZ compartments were characterized by staining for CD86 and CXCR4 expression. Although GC formation was impaired in CD19-Cre; $Id3^{loxp/loxp}$ mice, the ratio of B cells in the DZ versus the LZ were unaltered as compared to immunized wild-type mice (Figure 6a). To determine whether *Id3* expression affects cell growth in GC cells, the distribution across the cell cycle was examined in the dark and light zones of the germinal centers using PI staining. In line with previous studies, we found few cells in G2/M phase within the LZ while around 30% cells were in S/G2/M phase within DZ. We found that the cell cycle distribution of either DZ or LZ cells between control and CD19-Cre; $Id3^{loxp/loxp}$ mice was virtually identical (Figure 6b). To validate these findings GC B cells were labeled with 5-bromo-2'-deoxyuridine (BrdU) and examined for the fraction of $BrdU^{+}$ cells in the light and dark zones. Consistent with the analysis using PI as a marker, we found that wild-type and CD19-Cre; $Id3^{loxp/loxp}$ mice showed similar incorporation rates of BrdU across the light and dark zones of the germinal center of immunized mice (Figure 6c).

Role of *Id3* in B cell memory response

The *Id3*-GFP reporter mice showed that the $CD38^{+}IgG1^{+}$ compartment was associated with relatively high levels of *Id3* expression. To determine whether *Id3* expression is essential to generate a B cell memory response, we challenged both control and CD19-Cre; $Id3^{loxp/loxp}$ mice with NP-KLH plus adjuvant followed by boosting with NP-KLH 2 months post the initial immunization (Figure 7a). Slightly fewer $IgG1^{+}$ B cells were detected in CD19-Cre; $Id3^{loxp/loxp}$ mice 2 weeks after first immunization. However, these differences were no longer detectable by the time of boosting (Figure 8). Memory responses, checked both 7 days and 14 days post secondary immunization, were similar in control versus CD19-Cre; $Id3^{loxp/loxp}$ mice, when examined for IgM levels, including both high-affinity (NP_4-reactive IgM) and lower affinity (NP_{26}-reactive IgM) antibodies (Figure 7b). Interestingly, the generation of NP_4-reactive IgG1 antibodies was significantly perturbed in CD19-Cre; $Id3^{loxp/loxp}$ mice as compared to control mice (Figure 7b). In sum, these data indicate that Id3 expression is essential to generate an effective IgG1 memory response.

Id3 regulates GC formation and memory B cell function before GC entry

The studies described above utilizing CD19-Cre; $Id3^{loxp/loxp}$ mice revealed a critical role for *Id3* in orchestrating the development of GC B cells. To determine whether *Id3* also plays key roles at later stages of the germinal center reaction, plasma and/or memory B cell development, Cγ1-Cre; $Id3^{fl/fl}$ mice were immunized with SRBC. Immunized mice were examined 2 weeks later for the presence of GC B cells. The fraction and total number of GC B cells in immunized Cγ1-Cre; $Id3^{fl/fl}$ mice were comparable to that of immunized control mice (Figure 8a). IgG1-switched B cells and

plasma cell development also appeared to be unaffected in B cells of which *Id3* was deleted after they entered the GC reaction (Figure 8c). Following boosting, both the IgM and IgG1 recall response in Cγ1-Cre; $Id3^{fl/fl}$ mice was comparable to that of wild-type control mice, although differences were detectable in Cγ1-Cre; $Id3^{fl/fl}$ mice versus control mice (Figure 8c). Collectively, these results suggested that proper GC formation upon Ag stimulation requires *Id3* expression prior to entering the GC phase.

Role of *E2a* and *Heb* in B cell activation and GC formation

Previous results showed that lack of *E2a* expression led to impaired GC development although *Aicda* expression and CSR was not affected. E-proteins, including E2A, E2-2 and HEB may have redundant functions in controlling the above physiological process. To test this hypothesis, we crossed $E2a^{fl/fl}$ and $Heb^{fl/fl}$ mice with $Cd21^{Cre}$ mice 70. Both control and $E2a^{f/f}Heb^{f/f}Cd21^{Cre}$ mice were intraperitoneally immunized with NP-KLH plus adjuvants. Two weeks post immunization, mice were examined for GC formation, CSR, differentiation of $CD38^{+}IgG1^{+}$ "memory-like" B cells and PCs. Ablation of *E2a* and *Heb* expression in B cells was associated with decreased numbers of splenocytes as compared to that of control mice (Figure 9a). Fourteen days following immunization, fewer GC B cells were detected in the spleen of $E2a^{f/f}Heb^{f/f}Cd21^{Cre}$ mice (Figure 9b). We also observed a lower percentage of IgG1-switched B cells and $CD38^{+}IgG1^{+}$ "memory-like" B cells, while development of NP-reactive plasma cells was not affected by deficiency of *E2a* and *Heb* expression (Figure 9b). Consistent with these observations we found that the serum level of NP-specific immunoglobulin titers, measured by ELISA 2 weeks after NP-

KLH injection, was not altered upon *E2a* and *Heb* deletion despite impaired GC formation (Figure 9c). Taken together, the lack of *E2a* and *Heb* expression in B cells led to impairment in GC development while the formation and function of $IgG1^+$ plasma cells remained intact. These results suggested that the differentiation of plasma cells, even class-switched ones, can be uncoupled from the process of GC maturation.

DISCUSSION

Previous data have indicated that in the absence of *E2a* and *Heb*, GC formation upon antigen stimulation was impaired whereas class switch recombination, terminal differentiation into plasma cells and memory B cells still remained intact. Here we show that deleting those genes that encode proteins inhibiting the DNA-binding activity of E proteins did not enhance GC formation and IgG1 CSR. In contrast, *Id3* deficiency in B cells prior to GC entry led to clear impairment in GC formation, IgG1 CSR and a complete block of memory response in IgG1 sub-class. Since previous studies showed that ectopic expression of *Id3* in B cells abolished the induction of *Aicda* gene upon activation, this unexpected observation raises the question as to how are *E2a* and *Id3* expression independently regulated after B cells get activated?

E2a and *Id3* displayed very different expression patterns during those sequential stages following B cell activation, indicating they might have different regulatory functions in these processes. Compared with upregulated *E2a* expression during the GC phase, *Id3* only exhibited a prominent level of expression in the unstimulated naïve B cells and $IgG1^{+}CD38^{+}$ "memory-like" B cell populations. We suggest *E2a* expression is required for the clonal expansion of activated B cells within GCs and the induction of *Aicda* expression to promote IgG1 CSR. However, for those B cells escaping these "checkpoints" in GCs, the regulation by *E2a* is no longer required as *E2a* expression is downregulated in the post-GC B cells destined for becoming either plasma cells or memory B cells.

Id3, of which the expression is very high in naïve B cells, could be required for pre-GC checkpoints. Prior to GC entry, *Id3* expression is required to counteract *E2a*, which should be inactive at that moment so stimulated B cells would not enter GC phase prematurely. When *Id3* is absent, B cells upon antigen stimulation directly enter GC phase and proliferate prematurely without acquiring the necessary mutational events or gene expression changes. These B cells might be more susceptible to apoptosis and failed to accumulate mutations to generate high-affinity BCRs. Our observations that deletion of *Id3* after GC entry did not lead to impaired GC formation and IgG1 CSR partially substantiate this hypothesis. For those B cells already passing the pre-GC checkpoints, they need the presence of *E2a* to induce AID activity, rendering the inhibition by *Id3* no longer important.

MATERIALS AND METHODS

Mice

C57BL/6, *Id3*$^{fl/fl}$, *E2a*$^{fl/fl}$*Heb*$^{fl/fl}$, *Cd19*^{Cre}, *Cd21*^{Cre} and *Cγ1*^{Cre} mice were bred and housed in specific pathogen-free conditions in accordance with the Institutional Animal Care and Use Guidelines of the University of California, San Diego.

Flow cytometry

Single cell suspensions from bone marrow, lymph nodes and spleen were prepared, red blood cells lysed, counted and stained with the following antibodies: FITC-, PE-, APC-, APC-Cy7-, Pacific Blue-, Alexa Fluor 700-, Alexa Fluor 780-, PerCP-Cy5.5-, PE-Cy7- or biotin-labeled monoclonal antibodies were purchased from BD PharMingen or eBioscience including B220 (RA3-6B2), CD19 (1D3), CD38 (90), IgD (11.26), GL7 (GL7), CD95 (Jo-2), CXCR4 (2B11), IgM (R6-60.2), CD86 (GL1), IgG1 (A85-1), CD21 (7G6), CD23 (B3B4), c-kit (ACK2), CD25 (PC61), CD138 (281-2), CD93 (AA4.1), Sca1 (E13-161.7), CD150 (TC15-12F12.2), Flt3 (A2F10), IL7R (A7R34), Ly6D (49-H4), CD8 (53-6.7), Mac1 (M1/70), Gr1 (RB6-8C5), NK1.1 (PK136), Ter119 (TER119), TCRβ (H57), TCRγδ (GL3), CD3ε (2C11) and CD4 (GK1.5). Biotinylated antibodies were labeled with streptavidin-conjugated Qdot-605 (Invitrogen). Clone 2.4 G2 anti-CD16: CD32 (eBioscience) was used to block Fc receptors. Dead cells were removed from sorting and analysis by propidium iodide (PI) staining (Sigma-Aldrich). Data were collected on a LSRII (BD Biosciences) and analyzed with FlowJo software (TreeStar). Sorting was performed on a FACSAria (BD).

B cell isolation and culture

B cells from spleen were isolated with the B cell Isolation Kit (Miltenyi Biotec). B cells were cultured in RPMI-1640 medium plus 10% FBS, antibiotics, 2mM L-glutamine and β-mercaptoethanol (50μM). B cells were activated in complete medium at $1*10^6$ cells/ml with the indicated stimuli at the following final concentrations: 2.5% IL-4; 2.5μg/ml anti-CD40 (FGK45); 25μg/ml LPS (Sigma). Cells were harvested at the times indicated, washed and used for downstream analysis.

Enzyme-linked immunosorbent and enzyme-linked immunospot assay

Serum immunoglobulins and NP-specific antibodies were measured by enzyme-linked immunosorbent assay (ELISA) as described. NP-specific ASCs were detected by Elispot assay as described.

Quantitative PCR

RNA was prepared using RNeasy Column (Qiagen) and cDNA was prepared using Superscript III (Invitrogen) as directed by the manufacturer using random hexamer. Real-time PCR was performed in 20ul reactions using FastStart Universal SYBR Green Master (Rox) (Roche) on a Stratagene Mx3500p cycler. Primers were designed specifically for each transcript of interest to span over an intron and the amplicon to be less than 200bp. Housekeeping genes HPRT1 (hypoxanthine-guanine phosphoribosyltransferase) and 18s RNA (ribosomal RNA, 18S) were used as controls.

RNA Isolation for RNA-seq

RNA from purified or sorted B cells was isolated using RNeasy Column (Qiagen) with DNaseI on-column digest. DNA was further digested with TURBO DNase (Life Technologies) as directed. mRNA was purified using the Dynabead mRNA purification kit (Life Technologies) and starting with less than 75ug total RNA in 100ul total volume. 100-500ng enriched mRNA was incubated at 70°C for 10 minutes then immediately placed on ice. cDNA synthesis was then performed as described with the addition of actinomycin D. Removal of dNTPs was achieved by Probe Quant G50 Columns (GE). The samples were incubated for 2 hours at 16°C for second strand synthesis in the following mixture: 0.1x RT Buffer, 0.25mM $MgCl_2$, 1mM DTT (Life Technologies), 0.2mM each dAGCU, 0.75x Second Strand Synthesis mix, 5U E Coli ligase, 20U DNA Polymerase (NEB) and 5U RNase H (Life Technologies). Double stranded cDNA was column purified by DNA Clean and Concentrator Kit (Zymo Research) and sonicated on Covaris for 4 cycles of 60 seconds per cycle. Sonicated samples were column purified as above.

Library Preparation of RNA-Seq samples

Sonicated fragments were blunt ended with End-it DNA End-Repair Kit (Epicentre) and column purified as above. To the 3' end, "A" base was added with 15U Klenow Fragment 3' to 5' exo-, 1x NEB buffer 2, 0.2mM dATP and purified DNA, incubated at 37°C for 30 minutes before column purified as above. Illumina sequencing adaptors were incubated with quick Ligase (NEB) at 20°C for 30 minutes before column purification. Samples were size selected using 8% PAGE gel for 200-450bp. Purified sample was digested with AmpErase Uracil N-glycosylase at 37°C

for 15 minutes. Samples were then PCR amplified with Phusion Hot Start II DNA polymerase (Thermo Fisher Scientific), PCR primers and Index for the following program: 98°C for 30 seconds; 13-18 cycles of 98°C for 10s, 65°C for 30s, 72°C for 30; 72°C for 5 minutes. Samples were size selected again for 200-450bp fragments and gel extracted from a 8% PAGE gel with SYBR Gold (Life Technologies). Visualized with a trans-illuminator, a 200-450bp band was cut carefully to avoid primer dimers. DNA was extracted with a Gel Extraction Kit (Zymo Research). Concentration was measured by Qubit Fluorometric Quantitation (Life Technologies) and samples were delivered at 2ng/ul for sequencing which was performed at the UCSD Institute for Genomic Medicine on a HiSeq 4000 sequencer (Illumina).

RNA-Seq Analysis

Alignment and trimming of reads were done using the OSA algorithm mapping to the mm10 murine genome reference sequence in Arraystudio (Omicsoft). mRNA transcripts were quantified using RSEM methods (http://deweylab.biostat.wisc.edu/rsem) as implemented in Assaystudio. Abundance values (counts) were normalized and comparisons were drawn with calculated P-values through DESeq (http://www-huber.embl.de/users/anders/DESeq). Genes of which counts were <10 in all samples were removed. Heat maps and hierarchical clustering were generated using MultiExperiment Viewer software. Gene Ontology (GO) analyses and visualization files were generated using WebGestalt (http://bioinfo.vanderbilt.edu/webgestalt/login.php) as detailed in the following section.

Gene Ontology Analysis

Genes that were identified to have a greater than a 2-fold change (i.e.: $-1 < \log_2(\text{fold change}) < 1$) in gene expression by counts were submitted to functional annotation by Gene Ontology (GO) analysis by looking at Kyoto Encyclopedia of Genes and Genomes (KEGG) pathways associated through the Database for Annotation, Visualization and Integrated Discovery (DAVID) online tool (http://david.abcc.ncifcrf.gov).

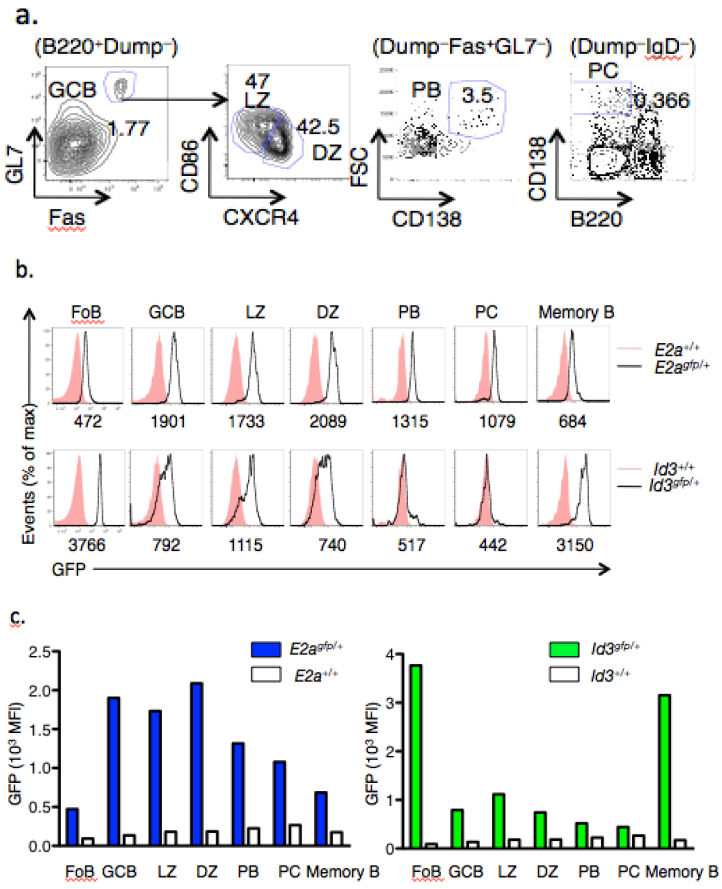

Figure 4.1 Analysis of E2A and Id3 expression in peripheral B cells from E2A-GFP or Id3-GFP reporter mouse.

(a) Strategy of gating different activated B cell subpopulations. Populations gated such as GC ($B220^{+}Dump^{-}Fas^{+}GL7^{+}$), DZ ($Fas^{+}GL7^{+}CXCR4hiCD86lo$), LZ ($Fas^{+}GL7^{+}CXCR4loCD86hi$), Plasmablast ($Dump^{-}Fas^{+}GL7^{-}CD138^{+}FSC^{hi}$) and PC ($Dump^{-}IgD^{-}B220^{-}CD138^{+}$). (b) E2a GFP expression (upper) and Id3 GFP expression (bottom), gated on unstimulated follicular B cells, $CD38^{+}IgG1^{+}$ "memory-like" B cells and the above subpopulations derived from the spleens of control, $E2a^{GFP/+}$ and $Id3^{GFP/+}$ mice. (c) Quantification of E2a GFP level (left) and Id3 GFP level (right) throughout different stages of peripheral B cell differentiation following Ag stimulation.

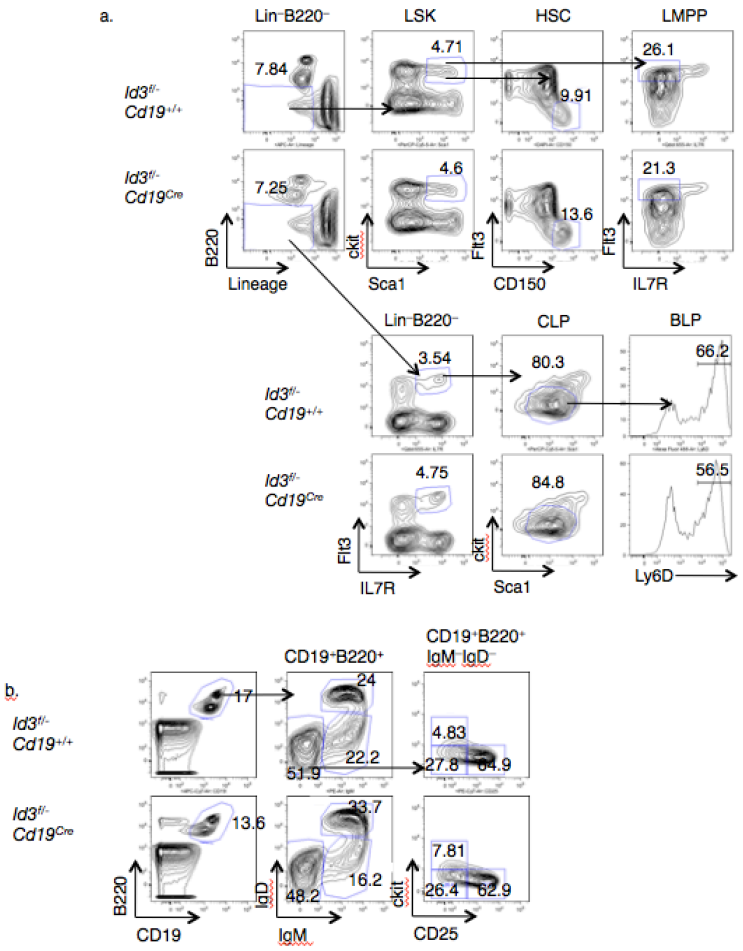

Figure 4.2 Early B cell development in the absence of *Id3*. Representative flow cytometric analysis of (A) LSK (Lineage$^-$Sca1$^+$ckit$^+$), HSC (Lineage$^-$Sca1$^+$ckit$^+$Flt3$^-$CD150$^+$), and LMPP (Lineage$^-$Sca1$^+$ckit$^+$Flt3$^+$IL7R$^-$), (B) CLP (Lineage$^-$Flt3$^+$IL7R$^+$Sca1^{lo}ckit^{lo}) and BLP (Ly6D$^+$ gated on CLP), and (C) pro-B (IgM$^-$IgD$^-$ckit$^+$CD25$^-$) and pre-B (IgM$^-$IgD$^-$ckit$^-$CD25$^+$)cells. Bone marrow cells were isolated as described and doublets were excluded based on FSC and SSC.

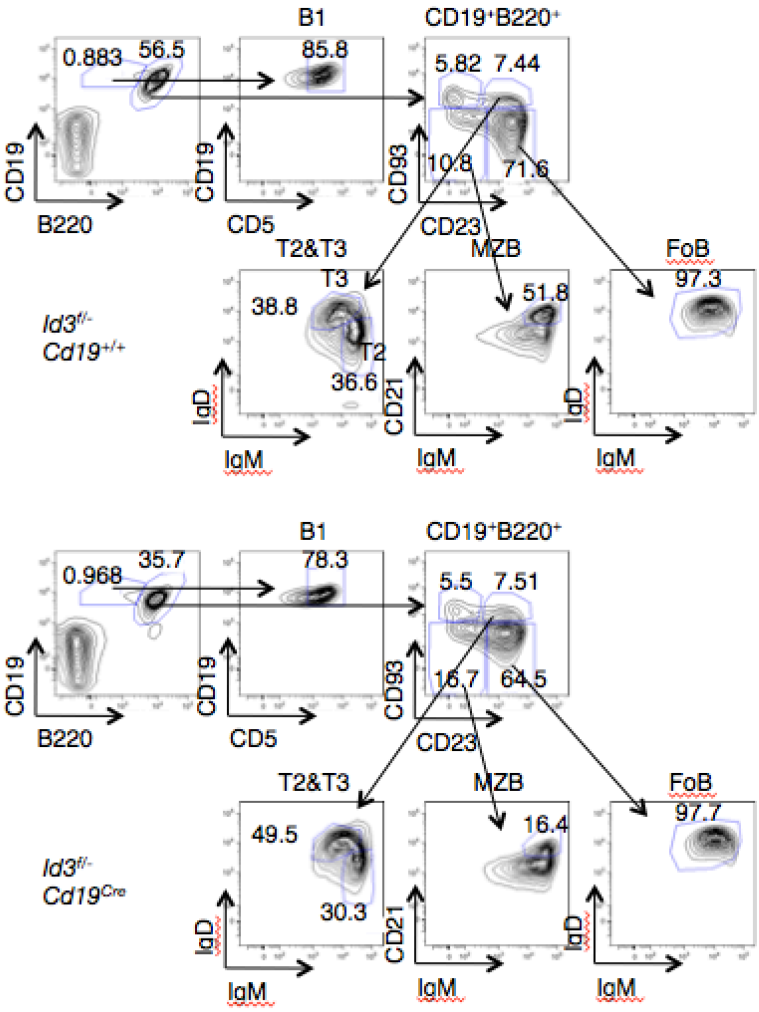

Figure 4.3 Follicular B cell development prior to the activation in the spleen.

Representative flow cytometric analysis of B1 ($B220^{-}CD19^{+}CD5^{+}$), T2 ($B220^{+}CD19^{+}CD93^{+}CD23^{+}IgM^{+}IgD^{lo}$), T3 ($B220^{+}CD19^{+}CD93^{+}CD23^{+}IgM^{lo}IgD^{hi}$), marginal zone B cells (MZB: $B220^{+}CD19^{+}CD93^{-}CD23^{-}IgM^{+}CD21^{+}$) and Follicular B cells (FoB: $B220^{+}CD19^{+}CD93^{-}CD23^{+}IgM^{med}IgD^{hi}$). Splenocytes were isolated as described and doublets were excluded based on FSC and SSC.

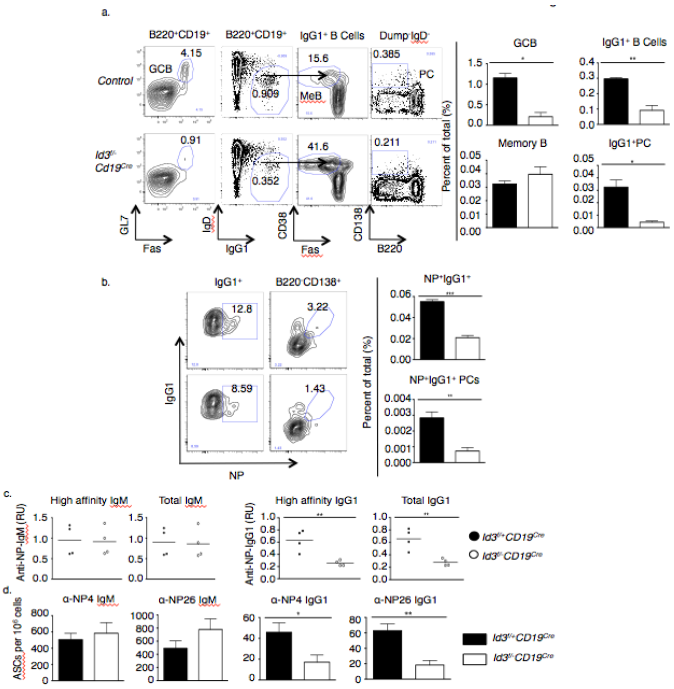

Figure 4.4 B cell differentiation following NP-KLH immunization.

(a) Flow cytometric analysis of activated B cell subpopulations derived from the spleens isolated from 8-week-old control (*Id3*$^{fl/-}$*Cd19*^{WT} and *Id3*$^{fl/+}$*Cd19*$^{Cre\ or\ WT}$) or Id3-CD19 cKO (*Id3*$^{fl/-\ or\ fl/fl}$*Cd19*^{Cre}) mice immunized with NP-KLH plus adjuvant. The two left panels indicate Fas versus GL7 and IgG1 versus IgD expression, gated on the B220^{+}CD19^{+} compartment derived from spleens of immunized control or Id3-CD19 cKO mice. The right two panels indicate Fas versus CD38, gated on the IgG1^{+}IgD^{-} compartment of B cells, and B220 versus CD138 expression, gated on the Dump^{+}IgD^{-} compartment. Numbers in plots indicate percent of Fas^{+}GL7^{+}, IgG1^{+}IgD^{-}, Fas^{-}CD38^{+}, and B220^{-}CD138^{+} cells. Right, percentages of GC (Fas^{+}GL7^{+}), IgG1^{+} B cells (IgG1^{+}IgD^{-}), "memory-like" B cells (IgG1^{+}IgD^{-}Fas^{-}CD38^{+}), and plasma cells (Dump^{+}IgD^{-}B220^{-}CD138^{+}) in splenocytes. (b) Flow cytometric analysis of NP-reactive IgG1-switched B cells (IgG1^{+}IgD^{-}NP^{+}) and NP-reactive PCs (Dump^{+}IgD^{-}B220^{-}CD138^{+}NP^{+}) from spleens isolated from 8-week-old control and Id3-CD19 cKO mice immunized with NP-KLH plus adjuvant. Numbers in plots indicate percent of IgG1^{+}IgD^{-}NP^{+} and Dump^{+}IgD^{-}B220^{-}CD138^{+}NP^{+} cells. Right, percentages of NP-reactive IgG1^{+} B cells and NP-reactive PCs in splenocytes. (c) Quantification of NP_4-reactive IgM and IgG1, NP_{26}-reactive IgM and IgG1in serum collected from control and Id3-CD19 cKO mice (n=4 per group) 14 d after immunization with NP-KLH. (d) Elispot analysis of NP_4- and NP_{26}-specific IgM and IgG1 ASCs in spleens on days 14 after NP-KLH immunization. Data are representative of at least four experiments (a, b, d; mean ± s.d.; control $n = 4$, *Id3*$^{f/-}$*Cd19*^{Cre} $n = 4$ independent biological replicates), one experiment (c; mean; control $n = 4$, *Id3*$^{f/-}$*Cd19*^{Cre} $n = 4$ independent biological replicates). * P<0.05, ** P<0.01, *** P<0.001 (two-tailed unpaired Student's t test).

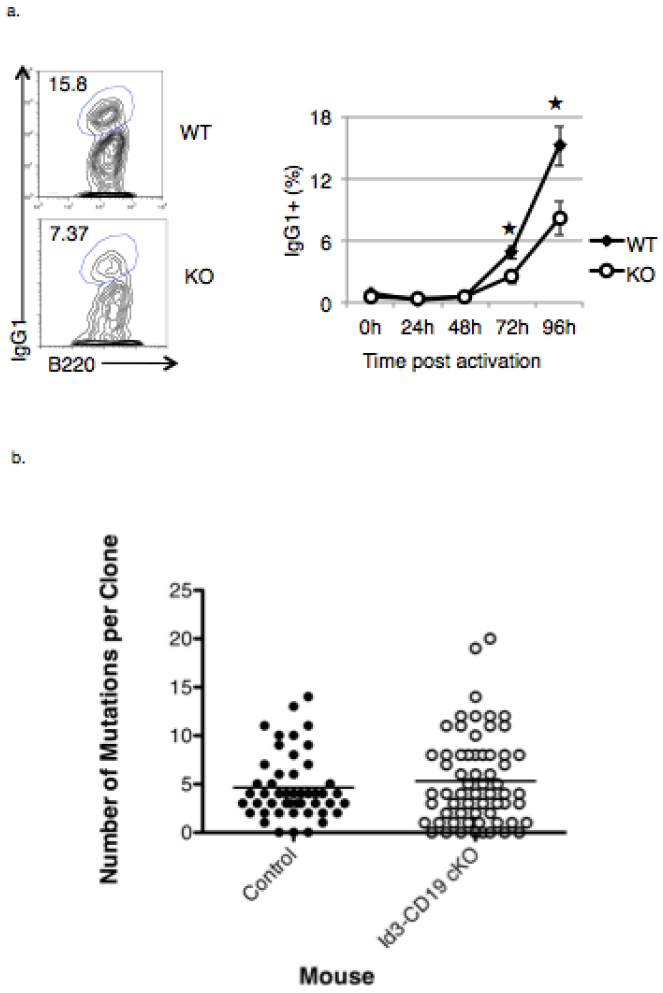

Figure 4.5 CSR and SHM of in vitro activated B cells.

(A) CSR to IgG1 of B cells isolated from WT or *Id3*$^{f/-}$*CD19*^{Cre} mice activated in vitro in the presence of LPS and IL-4 over 4 days. Percentage of IgG1^{+} B cells from WT (black) and *Id3*$^{f/-}$*CD19*^{Cre} (white) at each 24-hour time point was shown. (B) SHM of sorted germinal center B cells isolated from WT (black) or *Id3*$^{f/-}$*CD19*^{Cre} (white) mice immunized with SRBC measured by number of mutations per cell.

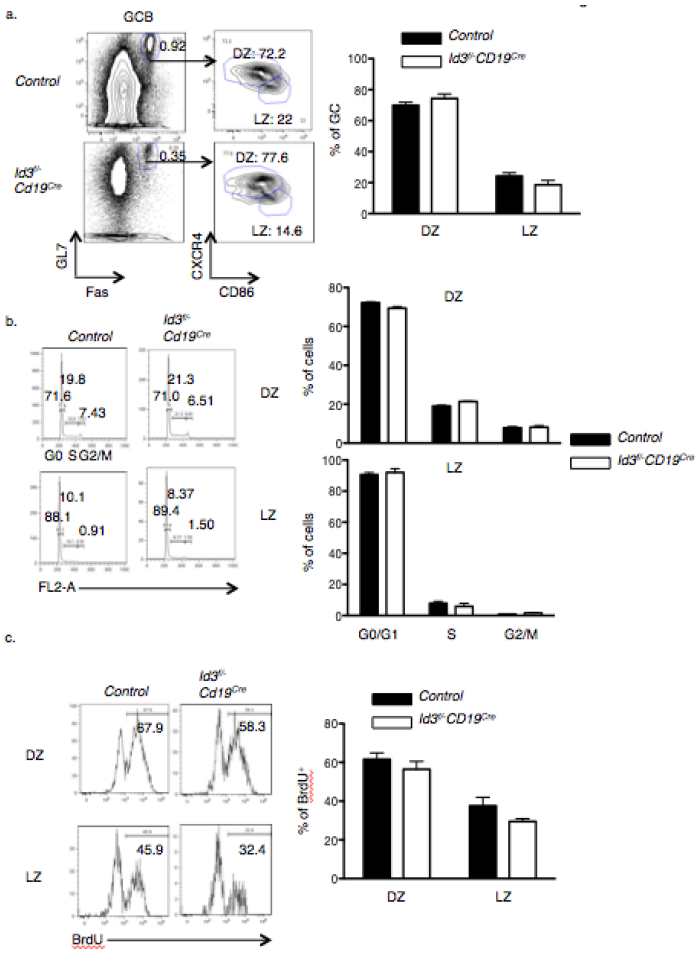

Figure 4.6 DZ and LZ characterization from GCs of WT and Id3-cKO mouse.

(a) Flow cytometric analysis of sub-compartmentalization into dark zone (DZ) and light zone (LZ) of GC B cells isolated from spleens of both control and Id3-CD19 cKO mice following sheep red blood cell (SRBC) immunization. Numbers in plots indicate percent of $Fas^{+}GL7^{+}$, $CXCR4^{hi}CD86^{lo}$, and $CXCR4^{lo}CD86^{hi}$ cells. Right, quantification of percentages of DZ/LZ within GCs from both control and Id3-CD19 cKO mice. (b) Cell cycle (DNA content) profiles of DZ (upper) and LZ (bottom) cells, gated as shown in (a). Right, Quantification of DZ or LZ cells in each phase of cell cycles. (c) BrdU incorporation of DZ (upper) and LZ (bottom) cells, as gated in (a). Right, percentage of $BrdU^{+}$ cells within DZ or LZ from both control and Id3-CD19 cKO mice immunized with SRBC. Data are representative of two experiments (a,b,c; mean ± s.d.; control n = 3, Id3-CD19 cKO n = 3 independent biological replicates).

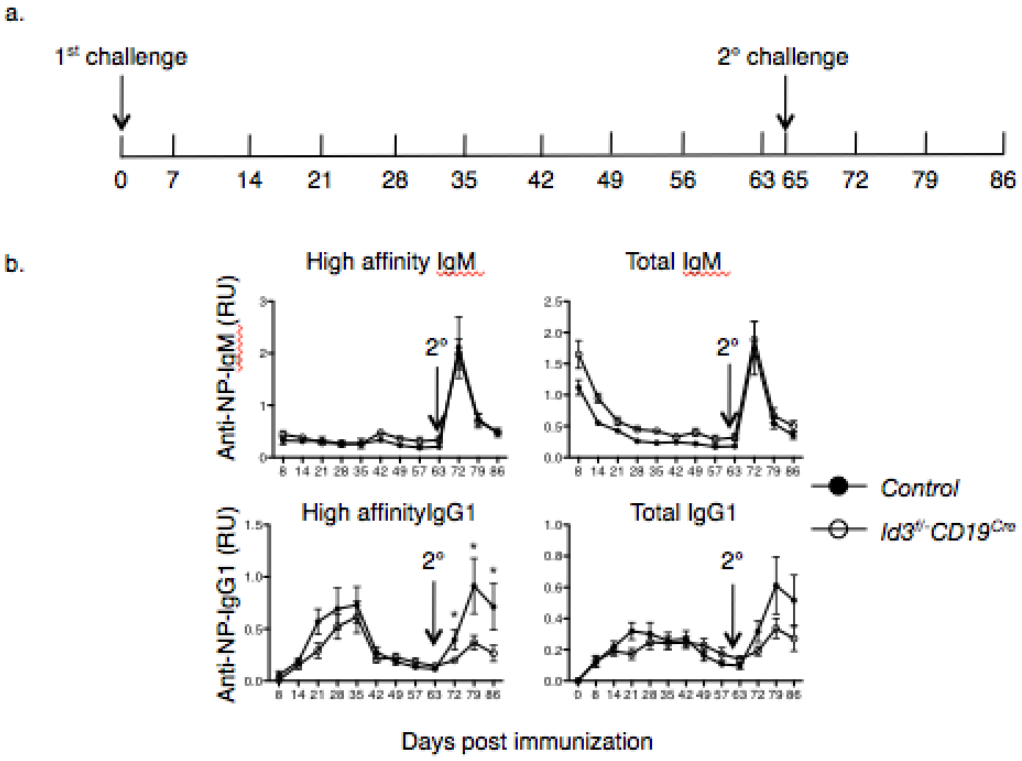

Figure 4.7 B cell memory response in the absence of *Id3*.

(a) Immunization strategy for studying memory response of B cells. For 1st challenge, both control and Id3-CD19 cKO mice were immunized with NP-KLH plus sigma adjuvant. For 2° challenge, mice were boosted with NP-KLH only. (b) Time-course analysis of NP4- or NP26-reactive IgM and IgG1 in serum from control and Id3-CD19 cKO mice immunized with NP-KLH plus adjuvant at day 0 and boosted with NP-KLH only at day 65 (downward arrows). Data are representative of two independent experiments (b; mean ± s.d. of n = 7 mice in control group and n = 8 in Id3f/-Cd19Cre group).

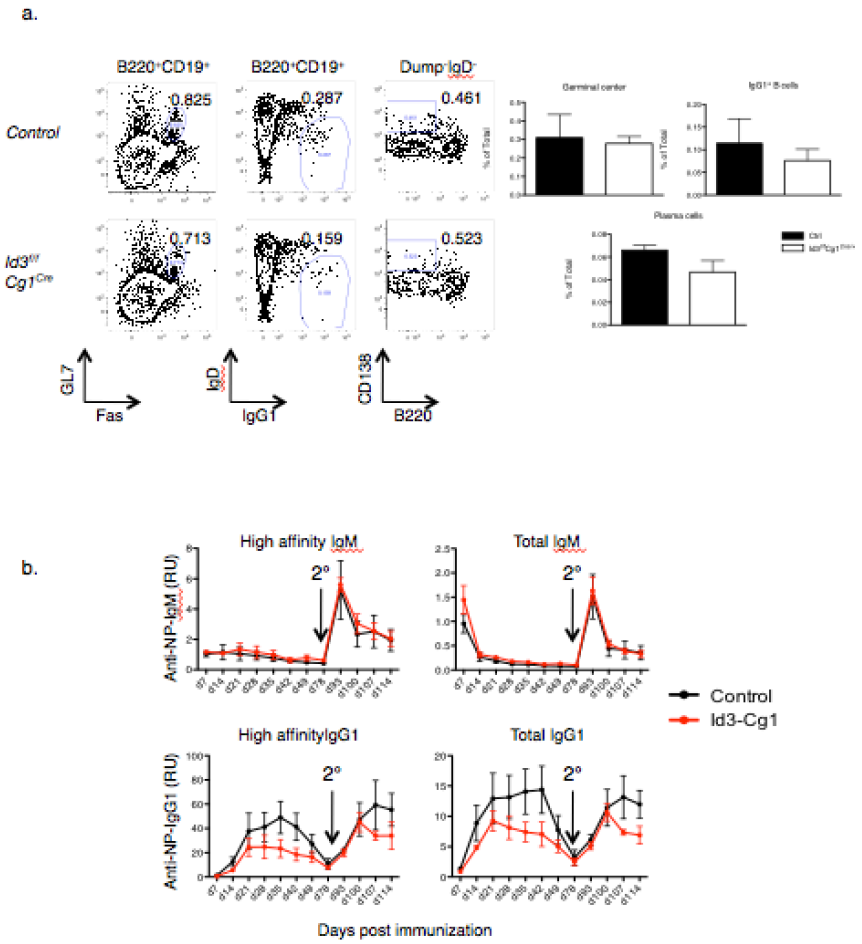

Figure 4.8 Primary and memory response when *Id3* is deleted after GC entry.

(a) Flow cytometric analysis of activated B cell subpopulations derived from the spleens isolated from 8-week-old control or Id3-Cg1 cKO ($Id3^{fl/fl}$ $C\gamma1^{Cre}$) mice immunized with NP-KLH plus adjuvant. The two left panels indicate Fas versus GL7 and IgG1 versus IgD expression, gated on the $B220^{+}CD19^{+}$ compartment derived from spleens of immunized control or Id3-Cg1 cKO mice. The right panel indicates B220 versus CD138 expression, gated on the $Dump^{+}IgD^{-}$ compartment. Numbers in plots indicate percent of $Fas^{+}GL7^{+}$, $IgG1^{+}IgD^{-}$, and $B220^{-}CD138^{+}$ cells. Right, percentages of GC ($Fas^{+}GL7^{+}$), $IgG1^{+}$ B cells ($IgG1^{+}IgD^{-}$), and plasma cells ($Dump^{+}IgD^{-}B220^{-}CD138^{+}$) in splenocytes. (b) Time-course analysis of NP_4- or NP_{26}-reactive IgM and IgG1 in serum from control and Id3-Cg1 cKO mice immunized with NP-KLH plus adjuvant at day 0 and boosted with NP-KLH only at day 78 (downward arrows). Data are representative of two independent experiments (b; mean ± s.d. of n = 5 mice in control group and n = 5 in $Id3^{f/f}C\gamma1^{Cre}$ group). * $P<0.05$ (two-tailed unpaired Student's t test).

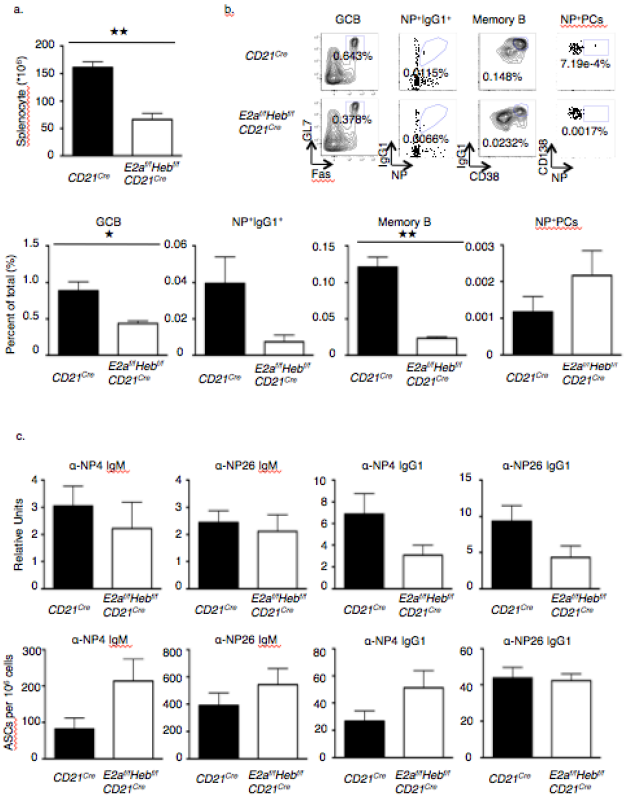

Figure 4.9 B cell activation and differentiation in the absence of *E2a* and *Heb* following NP-KLH immunization.

(a) Number of splenocytes isolated from 8-week-old control and $E2a^{f/f}Heb^{f/f}Cd21^{Cre}$ mice. (b) Flow cytometric analysis B cells derived from the spleens isolated from 8-week-old control ($E2a^{f/f}Heb^{f/f}Cd21^{WT}$) or $E2a^{f/f}Heb^{f/f}Cd21^{Cre}$ mice. Adjacent panels indicate Fas versus GL7 expression, gated on the $Dump^{-}B220^{+}CD19^{+}$ compartment derived from 8-week-old control ($E2a^{f/f}Heb^{f/f}Cd21^{WT}$) or $E2a^{f/f}Heb^{f/f}Cd21^{Cre}$ splenocytes; NP versus IgG1 and CD38 versus IgG1 expression, gated on $Dump^{-}B220^{+}CD19^{+}IgD^{-}$ compartment derived from 8-week-old control ($E2a^{f/f}Heb^{f/f}Cd21^{WT}$) or $E2a^{f/f}Heb^{f/f}Cd21^{Cre}$ splenocytes; NP versus CD138 expression, gated on $Dump^{-}IgD^{-}$ compartment derived from 8-week-old control ($E2a^{f/f}Heb^{f/f}Cd21^{WT}$) or $E2a^{f/f}Heb^{f/f}Cd21^{Cre}$ splenocytes. Numbers in plots indicate percent $Fas^{+}GL7^{+}$, $NP^{+}IgG1^{+}$, $IgG1^{+}CD38^{+}$, and $NP^{+}CD138^{+}$. Bottom, percentages of germinal center B cells ($Fas^{+}GL7^{+}$), NP-reactive IgG1-switched B cells ($NP^{+}IgG1^{+}$), $CD38^{+}IgG1^{+}$ "memory-like" B cells ($IgG1^{+}CD38^{+}$), and NP-reactive plasma cells ($NP^{+}CD138^{+}$) in splenocytes. (c) Upper, quantification of NP_4- and NP_{26}-reactive IgM and IgG1 in serum collected from control and $E2a^{f/f}Heb^{f/f}Cd21^{Cre}$ mice 14 d after immunization with NP-KLH. Bottom, Elispot analysis of NP_4- and NP_{26}-specific IgM and IgG1 ASCs in spleens on days 14 after NP-KLH immunization. Data are representative of at least four experiments (a, b, c; mean ± s.d.; control n = 3, $E2a^{f/f}Heb^{f/f}Cd21^{Cre}$ n = 3 independent biological replicates). * P<0.05, ** P<0.01 (two-tailed unpaired Student's t test).

Chapter IV, in part, is based on the material as it appears in Chen S, Miyazaki M, Fisch K, Chang AN, Murre C. *The antagonist HLH protein Id3 acts to enforce the germinal center checkpoint in B-lineage cells.* (In preparation, 2016). The dissertation author was the primary author of this draft in preparation.

Chapter V:

Insights and future directions

Previous studies indicated that *Foxp3* expression and other transcription factors such as *Ctla4* are critical for Treg-mediated suppression. However, studies performed during the last decade revealed there as a secondary module for regulatory T cells to carry out their suppressive activity against specific helper T cell subpopulations. In this study, we identified a subpopulation of Treg cells expressing the chemokine receptor CXCR5, a marker used to distinguish follicular helper T cells. Moreover, these CXCR5+ Treg cells can suppress Th2-mediated inflammation dependent on transcription factors *Id2* and *Id3*.

Checking the expression pattern of *Id2* and *Id3* in Treg populations during different developmental stages, we notice that *Id2* level is much higher in thymic Treg populations than in the periphery. This suggests Id2 might have important function in TCR-mediated thymic Treg differentiation. Even in those peripheral lymphoid organs, around 6% of CD25+ Treg cells express *Id2*. In the future, we can look into if these ID2+ Tregs are derived from their thymic progenitors or other precursor populations in the periphery. Furthermore, as *Id3* maintains high expression level in all Tregs, it may have important function during inflammatory conditions.

Those Treg cells lacking *Id2* and *Id3* expression display impaired suppressive function in lymphopenic or inflammatory situations, although they show normal suppressive activity in vitro as measured by thymidine incorporation. Such difference can be due to deficient homeostasis of Treg cells in the absence of *Id2* and *Id3*. Besides increased cell death, improper localization could also affect Treg homeostasis.

Abundance of *Id2* and *Id3* is required for establishing checkpoint of CXCR5+ Treg cells (follicular Treg, T_{FR}) at early phases. Later during differentiation, E proteins' expression and activity need to be upregulated to control progression into a fully mature T_{FR} phenotype. Actually, such balance and counteraction between E and Id proteins can also be found in other lymphocyte populations such as B cells. Using *Id3-GFP* reporter mice, we found high level of *Id3* in naïve follicular B cells. Nonetheless, once these B cells get activated by foreign antigens and pass the pre-GC checkpoints, *Id3* expression declines and *E2a* activity is increased.

Using *Id3-GFP* and *E2a-GFP* reporter mice, we found they exhibited very different expression patterns during various stages of B cell terminal differentiation, suggesting Id proteins may counterbalance E protein activity in this process. Before GC entry, Id3 is highly expressed in naïve B cells, inhibiting E protein activity and establishing a checkpoint for GC entry. Once activated B cells enter the GC phase, E proteins become active to enable clonal expansion and induce *Aicda* expression for further affinity maturation. Id proteins' inhibitory function is no longer in need at this stage, so we observe a clear declination of *Id3* expression throughout the GC phase. In those post-GC B cells, although Id3 expression is almost switched off in plasma cells, it may still have critical function in the regulation of terminal differentiation as indicated by its high level in CD38+IgG1+ "memory-like" B cells. A complete block of IgG1 memory response in the absence of *Id3* further substantiates this hypothesis. However, the cellular and molecular mechanism underlying this phenotype is far more complicated than a simple "cell intrinsic" effect.

Chapter VI:

References

1. Spangrude GJ, Heimfeld S, Weissman IL. Purification and characterization of mouse hematopoietic stem cells. *Science*. 1988;241(4861):58-62.

2. Mikkola HK, Orkin SH. The journey of developing hematopoietic stem cells. *Development*. 2006;133(19):3733-3744.

3. Kiel MJ, Yilmaz OH, Iwashita T, Yilmaz OH, Terhorst C, Morrison SJ. SLAM family receptors distinguish hematopoietic stem and progenitor cells and reveal endothelial niches for stem cells. *Cell*. 2005;121(7):1109-1121.

4. Papathanasiou P, Attema JL, Karsunky H, Xu J, Smale ST, Weissman IL. Evaluation of the long-term reconstituting subset of hematopoietic stem cells with CD150. *Stem Cells (Miamisburg)*. 2009;27(10):2498-2508.

5. Spangrude GJ, Heimfeld S, Weissman IL. Purification and characterization of mouse hematopoietic stem cells. *Science*. 1988;241(4861):58-62.

6. Akashi K, Traver D, Miyamoto T, Weissman IL. A clonogenic common myeloid progenitor that gives rise to all myeloid lineages. *Nature*. 2000;404(6774):193-197.

7. Kondo M, Weissman IL, Akashi K. Identification of clonogenic common lymphoid progenitors in mouse bone marrow. *Cell*. 1997;91(5):661-672.

8. Busch K, Klapproth K, Barile M, Flossdorf M, Holland-Letz T, Schlenner SM, Reth M, Hofer T, Rodewald HR. Fundamental properties of unperturbed haematopoiesis from stem cells in vivo. *Nature (London)*. 2015;518(7540):542-546.

9. Seita J, Weissman IL. Hematopoietic stem cell: self-renewal versus differentiation. *Wiley Interdiscip Rev Syst Biol Med*. 2010;2(6):640-653.

10. Dias S, Xu W, McGregor S, Kee B. Transcriptional regulation of lymphocyte development. *Curr Opin Genet Dev*. 2008;18(5):441-448.

11. Murre C. Developmental trajectories in early hematopoiesis. *Genes Dev*. 2009;23(20):2366-2370.

12. Semerad CL, Mercer EM, Inlay MA, Weissman IL, Murre C. E2A proteins maintain the hematopoietic stem cell pool and promote the maturation of myelolymphoid and myeloerythroid progenitors. *Proc Natl Acad Sci U S A*. 2009;106(6):1930-1935.

13. Rothenberg EV, Moore JE, Yui MA. Launching the T-cell-lineage developmental programme. *Nature Reviews Immunology*. 2008;8(1):9-21.

14. Carpenter AC, Bosselut R. Decision checkpoint in the thymus (vol 11, pg 666, 2010). *Nat Immunol*. 2011;12(3):271-271.

15. David-Fung ES, Yui MA, Morales M, Wang H, Taghon T, Diamond RA, Rothenberg EV. Progression of regulatory gene expression states in fetal and adult pro-T-cell development. *Immunol Rev*. 2006;209:212-236.

16. Ma CS, Deenick EK, Batten M, Tangye SG. The origins, function, and regulation of T follicular helper cells. *J Exp Med*. 2012;209(7):1241-1253.

17. Okada T, Moriyama S, Kitano M. Differentiation of germinal center B cells and follicular helper T cells as viewed by tracking Bcl6 expression dynamics. *Immunol Rev*. 2012;247(1):120-132.

18. Brunkow ME, Jeffery EW, Hjerrild KA, Paeper B, Clark LB, Yasayko SA, Wilkinson JE, Galas D, Ziegler SF, Ramsdell F. Disruption of a new forkhead/winged-helix protein, scurfin, results in the fatal lymphoproliferative disorder of the scurfy mouse. *Nat Genet*. 2001;27(1):68-73.

19. Wong J, Obst R, Correia-Neves M, Losyev G, Mathis D, Benoist C. Adaptation of TCR repertoires to self-peptides in regulatory and nonregulatory CD4+ T cells. *J Immunol*. 2007;178(11):7032-7041.

20. Chen W, Jin W, Hardegen N, Lei KJ, Li L, Marinos N, McGrady G, Wahl SM. Conversion of peripheral CD4+CD25- naïve T cells to CD4+CD25+ regulatory T cells by TGF-β induction of transcription factor Foxp3. *J Exp Med*. 2003;198(12):1875-1886.

21. Sakaguchi S, Yamaguchi T, Nomura T, Ono M. Regulatory T cells and immune tolerance. *Cell*. 2008;133(5):775-787.

22. Yamaguchi T, Hirota K, Nagahama K, Ohkawa K, Takahashi T, Nomura T, Sakaguchi S. Control of immune responses by antigen-specific regulatory T cells expressing the folate receptor. *Immunity*. 2007;27(1):145-159.

23. Takahashi T, Tagami T, Yamazaki S, Uede T, Shimizu J, Sakaguchi N, Mak TW, Sakaguchi S. Immunologic self-tolerance maintained by CD25+CD4+ regulatory T cells constitutively expressing cytotoxic T lymphocyte-associated antigen 4. *J Exp Med*. 2000;192(2):303-310.

24. Borghesi L, Hsu L, Miller JP, Anderson M, Herzenberg L, Herzenberg L, Schlissel MS, Allman D, Gerstein RM. B lineage-specific regulation of V(D)J recombinase activity is established in common lymphoid progenitors. *J Exp Med*. 2004;199(4):491-502.

25. Ehlich A, Martin V, Muller W, Rajewsky K. Analysis of the B-cell progenitor compartment at the level of single cells. *Curr Biol*. 1994;4(7):573-583.

26. Bassing C, Swat W, Alt F. The mechanism and regulation of chromosomal V(D)J recombination. *Cell*. 2002;109:S45-S55.

27. Rooney S, Chaudhuri J, Alt FW. The role of the non-homologous end-joining pathway in lymphocyte development. *Immunol Rev*. 2004;200:115-131.

28. Inlay MA, Bhattacharya D, Sahoo D, Serwold T, Seita J, Karsunky H, Plevritis SK, Dill DL, Weissman IL. Ly6d marks the earliest stage of B-cell specification and identifies the branchpoint between B-cell and T-cell development. *Genes Dev*. 2009;23(20):2376-2381.

29. Mansson R, Zandi S, Welinder E, Tsapogas P, Sakaguchi N, Bryder D, Sigvardsson M. Single-cell analysis of the common lymphoid progenitor compartment reveals functional and molecular heterogeneity. *Blood*. 2010;115(13):2601-2609.

30. Melchers F, Haasner D, Grawunder U, Kalberer C, Karasuyama H, Winkler T, Rolink AG. Roles of IgH and L chains and of surrogate H and L chains in the development of cells of the B lymphocyte lineage. *Annu Rev Immunol*. 1994;12:209-225.

31. Zhuang Y, Soriano P, Weintraub H. The helix-loop-helix gene E2A is required for B cell formation. *Cell*. 1994;79(5):875-884.

32. Allman D, Pillai S. Peripheral B cell subsets. *Curr Opin Immunol*. 2008;20(2):149-157.

33. Thomas MD, Srivastava B, Allman D. Regulation of peripheral B cell maturation. *Cell Immunol*. 2006;239(2):92-102.

34. Basso K, Dalla-Favera R. Germinal centers and B cell lymphomagenesis. *Nat Rev Immunol*. 2015;15(3):172-184.

35. MacLennan IC. Germinal centers. *Annu Rev Immunol*. 1994;12:117-139.

36. Victora GD, Schwickert TA, Fooksman DR, Kamphorst AO, Meyer-Hermann M, Dustin ML, Nussenzweig MC. Germinal center dynamics revealed by multiphoton microscopy with a photoactivatable fluorescent reporter. *Cell*. 2010;143(4):592-605.

37. Allen CD, Ansel KM, Low C, Lesley R, Tamamura H, Fujii N, Cyster JG. Germinal center dark and light zone organization is mediated by CXCR4 and CXCR5. *Nat Immunol*. 2004;5(9):943-952.

38. Muramatsu M, Kinoshita K, Fagarasan S, Yamada S, Shinkai Y, Honjo T. Class switch recombination and hypermutation require activation-induced cytidine deaminase (AID), a potential RNA editing enzyme. *Cell*. 2000;102(5):553-563.

39. Kinoshita K, Honjo T. Linking class-switch recombination with somatic hypermutation. *Nat Rev Mol Cell Biol*. 2001;2(7):493-503.

40. Reimold AM, Iwakoshi NN, Manis J, Vallabhajosyula P, Szomolanyi-Tsuda E, Gravallese EM, Friend D, Grusby MJ, Alt F, Glimcher LH. Plasma cell differentiation requires the transcription factor XBP-1. *Nature*. 2001;412(6844):300-307.

41. Shaffer AL, Lin KI, Kuo TC, Yu X, Hurt EM, Rosenwald A, Giltnane JM, Yang L, Zhao H, Calame K, Staudt LM. Blimp-1 orchestrates plasma cell differentiation by extinguishing the mature B cell gene expression program. *Immunity*. 2002;17(1):51-62.

42. Klein U, Casola S, Cattoretti G, Shen Q, Lia M, Mo T, Ludwig T, Rajewsky K, Dalla-Favera R. Transcription factor IRF4 controls plasma cell differentiation and class-switch recombination. *Nat Immunol*. 2006;7(7):773-782.

43. Fairfax KA, Kallies A, Nutt SL, Tarlinton DM. Plasma cell development: from B-cell subsets to long-term survival niches. *Semin Immunol*. 2008;20(1):49-58.

44. Ahmed R, Gray D. Immunological memory and protective immunity: understanding their relation. *Science*. 1996;272(5258):54-60.

45. Kurosaki T, Kometani K, Ise W. Memory B cells. *Nat Rev Immunol*. 2015;15(3):149-159.

46. Massari ME, Murre C. Helix-loop-helix proteins: Regulators of transcription in eucaryotic organisms. *Mol Cell Biol*. 2000;20(2):429-440.

47. MURRE C, MCCAW P, BALTIMORE D. A new dna-binding and dimerization motif in immunoglobulin enhancer binding, daughterless, myod, and myc proteins. *Cell*. 1989;56(5):777-783.

48. Semerad CL, Mercer EM, Inlay MA, Weissman IL, Murre C. E2A proteins maintain the hematopoietic stem cell pool and promote the maturation of

myelolymphoid and myeloerythroid progenitors. *Proc Natl Acad Sci U S A*. 2009;106(6):1930-1935.

49. Bain G, Maandag ECR, Izon DJ, Amsen D, Kruisbeek AM, Weintraub BC, Krop I, Schlissel MS, Feeney AJ, van Roon M, van der Valk M, te Riele HPJ, Berns A, Murre C. E2A proteins are required for proper B cell development and initiation of immunoglobulin gene rearrangements. *Cell*. 1994;79(5):885-892.

50. Busslinger M. Transcriptional control of early B cell development. *Annu Rev Immunol*. 2004;22:55-79.

51. Murre C. Developmental trajectories in early hematopoiesis. *Genes Dev*. 2009;23(20):2366-2370.

52. Welinder E, Mansson R, Mercer EM, Bryder D, Sigvardsson M, Murre C. The transcription factors E2A and HEB act in concert to induce the expression of FOXO1 in the common lymphoid progenitor. *Proc Natl Acad Sci U S A*. 2011;108(42):17402-17407.

53. Lin YC, Jhunjhunwala S, Benner C, Heinz S, Welinder E, Mansson R, Sigvardsson M, Hagman J, Espinoza CA, Dutkowski J, Ideker T, Glass CK, Murre C. A global network of transcription factors, involving E2A, EBF1 and Foxo1, that orchestrates B cell fate. *Nat Immunol*. 2010;11(7):635-643.

54. Naito T, Tanaka H, Naoe Y, Taniuchi I. Transcriptional control of T-cell development. *Int Immunol*. 2011;23(11):661-668.

55. Quong MW, Harris DP, Swain SL, Murre C. E2A activity is induced during B-cell activation to promote immunoglobulin class switch recombination. *EMBO J*. 1999;18(22):6307-6318.

56. Sayegh CE, Quong MW, Agata Y, Murre C. E-proteins directly regulate expression of activation-induced deaminase in mature B cells. *Nat Immunol*. 2003;4(6):586-593.

57. Norton JD, Deed RW, Craggs G, Sablitzky F. ID helix-loop-helix proteins in cell growth and differentiation. *Trends Cell Biol*. 1998;8(2):58-65.

58. Bain G, Cravatt CB, Loomans C, Alberola-lla J, Hedrick SM, Murre C. Regulation of the helix-loop-helix proteins, E2A and Id3, by the Ras-ERK MAPK cascade. *Nat Immunol*. 2001;2(2):165-171.

59. Engel I, Johns C, Bain G, Rivera RR, Murre C. Early thymocyte development is regulated by modulation of E2A protein activity. *J Exp Med*. 2001;194(6):733-745.

60. Ikawa T, Fujimoto S, Kawamoto H, Katsura Y, Yokota Y. Commitment to natural killer cells requires the helix-loop-helix inhibitor Id2. *Proc Natl Acad Sci U S A*. 2001;98(9):5164-5169.

61. Boos MD, Yokota Y, Eberl G, Kee BL. Mature natural killer cell and lymphoid tissue-inducing cell development requires Id2-mediated suppression of E protein activity. *J Exp Med*. 2007;204(5):1119-1130.

62. Maruyama T, Li J, Vaque JP, Konkel JE, Wang W, Zhang B, Zhang P, Zamarron BF, Yu D, Wu Y, Zhuang Y, Gutkind JS, Chen W. Control of the differentiation of regulatory T cells and T(H)17 cells by the DNA-binding inhibitor Id3. *Nat Immunol*. 2011;12(1):86-95.

63. Nakatsukasa H, Zhang D, Maruyama T, Chen H, Cui K, Ishikawa M, Deng L, Zanvit P, Tu E, Jin W, Abbatiello B, Goldberg N, Chen Q, Sun L, Zhao K, Chen W. The DNA-binding inhibitor Id3 regulated IL-9 production in CD4(+) T cells. *Nat Immunol*. 2015;16(10):1077-1084.

64. Miyazaki M, Rivera RR, Miyazaki K, Lin YC, Agata Y, Murre C. The opposing roles of the transcription factor E2A and its antagonist Id3 that orchestrate and enforce the naïve fate of T cells. *Nat Immunol*. 2011;12(10):992-1001.

65. Sayegh CE, Quong MW, Agata Y, Murre C. E-proteins directly regulate expression of activation-induced deaminase in mature B cells. *Nat Immunol*. 2003;4(6):586-593.

66. Xu Z, Zan H, Pone EJ, Mai T, Casali P. Immunoglobulin class-switch DNA recombination: induction, targeting and beyond. *Nat Rev Immunol.* 2012;12(7):517-531.

67. Teng G, Papavasiliou FN. Immunoglobulin somatic hypermutation. Annu Rev Genet. 2007;41:107-120.

68. Muramatsu M, Kinoshita K, Fagarasan S, Yamada S, Shinkai Y, Honjo T. Class switch recombination and hypermutation require activation-induced cytidine deaminase (AID), a potential RNA editing enzyme. *Cell*. 2000;102(5):553-563.